INDEX

SUMMARY

A new three-dimensional elastomeric substrate was created to allow precise cellular force measurements while providing the cells with a complex, nature-like environment. The substrate consisted of elastomeric arrays of micrometer-sized pillars projecting from the same elastomer substrate and organized in square lattices. Cells used in the study were cardiac myocytes extracted from rat foetuses. The myocytes were allowed to adhere to the microarray; subsequently, contracting cells were chosen for the analysis. The cells were studied with confocal laser scanning microscopy (CLSM).

To evaluate the data, a new approach to the elasticity theory was necessary, as soft micropillars protruding from equally soft substrate required a different approach than described up to now. After implementations of necessary corrections, two models with regard to cellular force spatial distribution were proposed and used to calculate possible cellular forces. The obtained force magnitude was then compared with results obtained by other researchers. Also, contraction amplitude and frequency were discussed.

1. INTRODUCTION

The ability to perform experiments on small scales is very appealing. Lab-on-chip techniques, at first used by chemists to work with miniscule amount of reagents, gain popularity in other branches of research as well. (Nature Insight, 2006) In particular, micro-devices allow studies of single cell behaviour. Single cell experiments are already intuitively attractive and have furthermore proven to be very valuable for the study of numerous cellular phenomena (Balaban et al. 2001, Geiger et al. 2001). This is why the methodology of a single-cell experiments has been vividly discussed for years and we believe it is highly desirable to improve the existing techniques.

Numerous studies showed that cells answer not only to chemical stimuli but also to mechanical ones (e.g. stiffness and texture of the substrate they adhere to (see chapter 1.2 CELLULAR BEHAVIOUR VS. MECHANICAL PROPERTIES OF THE ENVIRONMENT: Geiger and Bershadsky 2001, Balaban et al. 2001, Yeung et al. 2004, Tomasek et al. 2002). Not only do muscle cells, while contracting, apply forces to the surrounding tissue; other actively moving cells do as well (Balaban et al. 2001, Roy et al 1997). The greatest cell 'walkabout' takes place during embryo development but it never ceases throughout the lifespan of an organism (Juliano and Haskill 1993). Although the body structures may look static at the first sight, cells migrate constantly inside and between tissues. For example, immune cells penetrate tissues searching for germs, skin cells move towards wounds in order to close them and neurons grow, forming new connections (Cooper and Hausman 2007, Britland et al. 1997, Doolabh et al. 1996).

Topography and mechanical properties of cellular environment play a crucial role in regulating cellular processes for example migration (Pelham & Wang 1997, Choquet et al. 1997, Lo et al. 2000), proliferation (Boateng et al. 2003), differentiation and tissue formation (Hamilton et al. 2004, Huang and Ingber 1999, Engler et al. 2004, Dike et al. 1999, Powers et al. 2002, Norman et al. 2005, Ben-Ze'ev et al. 1988). Apoptosis (programmed cell death, 'cellular suicide') is also influenced by the mechanical stimuli (Dike et al. 1999, Discher et al 2005). What is more, environment influences cell morphology (shape) (see also chapter 3 DISCUSSION) (Ben-Ze'ev et al. 1988) and alignment (Boateng et. al. 2003, Bursac et al. 2002). It affects cytoskeletal structure (Motlagh et al. 2003, Yeung et al. 2004), gene expression (Brunette 1984, Webb et al. 2003) and protein synthesis and activation (Seko et al. 1999, Yi et. al. 2003, Vogel, Sheetz 2006) or calcium dynamics (Yin et al. 2004, le Guennec et al. 1991). Despite this, cells have usually been studied on flat, hard substrates, like plastic Petri dishes, which resemble natural tissue neither in stiffness nor in texture. In later experiments, more sophisticated elastomeric systems were created (Balaban et al. 2001) but still they resembled tissues in few aspects only. They enabled precise force measurements but did not bear a resemblance to natural tissue structure. Alternatively, they offered the cells

tissue-like environment (Sheu et al. 2001, Pizzo et al. 2005) but gave no quantitative information about cell mechanics. Therefore, there is need for novel systems, tailored to cellular specifics and at the same time, allowing precise force measurements.

In this chapter, heart muscle cells are introduced and the cellular response to mechanical stimuli is described together with numerous devices built in the past to study cellular mechanical properties.

1.1. CARDIAC MYOCYTES

1.1.1. CONTRACTION MECHANISM

The **cardiac myocyte**, also called heart muscle cell, is responsible for heart beating. Cardiac muscle tissue, called myocardium, can contract rhythmically and in a synchronized way because its cells are electrically connected with so called gap junctions - channels which allow the flow of different molecules and of electric currents between the cells while keeping the tissue mechanically tightly bound. A complex system of pacemakers ensures that the heart contracts in a proper way. Interestingly, those pacemakers continue working even after the heart is disconnected from the nervous system (Sotowska-Brochocka, 2001).

The 'electricity' of the heart, (just as the 'electricity' of the nervous system or muscles) is **ion based**. Influx and efflux of sodium, potassium and calcium cations as well as chloride anions[1] into the cells create an electrical potential difference between the inside and outside of the cell. Changes of this potential difference, in turn, triggers cell contraction (in case of muscle cells) or signal transfer (in case of neurons). As each cell is surrounded by a lipid **cell membrane**, practically impermeable to ions, cells posses a sophisticated system of ion channels and ion pumps. They are complex proteins, positioned inside cell membrane that let the ions in and out of the cell. Channels transfer the ions with the ion concentration gradient while pumps use energy to accumulate or remove the ions against the gradient (Berg et al. 1997).

Heart muscle cells contract in response to a changing potential difference between the outside and the inside of the cell. The potential triggering a contraction is called the cardiac action potential. It varies significantly in different regions of the heart that causes the different electrical characteristics of various portions of the heart, cf. Fig 1-A and Fig. 1-B. (Malmivuo and Plonsey 1995). The standard model used to understand the cardiac action potential is the

---

[1] different types of ions are used in different kinds of cells

action potential of the ventricular myocyte (see Fig. 1-A). The action potential has 5 phases, numbered 0-4 (Klabunde 2004). Phase 4 is called the resting membrane potential and describes the membrane potential when the myocyte is not being stimulated. The resting membrane potential is caused by the difference in ion concentration across the cell membrane. The normal resting membrane potential in the ventricular myocardium is about -85 to -95 mV. The ventricular cell remains in the phase 4 till an external electrical trigger, usually by a neighboring cell, stimulates it. However, some of the cardiac myocytes, for example sinoatrial myocytes, may undergo spontaneous depolarisation (that is, they contract without being stimulated), in which an action potential is generated without any external trigger. They are called pacemaker cells, as they, stimulating the adjacent cells, cause the whole heart to contract. Their action potential has a specific phase 4, called a prepotential (see Fig. 1-A). As the potential increases to the firing (contraction) level (around -40 mV) the rapid depolarisation phase (phase 0) begins. In phase 1 the action potential has a positive peak while phase 2, is a potential plateau. Phase 3, depolarisation, leads to the reconstruction of the resting membrane potential. For a moment, the potential can fall even lower than –85 mV; this phenomenon is called hyperpolarisation. For more details, see Malmivuo and Plonsey (1995).

Due to the spontaneous depolarisation, some cardiac myocytes may continue to contract regularly even if isolated as, in principle, no external trigger is necessary to excite them. Despite that fact, cardiac myocytes are usually stimulated during experiments either with calcium ions or by applying an electrical potential to them. This approach is understandable in some kinds of experiments as relatively few isolated cells retain their ability to contract. To our best knowledge, however, it is not certain how external triggers influence the natural character of cell contractions. For this reason, one cannot keep for certain the behaviour of artificially stimulated heart muscle cells is similar to their *in vivo* activity (Sotowska-Brochocka 2001, Bryszewska and Leyko 1997).
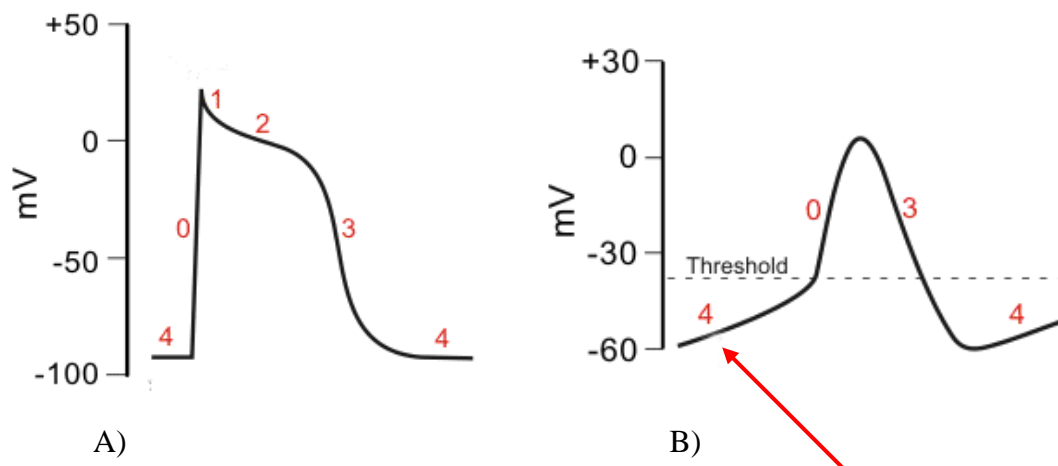
Fig. 1-A Cardiac action potential phases. A) Ventricular myocyte B) Sinoatrial myocyte. The prepotential of the pacemaker cell is indicated with an arrow. (Klabunde 2004)
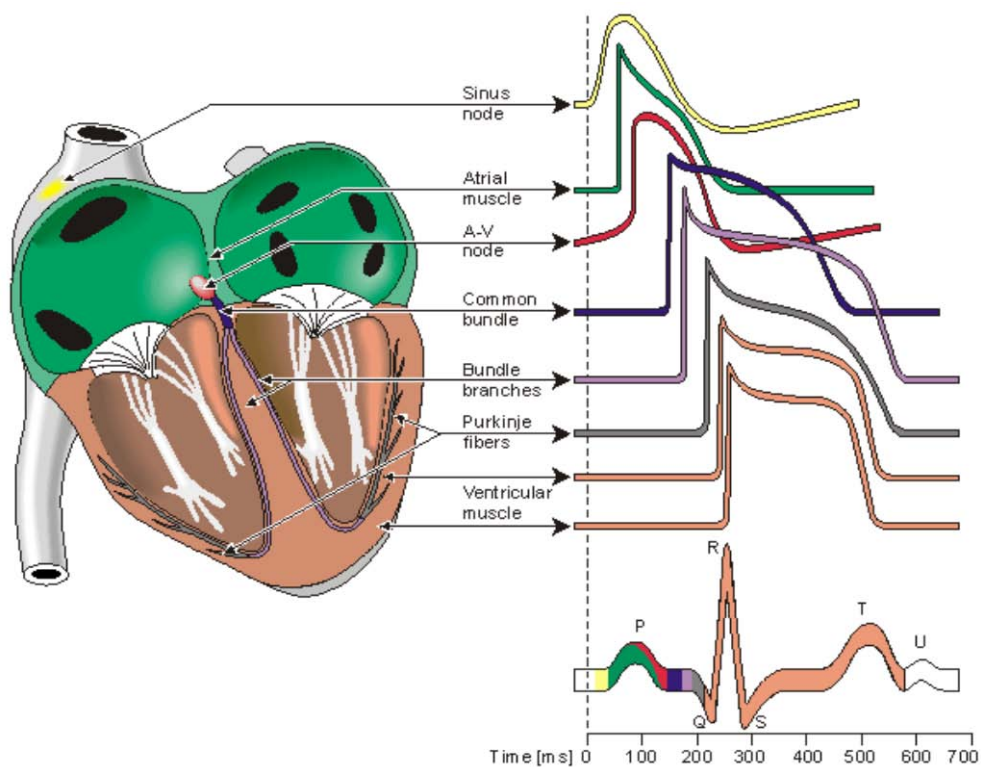
Fig. 1-B Different types of cardiac myocyte action potential. Note the prepotential on AV-node cells. Activity period of each kind of cells is depicted on an ECG graph (Malmivuo and Plonsey 1995).

1.1.2. CYTOSKELETON

Each eucariotic (non-bacterial and non-archaean) cell possesses a **cytoskeleton** – the protein scaffold taking part in such processes like cell migration, division, morphology change, intercellular transport, mechanosensing and resistance against mechanical stress (Cooper and Hausman 2007). Also archaean and bacterial cells possess a complex system of proteins that play a similar role although their cytoskeleton molecules and functions are far less complex (Shih and Rothfield 2006, Michie and Löwe 2006). Although the word 'skeleton' reminds of a static, unchanging structure of bones, the cytoskeleton structures are not static; its fibres and meshes can appear and dissolve easily, depending on cell needs. It is indeed more a scaffold that can be assembled and disassembled on demand. Another difference between skeleton and cytoskeleton is that the latter is able to exert active forces; cytoskeleton is both the "bones" and the "muscles". There are several force-generation complexes known (Cooper and Hausman 2007; Bao 2002); in this thesis I will describe only the actin – myosin complex because it is directly responsible for cardiac myocyte contractions.

The 'workhorse' of cardiac myocytes is a duo consisting of actin and myosin II proteins. Actin is a polymer protein, capable to assemble into long filaments. Two parallel actin strands twist around each other in a helical formation, giving rise to microfilaments of the cytoskeleton. Microfilaments measure approximately 7 nm in diameter with a loop of the helix repeating every 37 nm.

Myosin II is a motor protein i.e. the protein that performs mechanical work. In muscle, actin and myosin are organized into actomyosin contractible myofibrils. Myosin molecules undergo a cycle during which they attach to actin filaments (called also thin filaments), exerting a tension, and then depending on the load, perform a power stroke that causes the actin filaments to slide past, shortening the muscle. For contraction, the myosin molecules are bundled laying between two separate actin filaments and the bundle (called a thick filament) simultaneously "walks", sliding the actin filaments closer to each other. This results in the shortening, or contraction, of the actin bundle. A thick filament-thin filament functional unit is called a **sarcomere** (see fig 1-C). As myofibrils in a cardiac myocyte are arranged in parallel, their simultaneous activity causes the whole cell to contract (Berg et al. 1997; Bryszewska and Leyko 1997; Cooper and Hausman 2007).
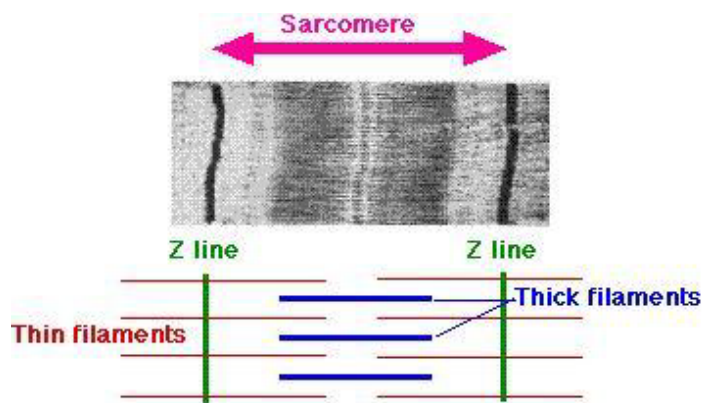
Fig. 1-C A sarcomere structure. Z-line contains sarcomere-stabilizing proteins.

1.1.3.   CELLULAR ADHESION

Cells are very selective with regard to the chemistry of the environment they adhere to. Cells adhere to their environment and another cells with help of proteins, namely integrins, cadherins and selectins (Gumbiner 1996, Vogel, Sheetz 2006). Integrins serve as anchors, binding to specific **extracellular matrix (ECM)** proteins only (Gumbiner 1996). They are also an important part of the force transfer and possibly force sensing system, taking an active part in cell response to mechanical forces (Katsumi et al. 2005).

ECM is the non-cellular part of animal tissue that usually provides structural support to the cells in addition to performing various other important functions. It is a complex, three dimensional mesh of fibrils. It consists of various proteins as well as many non-protein molecules. ECM is by no means a passive substrate – it forms, together with cells anchored to it, a sensitive and dynamic system. The connections between the cell contractile apparatus and ECM in adult cardiac myocytes are called **costameres** (Pardo et al. 1983). They provide a direct linkage to the ECM (see Fig 1-D). In addition to their role in cell anchorage, Danowski and co-workers (1992) demonstrated that costameres are sites where contractile forces are directly transmitted to the surrounding ECM. Due to integrin binding selectivity, all the devices cells are supposed to adhere to must be covered with appropriate ECM proteins before cell seeding. There are numerous ECM proteins which encourage cellular adhesion, for example: fibronectin, laminin or collagen (Gumbiner 1996, Badylak 2002). Malfunction of the cell adhesion system may have grave effects for the organism, including cancer formation and metastasis (Schwartz and Ingber 1994).

However, when isolated and cultured on Petri dishes as single cells, cardiac myocytes reorganize the costameres to adapt to the two-dimensional culture environment (Simpson et. al. 1993). Such adaptation results in adhesive structures that bear a resemblance to focal adhesion sites (FAS) which serve both as anchors as well as most likely mechanosensors for cells adhering to flat substrates (Geiger and Bershadsky 2002, Zamir and Geiger 2001). FAS are anchoring protein complexes of the cells, described in many cell types adhering to **flat** substrates. Focal adhesions consist of about 100 proteins. Moreover, **stress fibres** (actin filament bundles) are also formed in cardiac myocytes adhering to flat substrates. Stress fibres are actin bundles that generate and bear mechanical stresses and are anchored at the cell base to underlying ECM through integrins (Hu et al. 2003, Katz et al. 2000).
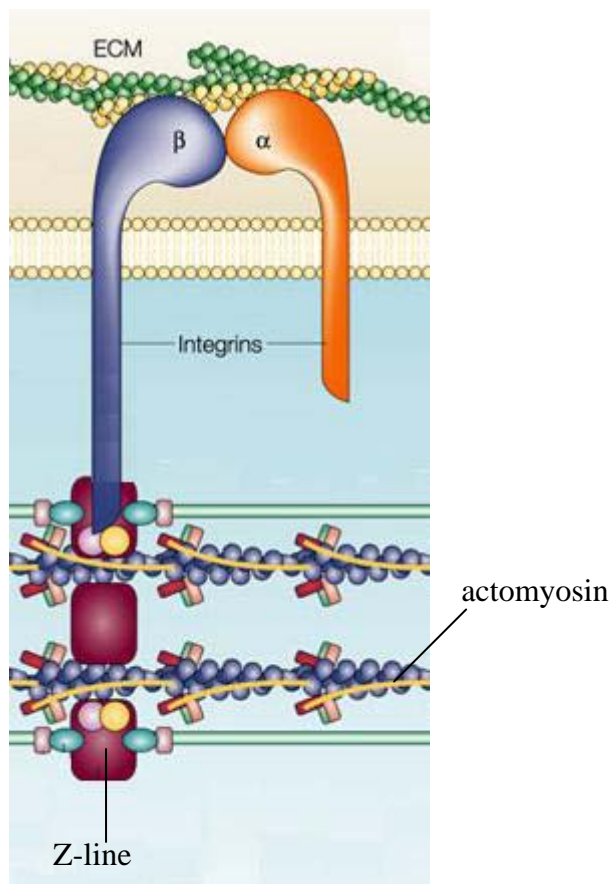
Fig. 1-D A costamere structure (after Liew and Dzau 2004).

1.2. CELLULAR BEHAVIOUR VS. MECHANICAL PROPERTIES OF THE ENVIRONMENT

Stiffness and topography of cellular substrates play a crucial role in tissue formation and wound healing as well as in embryogenesis (developing of the embryo). It regulates such phenomena as cell proliferation and migration. Moreover, it influences cell morphology (Boateng et. al. 2003, Craighead et al. 2001, Tan et al. 2001, Yeung et al. 2004, Pelham and Wang 1997, Engler et al. 2004). Cardiac myocytes cultivated on a flat substrate show no direction preference while when cultivated on a micro-grooved substrate they orient along the grooves, (see Bursac et al. 2002). Also, Lo et al. (2000) describe a 3T3 fibroblast cell line, moving along a rigidity gradient. In that experiment, the cell substrate consisted of two parts of different stiffness. The cells preferred the stiffer part; when already located on the stiffer side, they did not enter the more compliant one (see Lo et al. 2000). Mechanotaxis was also observed for NIH/3T3 fibroblasts and bovine pulmonary arterial endothelial cells by Gray and co-workers (2003).

Providing injured neurons with proper mechanical conduits positively affects cell regeneration and steers neuronal growth (Britland et al. 1997, Doolabh et al. 1996). What is more important, flat, uniform surfaces may fail as a substrate for artificial tissue cultures in spite of appropriate stiffness. Formation of liver and heart tissue 'patches' as well as angiogenesis *in vitro* is strongly affected by substrate topography (Curtis and Wilkinson 1997, Powers et. al. 2002, Zimmermann et al. 2000, Ben-Ze'ev et al. 1988, Dike et al. 1999). Angiogenesis (blood vessel formation), a process vital for tissue engineering and tumour formation, can be inducted with proper substrates (Sarkar et al. 2005, Hamilton et al. 2004). In case of cardiac myocytes, substrate topography influences not only cell shape but also the number of gap junctions (Entcheva et al. 2004). External forces, substrate rigidity and topography influence cells on the molecular level, manipulating such vital processes as gene expression (Webb et al. 2003, Dalby et al. 2002, Brunette 1984), protein synthesis and distribution (Yi et. al. 2003), protein activation (Seko et al. 1999), ion channel opening (le Guennec et al. 1991, Martinac 2004) and many other molecular processes (Vogel 2006, Motlagh et. al. 2003, Yin et. al 2004, Kung 2005, Mossman et al. 2005, Tamada et al. 2004, Geiger and Berschadsky 2002). Fibroblasts need external forces to differentiate and form normal tissues (Tomasek et al. 2002). Fibroblast cytoskeleton of cardiac myocytes and fibroblasts may reorganize prominently in response to topography (Entcheva and Bien 2003, Dalby et al. 2005). Substrate properties and external forces may even induce apoptosis – programmed cell death (Discher et al. 2005, Chen et. al. 1997, Numaguchi et al. 2003). Chen and co-workers (1997) cultivated cells on small, square islands covered with proteins cells

could attach to. Depending on the island size, cells either spread and survived or underwent apoptosis (Chen et. al 1997).

Moreover, many cell types orient and may move rapidly along fibres of a fairly narrow range of diameters (5–50 μm^2). This phenomenon was used to repair ripped tendons. The cells were encouraged to grow in a proper direction by placing a thin collagen fibre into an injured tissue (Curtis and Riehle 2001). It is also known that the ECM plays a vital part in tissue formation and regeneration (Badylak 2002).

Last but not least, proper tissue formation requires specific force application. A simple example is putting patients with broken limbs under traction. If no force is applied to the regenerating bone, it may deform (Curtis and Riehle, 2001). Tension, generated in ECM may also stimulate blood vessel formation and many other formation processes (Huang and Ingber 1999). Summarizing, one cannot overestimate the role played by external forces and substrate mechanical properties in tissue and cell regulation. The underlying mechanism of that influence is, however, poorly understood. The existing models suggest that strain, caused by external forces on the cell membrane, deforms proteins which in turn activates or deactivates them (Vogel and Sheetz 2006, Vogel 2006, Khan and Sheetz 1997, Perozo et al. 2002, Bao 2002). Tensegrity is also proposed as the principle regulating cell reactions to mechanical stimuli (Ingber 1998, Wang et al. 2001).

Still, despite the obvious importance of various mechanical properties of cellular substrates, cellular force measurements usually are conducted under highly non-physiological conditions. Therefore, creation of a cellular substrate characterized both with complex topography and giving the possibility of quantitative measurements is a challenging and attractive task.

1.3. CELL FORCE MEASUREMENT

Many cells move on their substrates. Although this migration mechanism is not fully understood, the cells must adhere to the substrate in order to push or pull their bodies forward. By doing so, they apply forces to the substrate. In order to study cellular migration mechanism and forces, numerous devices were created in the past. Also, many ingenious experimental set-ups were constructed to study contracting cells and the magnitude of forces exerted by cells. We will now review those techniques, concentrating on their most important advantages as well as disadvantages.

---

[2] this phenomenon is called 'contact guidance'.

1.3.1. DEVICES PROBING FORCES ON THE BASAL SURFACE OF A CELL

1.3.1.1. THIN FILMS

The first system developed to visualize cellular forces consisted of a layer of a liquid prepolymer called *PDMS* coated with a thin skin of crosslinked *PDMS* rubber, supported on a coverslip glass (Harris et al. 1980). Liquid *PDMS* was crosslinked with heat from a Bunsen burner. In order to produce films of different stiffness, various prepolymers and crosslinking times were used. As the resulting film was attached to the coverslip, it did not crumple and misshape during the experiment; it was also much easier to handle than the free film.

The films were next covered with ECM proteins to facilitate cell adhesion, placed in cell culture dishes and cells were allowed to adhere to them. As cells adhered and migrated, they deformed the film surface, creating wrinkles, see Fig. 1-E. The direction of force could be deduced from the wrinkles shape. The force magnitude was estimated by comparison to forces applied with the calibrated glass micropipettes under assumption that equal forces result in the same wrinkling pattern. This method by its nature is only semi-quantitative as precise force measurements were impossible. Still, it inspired creation of more sophisticated systems.
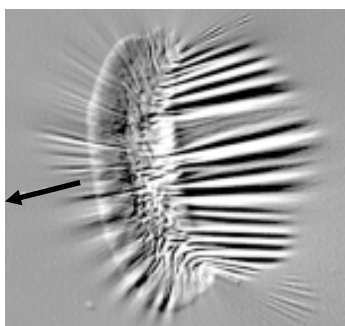
Fig. 1-E Cell wrinkling a thin silicone film. A motile fish keratocyte[3] exerts forces – visualized due to wrinkles – on a substrate. Direction of cell movement is indicated with the black arrow. (Beningo and Wang, 2002)

1.3.1.2. PATTERNED SUBSTRATES

A quantitative improvement was made by the introduction of **patterned hydrogels and elastomers** as the force detectors. For example, a mixture of acrylamide and

---

[3] Cornea cell

bisacrylamide was spread on glass coverslips previously activated by silanization[4]. To enable cellular adhesion, the polymer was in turn coated with ECM proteins. To visualize cellular forces fluorescent beads were mixed with the prepolymer (Pelham and Wang 1997, Dembo et al. 1996). Tracking the movement of the fluorescent beads with the aid of light microscope made quantitative studies of forces possible and enabled precise measurement of cell trajectory (Oliver et al. 1995, see Fig. 1-F). The serious drawback of the method is that beads are spread randomly, complicating the force magnitude calculation (Cesa 2007, Cesa et al. 2007).

This weakness was overcome by Balaban and co-workers who used patterned elastomer substrates. A still fluid two-component silicone elastomer mixture Sylgard[5] was cured on glass coverslips, resulting in non-wrinkling substrates with controllable mechanical properties[6].To enable tracking of the elastomer film deformation, a pattern of microdots was imprinted by curing the still liquid pre-elastomer pressed between a glass coverslip and a silicon master patterned with the negative of the dot pattern[7]. Alternatively, a microdot pattern can be printed on the plain substrate. Pattering and printing is not limited to microdots since, essentially, any structural form of position label can be implemented (for example squares or grids). Pattern deformation and the technique of pattern creation are shown in Fig. 1-G.

1.3.1.3.   MICRO- CANTILEVERS AND NEEDLES

First methods exploring microbeam bending to calculate the cellular force magnitude used single beams made of different materials. Those methods were used to estimate myocyte (muscle cell) contraction forces in contrast to the methods described above, serving mainly to study cell migration forces. The myocytes were fastened to steel microcantilevers (Tasche et al. 1999), polysilicon microbeams (Lin et al. 1995), glass needles (Puceat et al. 1990), or carbon microfibers (Nishimura et al. 2004) and stimulated to contract. For example, a cardiac myocyte was clamped between a stiff and a compliant fibre. The stiff fibre served as an anchor and was practically immobile while the compliant one bent as the cell contracted. Deflection of the compliant fibre was then recorded with a piezoelectric element (Nishimura et al. 2004, Yasuda et al. 2001). In an even more complicated alternative method, myocytes were mounted with the aid of a microscope between the tungsten needles of a force sensor and a piezoelectric translator using a polyurethane varnish. The piezoelectric translator was used to apply length changes to the cardiac myocyte. A piece of steel foil which moved as the

---

[4] covering the surface with chloroalkylosilanes as this increases the polymer wetting of the surface.

[5] Sylgard 184 (Dow Corning)

[6] PDMS is a two-component elastomer. By mixing the two components in different ratio one obtains an elastomer of different stiffness, see Appendix B

[7] Such silicon masters can be produced with standard photolithography techniques.

cell contracted, reflected a laser beam. Beam movement was detected by a photodiode. From the measured beam deflection and the needles' properties, one was able to calculate myocyte force magnitude (Tasche et al. 1999). The piezoelectric set-up and myocytes mounted between the microneedles are shown on Fig. 1-H and 1-I.
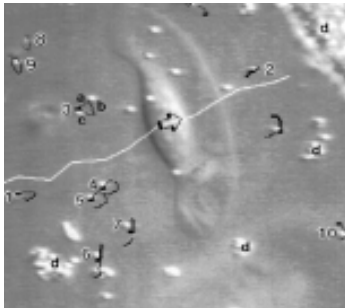
Fig. 1-F Motile fish keratocyte on a silicone substratum. Black tracings indicate the trajectories of embedded beads. Notice the fact that the beads are located irregularly. (Oliver, T. et al. 1995).
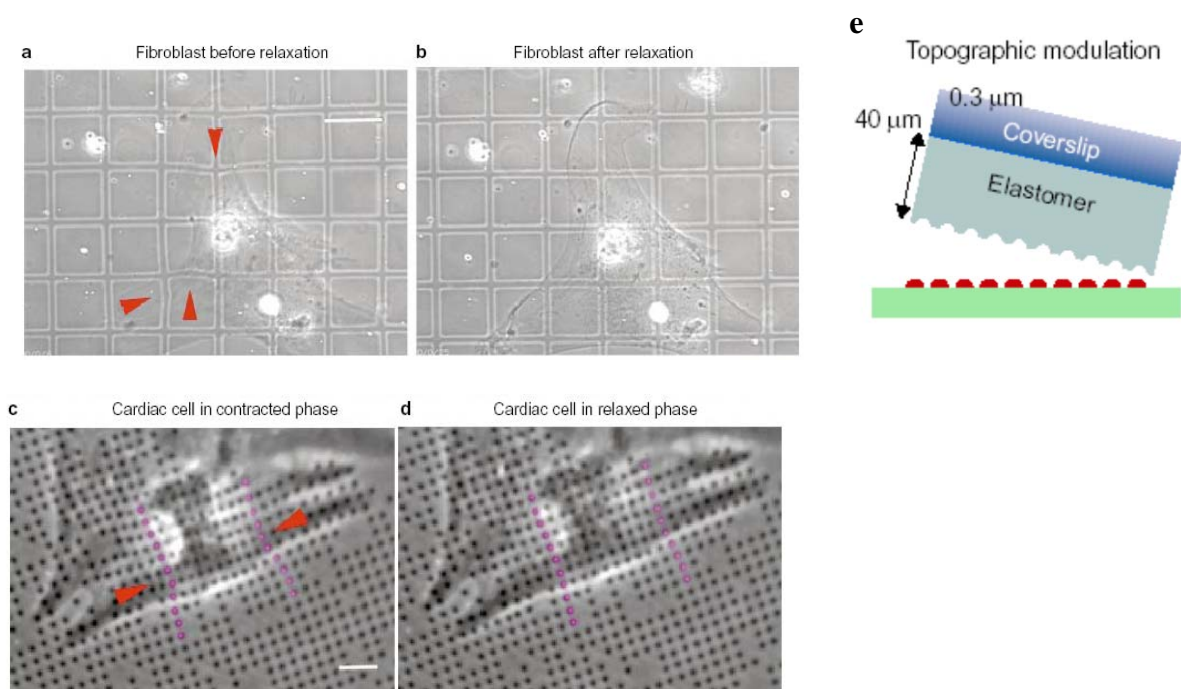
Fig. 1-G Cells on patterned surfaces a). A rat cardiac fibroblast plated on a large grid pattern. The cell distorts the elastomer (arrowheads). b) The same cell as in A), 10 min after relaxation. Notice the recovery of the regular grid pattern. Grid pitch = 30 μm. c) A contracting cardiac myocyte plated on elastomer with embedded photoresist pattern of dots (bar = 6 μm). The magenta dots show the deformation of the elastomer. Grid pitch = 2 μm. d) Relaxed phase e) Micropatterned elastomer preparation - separation of the elastomer form the silicon master (green with red dots on top) yields a pattern on the elastomer surface. (Balaban et al. 2001).

1.3.1.4. MICROFABRICATED POST-ARRAY DETECTORS (mPADs)

The multipillar system allowing discrete cellular force measurement, called **microfabricated post-array detector** (mPAD) (du Roure et al. 2005) consists of a regular array of micrometer-sized posts made of an elastomer (Li et al. 2007), see Fig. 1-J. The posts were coated with an ECM protein to allow cell adhesion. The microposts were packed so densely that the seeded cells were not able to penetrate in between and remained on top of the posts. Alternatively, the posts stood further apart but only their tops were covered with an ECM protein while the rest of the substrate was not adhesive. So, again, the cells adhered to the post tops. Only when cells exerted forces, the posts bent; force magnitude and direction could then be easily calculated from the measured post deflection amplitudes[8]. mPADs gave the possibility to study with sub-cellular spatial resolution. (du Roure et al. 2005, Zhao et al. 2006). A similar system was proposed by Li et al. (2007). They, however, calculated the post bending forces numerically using finite elements algorithms.
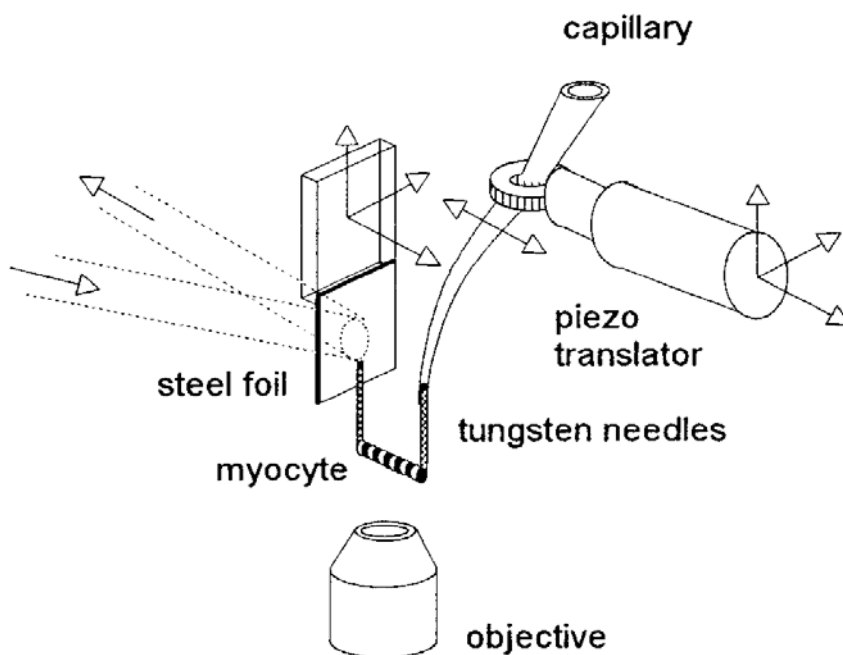
Fig. 1-H Experimental setup of Tasche and coworkers (1999), used to study forces of single cardiac myocytes. A myocyte was spanned between two tungsten microneedles. One of the needles could be moved with the help of a piezotranslator; to another one a steel foil, serving as a mirror, was attached. A laser beam, reflected from the foil, helped to monitor myocyte contractions.

---

[8] The relevant aspect of elasticity theory is discussed in detail in section 2.3 MODELLING OF ELASTICALLY ANCHORED PILLARS.
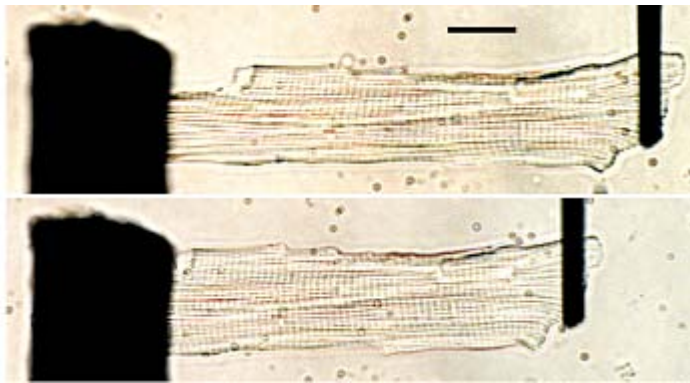
Fig. 1-I Single myocytes held between a pair of carbon graphite fibres. Bar = 20 μm. (Yasuda et al. 2001).

1.3.1.5. MEMS

Yet another method is based on microelectromechanical systems (MEMS) technology (Lin et al., 2000; Tan et al., 2003). A myocyte was clamped between polysilicon plates, attached in turn to flexible polysilicon beams (shown in Fig. 1-K). Upon myocyte contraction, the beams bent and the change of cell length was optically determined. The force was estimated from the displacement magnitude and the beams' spring constant.
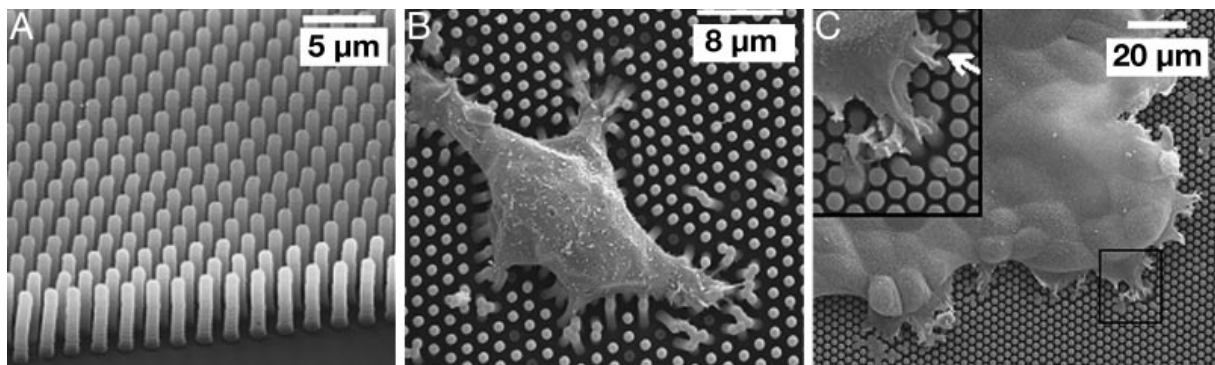
Fig. 1-J Closely spaced posts microfabricated by PDMS elastomer moulding. A) The regular array of microposts. *B*) Single cells lying on the bed of microposts. Post deflection is clearly visible. *C*) A cell monolayer. A magnified view of the area is shown in the upper left corner. Cells spread only on top of posts. (After du Roure et al. 2005).
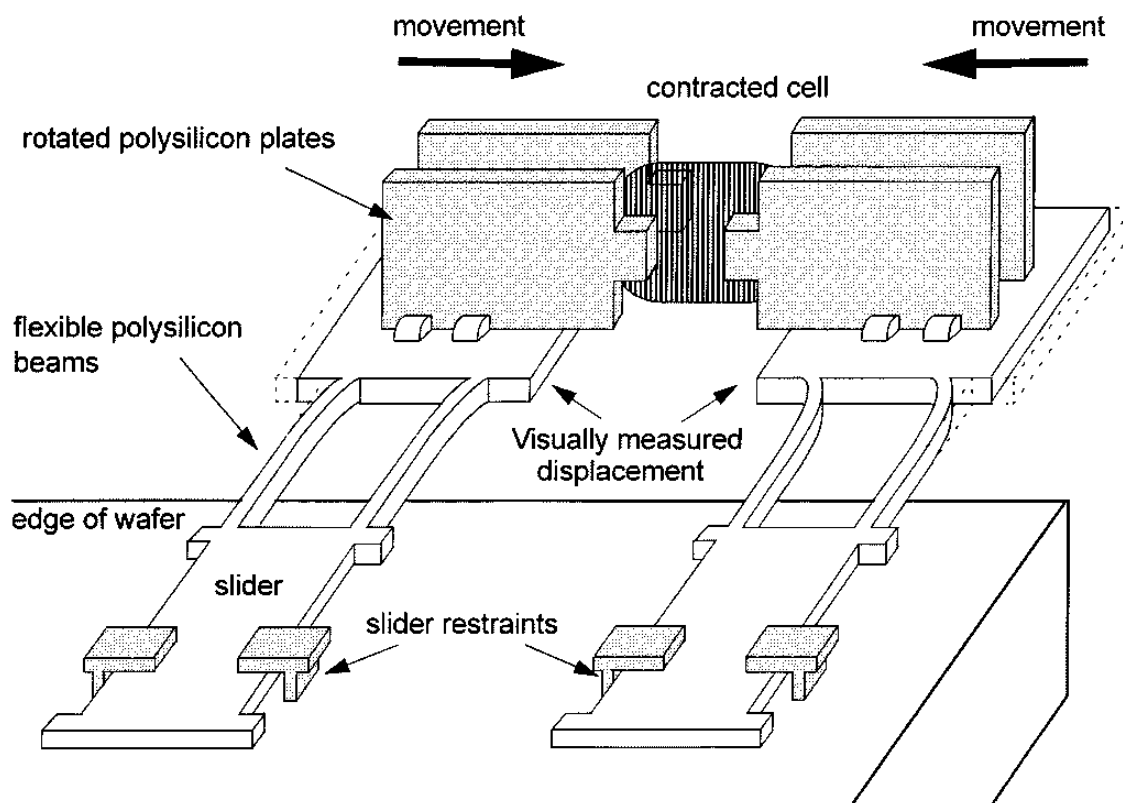
Fig. 1-K Schematic diagram of a MEMS micromachine. The cell was clamped between the four plates, attached to compliant microbeams. Displacements caused by the cell were optically measured. (after Lin et al. 2000).

In all the devices described above, the cells were placed on a flat or quasi-flat substrate. Since *in vivo* cells experience substantially more complex, three dimensional surroundings, three dimensional force microsensors were also explored most recently.

1.3.2. THREE DIMENSIONAL MATRICES

The need of studying cellular behaviour in as much as possible biomimetic conditions lead to creation of various three dimensional substrates for cells. These were meshes or 'sponges' either obtained from natural tissues by removing their cellular components (Pizzo et al. 2005, Roy et al. 1997) or made of different polymers: proteins like collagen (Sheu et al. 2001), biodegradable polymers and alginates (Ma et al. 2005) etc. Various matrix types are shown on Fig 1-L. A combination of patterned elastomer substrates with collagen meshes was also used (Norman et al. 2005). Norman and colleagues embedded a pattern consisting of

rows of parallel grooves into a collagen matrix, forming a complicated, three dimensional environment. The idea of the experiment was to combine the aligning properties of grooves with a quasi-natural mesh of collagen.

The cells may be then positioned in the matrix by simple seeding, mixing with the liquid prepolymer, 'planting' with the help of micromachines or 'steered' by chemical and mechanical gradients, depending on the scaffold structure and use (Curtis and Riehle 2001). Cellular forces could be estimated by measuring the displacement of matrix fibres or fluorescent labels embedded into the mesh.

There were, however, few experiments which estimated forces cell exert on meshes (Roy et al. 1997).
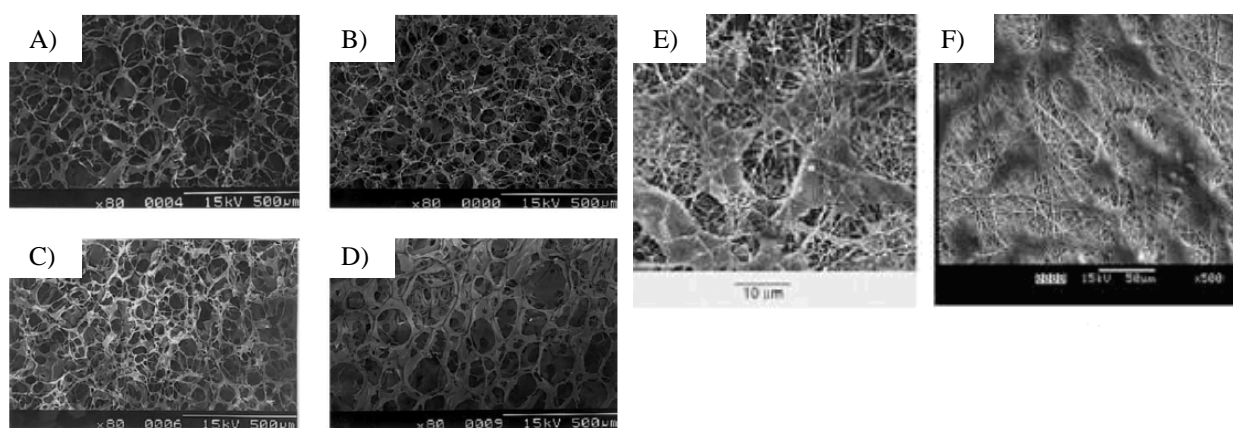
Fig. 1-L 3D matrices A) – D) SEM photographs of collagen matrices crosslinked with various concentrations of glutaraldehyde (After Sheu et al. 2001). E) and F) Similarity between native ECM protein structure and polymeric nanofibre matrix. E) Fibroblasts cultured on collagen fibrils of rat cornea; F) endothelial cells cultured on nanofibre matrix (after Ma et al. 2005).

1.4. ADVANTAGES AND DRAWBACKS OF CELLULAR FORCE MEASUREMENT SYSTEMS

Since numerous devices exist to measure cell forces the following questions arise. What are the differences between them? Why should we work on yet another one?

The first set-ups consisted of thin elastic films which wrinkled under the application of mechanical force. This system was quick and easy to produce; however, no quantitative information about the forces could be obtained. As the next approach, patterned elastomer surfaces were created. This approach demanded a far more complex experimental set-up as it required sophisticated software and microtechnologies but it enable both force directions and magnitudes measurements. However, force calculation is complex and time-consuming, as the deformations caused by an isolated force at one single point spread all over the whole

substrate. Moreover, the flat substrates induced morphological and biochemical changes in the cells on them. Thus cell behavior on flat elastomer films might not reflect physiological processes. Cell morphology does change dramatically in response to substrate geometry, even if chemical and mechanical properties of the substrate remain unchanged. Thus, results obtained with the help of flat geometry systems may not be transferable to cells *in vivo*. For example, tissue formation requires proper substrate geometry and usually cannot be observed in flat geometry experimental systems (see chapter 1.2 CELLULAR BEHAVIOUR VS. MECHANICAL PROPERTIES OF THE ENVIRONMENT for detailed information).

To avoid the problem of complex force vector calculation, set-ups enabling discrete force measurement were built, for example microfabricated post-array detector (mPADs) and microneedle systems. Critics of those set-ups point out, however, that both mPADs as well as microneedles form a highly unnatural environment for cells. Actually, its geometry is practically flat and does not differ much from geometries of previous systems. This is because the micropost dimensions are small. In the work of du Roure et al. (2005), the micropost diameter varied from 1 to 2 µm, the micropost height was 3-8 µm and the lattice constants of post array were in the range of 2-4 µm. Li et al. (2007) used microposts of 2 µm diameter, 6 µm height and with a lattice constant of 4 µm. Therefore, mPADs geometry, being specific and unnatural, may influence cellular behaviour considerably as the area of the adhesive spots on the substrate alone is already able to decide the cell fate (Discher et al 2005, Chen et al. 1997, Curtis and Wilkinson 1997).

Sponges and meshes, on the other hand, offer a highly biomimetic environment. Not only are they three dimensional, they also form complex nets of fibres, resembling the ECM most of all the systems described. However, quantitative analyses of those systems are problematic. First, microscopic observation of thick samples is difficult, as most of meshes are non-transparent. Second, in the case of meshes obtained from natural proteins, a phenomenon of mesh reorganization occurs in the matter of hours – the cells tend to actively rearrange mesh fibres. Even if the mesh is isotropic at the beginning, it becomes highly anisotropic under the influence of cells, which potentially leads to serious errors during force calculation. Third, even if the mesh remains homogenous as a whole it may exhibit local anisotropy of the network stiffness or the fibre direction. Those anisotropies may exist on small scales (µm range) only but could be sensed by the cells triggering a physiologically appropriate response and influencing cellular behaviour in the network. For the same reason – local anisotropy – displacement of markers, embedded into the mesh cannot be considered a reliable way to calculate cellular forces. Still, it may be a useful tool to study cell migration and ECM reorganization phenomena.

Another category of force measurement devices seems to avoid all the problems mentioned above. To this group belong microcantilever and magnetic bead devices, as well as MEMS. Here, the myocyte, contracting, deflects a carbon fibre, a microcantilever or moves a

small bead. The geometry of the systems is simple and well known, force magnitude calculation is easy and theoretically well founded. No such phenomena as mesh anisotropy come into play. Still, the cell is placed in an extremely unphysiological environment which may affect its behaviour considerably. What is more, the myocytes are actually lacking any substrate here, one cannot study such cellular phenomena like reaction to microtexture or stiffness of the environment which could be studied by micropatterned substrates or meshes, for example. Also, only strongly contracting cells may be used. There are also more serious problems occurring. As the authors of the method admit themselves, the system may be cantankerous and requires a lot of practice to handle. This is because the myocyte must be somehow attached to the system. It requires a lot of manipulation and the usage of an adhesive. The adhesive, however, may affect the cell membrane and as the result the whole cell in an unknown way. The problem can be diminished by using an ECM protein instead of an adhesive.

Another problem is cell excitation. It is necessary to excite the cell with the help of electric pulse or calcium ions. Therefore, for example cell natural frequencies cannot be studied (as the external trigger commands the pace). Also, artificial excitation may affect contraction amplitude. To our best knowledge this possibility has not been investigated yet.

The main advantages and disadvantages of various measurement set-ups are collected in Table 1-1.

Most of the techniques share the drawback of unnatural geometry. This is a common gravely negative aspect. As discussed in detail in section 1.2 CELLULAR BEHAVIOUR VS. MECHANICAL PROPERTIES OF THE ENVIRONMENT, geometrical and mechanical properties of the substrate have an tremendous effect on various cellular processes. Thus, geometry influences on myocyte contraction cannot be ruled out. Just the opposite, such influences are to be expected. On the other hand, the only *in-vivo* like system, namely 3D matrices, possesses numerous, hard to control parameters. Also, force measurement is only qualitative there.

Rather than reanalysing the existing cellular force data from various discussed methods with more realistic elastomechanical theoretical models we decided to create a new, precisely tailored micropillar array substrates for cellular force measurements. For such systems micropillar deflection can be easily modelled and the force magnitudes precisely evaluated. Inspiration for a particular technical solution employed here came from work of du Roure and coworkers (2005) and Yasuda and coworkers (2001). Du Roure et al. cultivated the cells on top of a layer of elastomeric microposts and, by measuring post deflection, estimated cellular force magnitude. Yasuda et al. attached a contractile cell between two microfibres and again used fibre deflection to calculate the forces in question. Our idea was to combine the two approaches. As in the experiments of du Roure et al. cells would be grown on an elastomeric surface with a regular **array of micropillars.** However in contrast to this work,

the micropillar dimensions and distances between them would suffice to let the cells adhere not only on pillar tops, but also along the full length of the micropillars and in-between.

Such a geometry mimics pretty well a normal tissue where cells are located between other cells and ECM fibres. It provides the cells with a variety of environments to choose from, too. Most important for the present study, the cells adhered to the micropillars and bend them upon contracting. This process can be optically monitored. The measured micropillar deflections are the bases for a calculation of cell forces. However, appropriate theoretical elastomechanical model needs to be determined first.

Typical micropillar arrays consisted of rows of pillars about 25 μm tall and 10 μm in diameter. The elastomer pillars resided on a layer from the same elastomer with a thickness of tens of micrometers. The elastomer layer rested on a glass coverslip (see Fig. 1-M). In the present study crosslinked *PDMS* elastomer (silicone rubber) was chosen as elastomer because it was proven to be suitable for cell force measurements (for more information about *PDMS*, see Appendix B).

The work of Cesa et al. (2007) served as a rich source of ideas. Cesa created micropatterned *PDMS* elastomer surfaces to measure cardiac myocyte contraction forces. The following procedures of Cesa were used in this work:

- *PDMS* elastomer calibration method (see Appendix B)
- Preparation of *PDMS* elastomer substrates for cell seeding 1.6.2 THE MICROPILLAR SUBSTRATE and 1.6.3 PREPARATION OF *PDMS* ELASTOMER SUBSTRATES FOR CELL SEEDING

The use of the equations for the bending of a rigidly clamped beam as used in earlier works was out of question (see for example Fig. 1-N). The model adopted in this work, referred to as 'elastically anchored pillars' is due to Rudolf Merkel and takes into account the softness of the pillar anchoring to the substrate.

Table 1-1 Comparison of cell force measurement devices.

Device	advantages	disadvantages
Thin films	Easy to make	Flat Only qualitative results
Patterned substrates	Measurement of force magnitude and direction is possible	Flat Complicated evaluation algorithm
Microcantilevers, microneedles	Easy force measurement	No cell-substrate interaction A lot of cell manipulation Highly artificial cell environment Cells have to be stimulated to contract
mPADS	Easy force calculation	Flat, very specific geometry Classic equations lead to force overestimation
3D matrices	Biomimetic environment	Only qualitative measurement possible Many uncontrolled matrix parameters Matrix reconstruction by cells
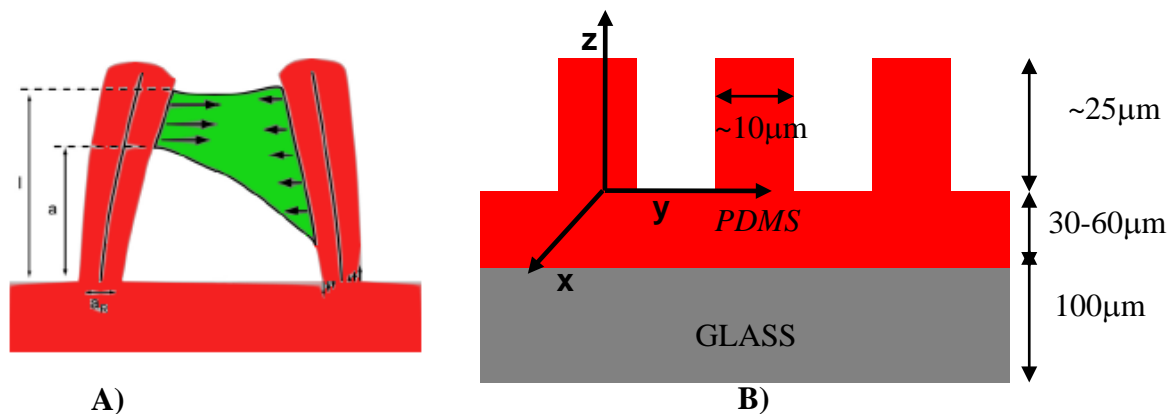
Fig. 1-M The basic features of the micropillar system. A) Two micropillars (red) connected by a cell (dark green). Cells apply transversal tensions (bold arrows) to both pillars (neutral axes depicted). The torque acting on each pillar is balanced by normal tensions within the pillar, depicted for the right pillar. Note that pillar diameter is not constant – they widen slightly. B) Main dimensions of the system. As micropillar diameter and height varied slightly from substrate to substrate, the typical values are given. Further shown are the coordinate system and the geometrical parameters of the pillars.
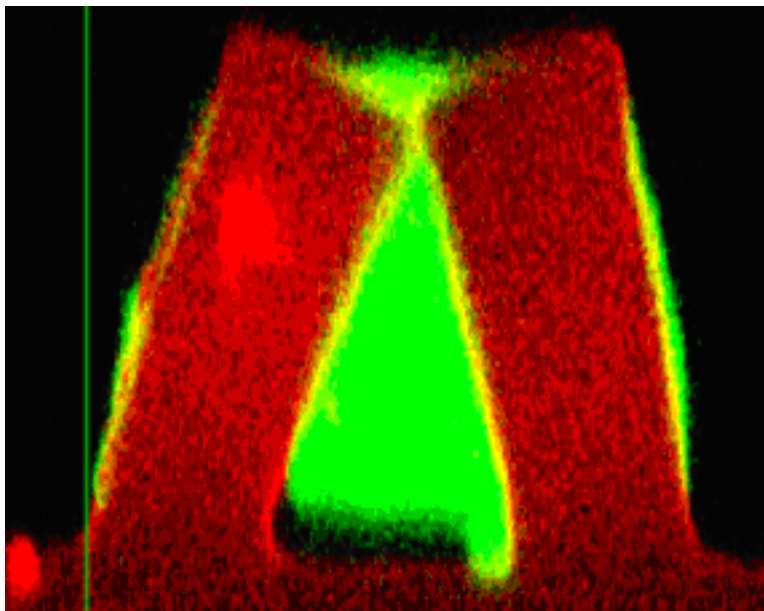
Fig. 1-N Micropillars bent by a cell (CLSM scan, cell dyed with calcein and pillars with DID). A cell is shown in green and pillars in red. The green line shows the direction perpendicular to the surface. The pillars are not rigidly clamped. Micropillar diameter is approximately 10 μm.

1.5. MICROPILLAR ARRAY SUBSTRATE

Three micro-lithography techniques were used to create the micropillar elastomer substrate for cells:

- **Electron beam lithography (EBL)** is a method of 'drawing' with a beam of electrons. It allows creation of submicrometer-sized features but tends to be slow (see Appendix C).

- **Optical lithography (**also called **photolithography)** is a method of transferring, by means of optical methods, the pattern from a photomask to a photoresist layer deposited on the wafer surface. It is much faster and cheaper than EBL[9] and allows many wafers to be produced from one photomask (see Appendix C).

- **Micromolding** (**Replica molding)** is a soft lithography technique. It is called 'soft' because it uses elastomers i.e. soft, elastic polymers. It is often applied in life science where harsh or toxic chemicals, UV or X-ray radiation and high temperatures cannot be used.

The main steps of photolithography and replica molding techniques, applied in this work, are shown in Fig. 1-O.

1.6. PROCESSING TECHNOLOGY FOR MICROPILLAR ARRAYS

First, a photomask had to be designed and prepared. Although photomask preparation is a standard process, widely used in microchip industry, each mask must be tailored to fit the needs of the user. Also, as mask creation is an expensive process, it was important to create the final version of the mask in as few trials as possible. In our case, the following requirements had to be met:

1. A square pillar shape was chosen to simplify the design process and the actual electron beam writing. (Had we used circles instead of squares, the required program

---

[9] The difference between EBL and optical lithography is that EBL is a serial technique (features are written one after the other) while optical lithography is parallel (all features written at the same time.) Therefore EBL is always much slower than optical lithography.

would exceed processor and memory capacities as circles must be replaced by tiny trapezoids which would require substantial computation power for EBL[10]).

2.   As no prior information about cellular behaviour on the planned micropillar topography was available, a wide range of inter-pillar distances were chosen for the experiments: every single cellular substrate contained eight areas (marked with different colours in Fig 1-P) of different inter-pillar distances, see Table 1-2.

3.   Two types of squares were written on the mask with 10 x 10 and 5 x 5 μm side length denoted group I and II respectively in Fig 1-P, offering an unique possibility to study cellular behaviour in chemically uniform but topographically different environment.

Once the pattern had been developed, the mask was a pattern of non-transparent squares drawn on a quartz glass plate by EBL.
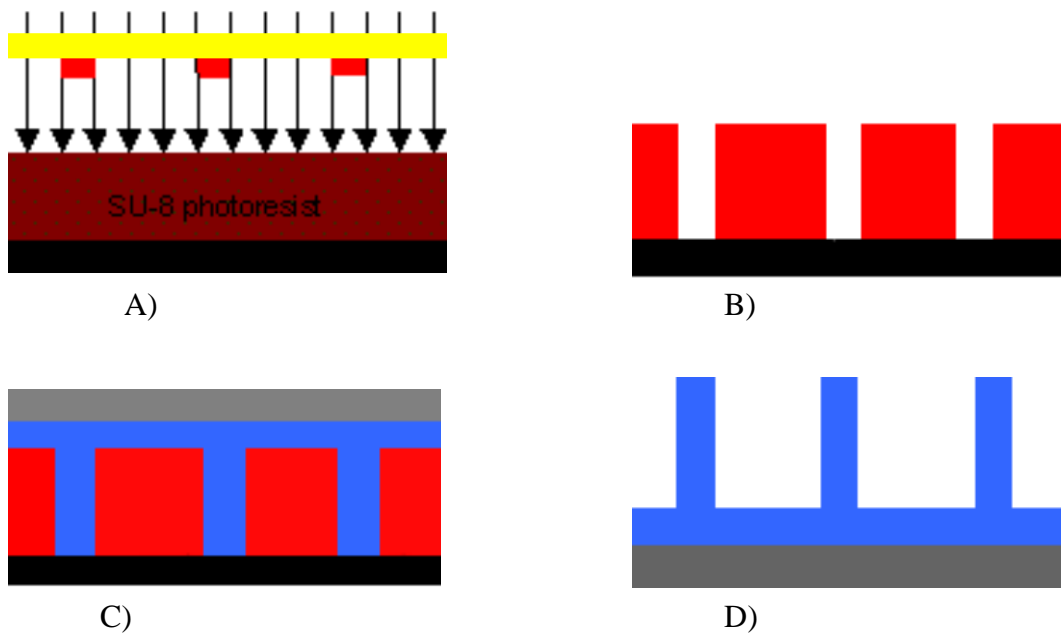
Fig. 1-O The main steps of micropillar array preparation. A) An uncured photoresist layer (brown) rests on a wafer (black) and is irradiated by UV light through a photomask (yellow). The chromium pattern (red) blocks some of the light and is transferred into the resist. B) The cured photoresist (red) is developed i.e. its irradiated parts are washed away. C) A prepolymer (blue) is filled into the photoresist structure and cured with a cover slip (grey) on top. D) The microarray is separated from the photoresist master.

---

[10] Mona Nonn, personal communication

Table 1-2 Lattice constants (LCs) of the groups I and II shown in the figure above. To guarantee environment variability, LCs cover the range from 15 to 110 μm.

Symbol of the region	Lattice constant (μm) – group I	Number of rows group I	Symbol of the region	Lattice constant (μm) – group II	Number of rows group II
Ia	20	70	*IIa*	15	80
Ib	25	50	*IIb*	20	60
Ic	30	40	*IIc*	25	50
Id	35	35	*IId*	30	40
Ie	45	25	*IIe*	40	35
If	60	20	*IIf*	55	25
Ig	80	15	*IIg*	75	15
Ih	110	12	*IIh*	105	12
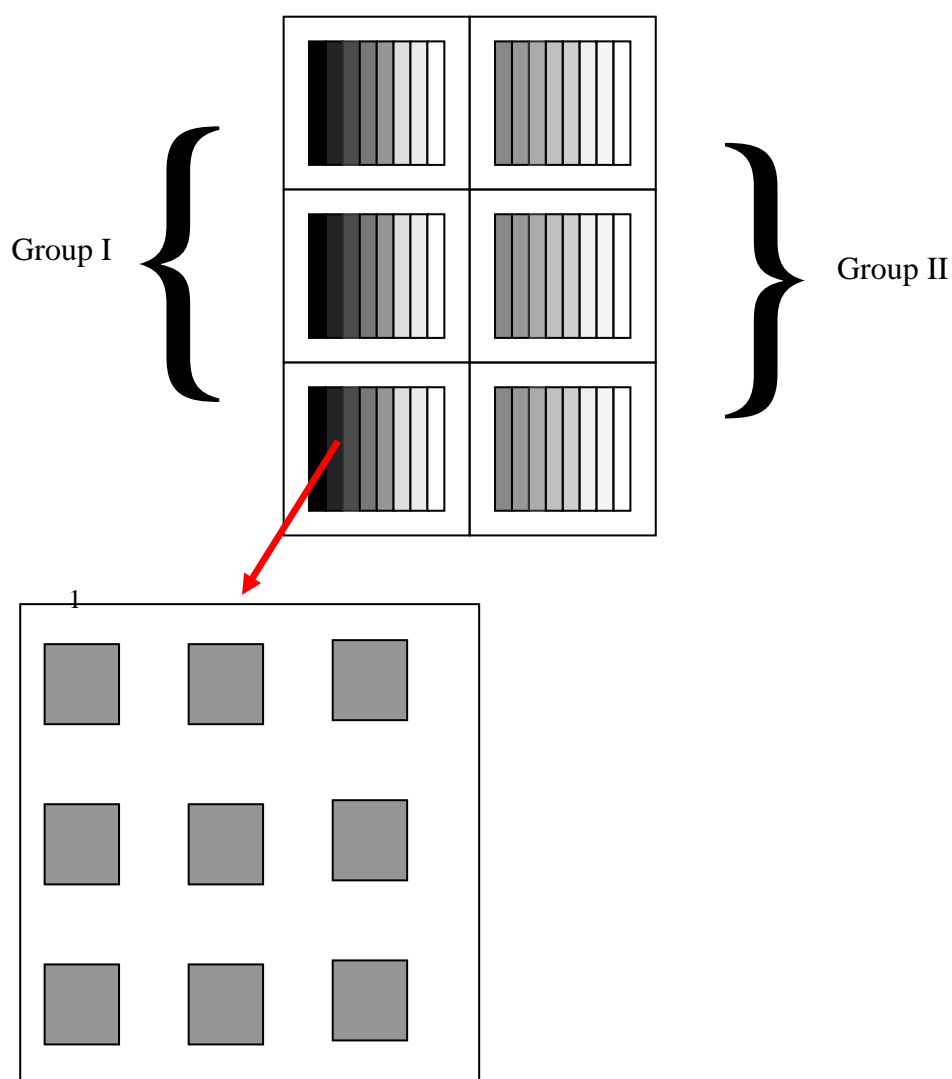
Fig. 1-P A scheme of the mask used in this thesis. Six masters can be prepared simultaneously to reduce the time necessary to produce the masters. Each master consists of a regular pattern of squares, of 10 or 5 μm side length in group I and II[11], respectively. There are eight regions on each wafer; differing solely in inter-pillar distance (see Table 1-2).

---

[11] However, the group II micropillars has never been used in further experiments, see APPENDIX C, chapter ALTERNATIVE MICROARRAY PREPARATION PROCEDURES.

1.6.1. THE MASTER

The mask pattern was transferred into photoresist which was in turn used as **master** for the micropillar structure. A layer of a photosensitive material (SU-8 photoresist, see Appendix B) was deposited on the silicon wafer. The mask was secured atop of the layer and the photoresist exposed to UV light through the mask. The height of the future micropillars (25 μm) was defined by the thickness of the photoresist layer. The regions of photoresist covered by the non-transparent elements of the mask remained unaffected, while the rest got irradiated. The unaffected part of the photoresist was then removed, leaving behind a 3D structure of holes in the resist.

The master preparation is described in detail in Appendix D. In summary, the main process parameters were as follows:

1. Silicon wafer pre-treatment: 180°C, 10 min.
2. Spin-coating of *SU-8* photoresist: 2000 rpm
3. Pre-exposure bake: 90°C, 5 min
4. Exposure time: 25 s
5. Post-exposure bake: 90°C, 30 s
6. Development ~ 6 min.
7. No hard bake

The quality of the masters produced in this process is shown in Fig. 1-R. The masters were broken in half and mounted onto scanning electron microscopy (SEM) stubs, gently blown with nitrogen to remove splitters and dust, and subsequently sputtered with gold. Scanning electron microscopy (Gemini 1550, Carl Zeiss, Jena, Germany) was performed at 10 kV at a 20 degree angle. The microchannels reached through the whole photoresist layer and were rectangular in shape, see Fig. 1-Q. To facilitate separation of the micropillar substrate from the master, the master surface was covered with silicone repellent layer from silane prior to the use.

A)

B)
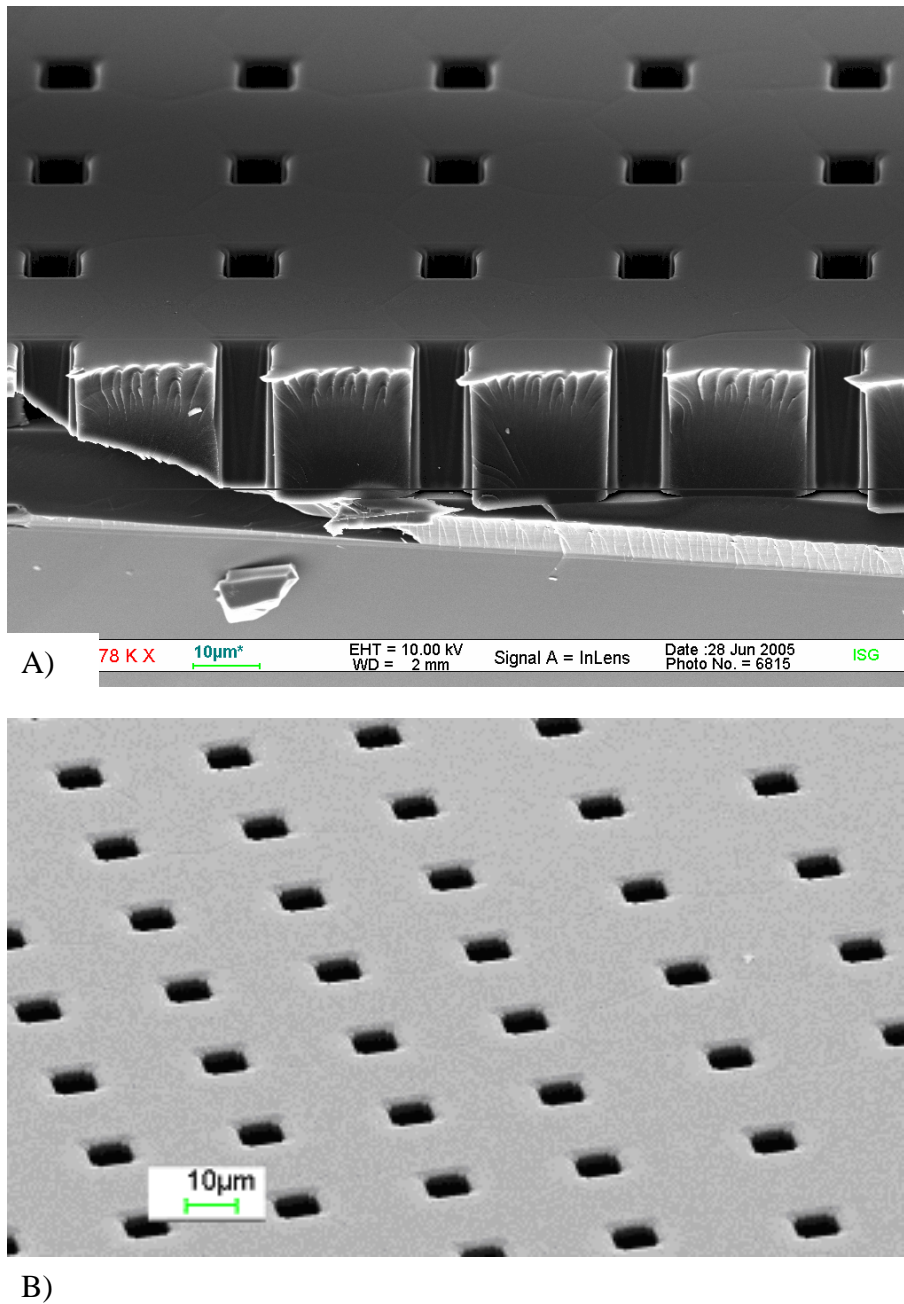
Fig. 1-Q *SU-8* **layer with microhole structure. A) The master was broken to visualize the microholes. Cracks are artifacts, formed during breaking. B) Rounded corners of the microholes. The border between stripes of different lattice constants visible.**

1.6.2. THE MICROPILLAR SUBSTRATE

The poly(dimethylosiloxane) *(PDMS)* prepolymer was used as micropillar substrate material. The *PDMS* prepolymer was prepared by mixing polymer base and cross-linking agent at a predefined ratio. A tiny droplet of the prepolymer mixture was dispensed directly on the photoresist structure. It was too viscous to spread by itself, therefore spreading was encouraged with a nitrogen stream. Low amounts of prepolymer had to be used to prevent the mixture from flowing over the edges of the master which would lead to non-uniform *PDMS* elastomer thickness. Also, the excess of cured *PDMS* elastomer would glue the coverslip and the microslide together, making their separation difficult. The masters with *PDMS* on top were subsequently put into an desiccator and degassed with a pump[12] for about 30 min to remove air bubbles trapped in the prepolymer during mixing and to enable the mixture to flow into microholes. Glass spacers were placed on the sides of the master to ensure repeatable *PDMS* elastomer layer thickness base, see Fig. 1-R. As *PDMS* elastomer thickness was of decisive importance for CLSM microscope examination, very thin, 80 μm coverslips were used as spacers. The *PDMS* layer was carefully covered with a coverslip. It was essential not to trap air bubbles between the glass and the prepolymer. 80 μm coverslips were also tested as cover of the *PDMS* layer. They, however, tended to bend and break very easily. To avoid coverslip bending and breaking, a piece of microslides were placed on the coverslips. The whole 'sandwich' was then fixed with 2 paperclips. To avoid bending of the coverslip, they were carefully positioned to exert pressure only on the spacers, not on the space between them. The *PDMS* was cured overnight (for 16 h) at 60°C.

Separation of the *PDMS* elastomer substrate from the *SU-8* master is a difficult task despite the silicone repellent layer from silane placed between the *PDMS* elastomer and the master. In this process the *PDMS* elastomer layer often is ripped and remained stuck to the glass or the thin coverslips cracked. The problem was essentially solved by injecting a small droplet of 2-propanol (using a syringe with a thin needle) between the *SU-8* master and the cured *PDMS* elastomer substrate. Afterwards, glass and master were carefully pulled apart (see Fig 1-S; Cesa 2007).

---

[12] Any type of vacuum pump suffices. One can simply estimate the time of degassing by observing the *PDMS* surface: it should be degassed till no air bubbles are visible.
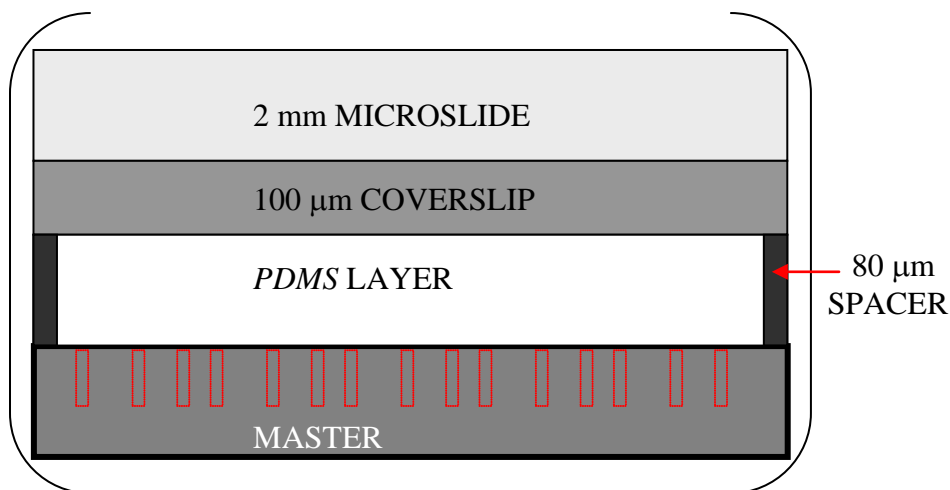
Fig. 1-R Scheme of the set-up used to create *PDMS* elastomer substrates. Not to scale.

A) B)
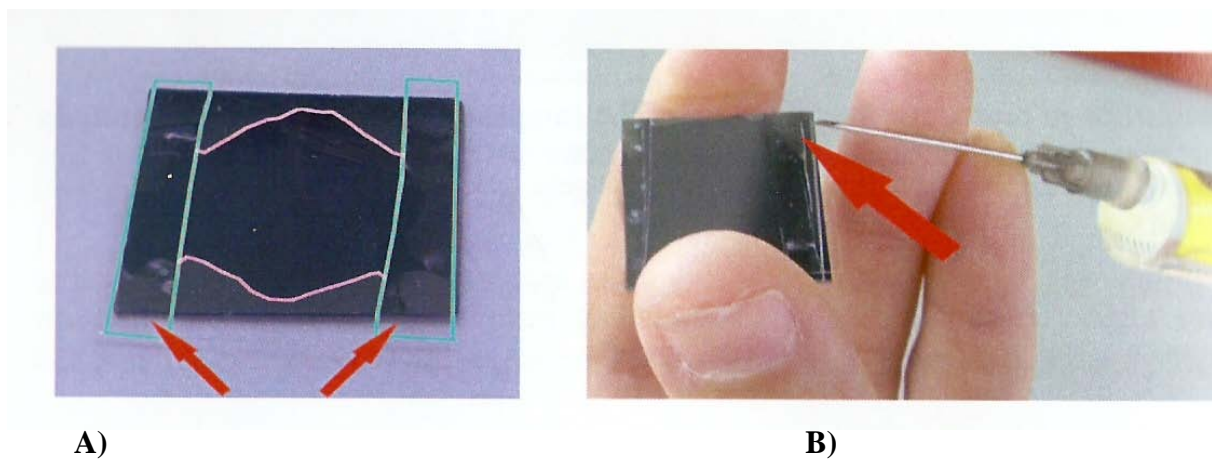
Fig. 1-S Separation of the *PDMS* elastomer substrate from the master. A) The substrate after curing, still attached to the master. Spacers are marked with blue lines, the outline of the *PDMS* elastomer with magenta lines. B) A droplet of 2-propanol was used to facilitate *PDMS*-master separation. Pictures taken from Cesa (2007).

The quality of the micropillar substrate was characterized with the help of SEM and CLSM. Pillar geometry varied as both the pillar diameter and its cross-section shape differed slightly from pillar to pillar. In general, pillar width increased to some extent with height. Their cross-sectional shape was practically square at the pillar base and rounded substantially with height, see Fig 1-T and 1-U. Such shape imperfections are common for structures moulded in soft elastomers and created in thick photoresists.
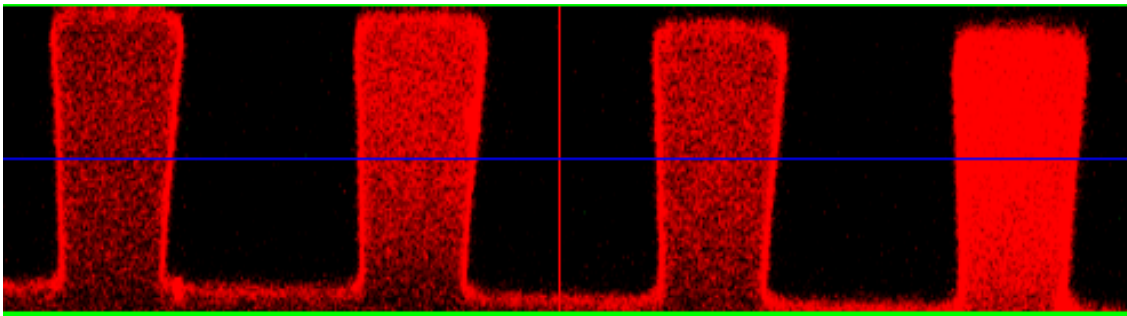
A)
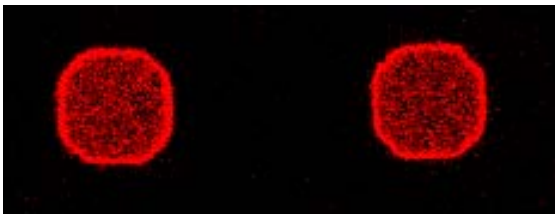
B)
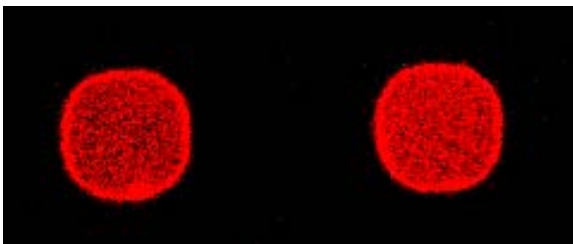
C)

Fig. 1-T CLSM scan of stained micropillars (red). A) seen from the side. The pillar shape is slightly conical, widening with pillar height. The red, green and blue lines originate from CLSM display program. B-C) Change of the pillar cross section with height. B) A pillar cross-section taken 2 μm above the substrate. C) A cross-section of the same pillar taken at a height of 12 μm. A micropillar is about 10 μm wide in diameter.
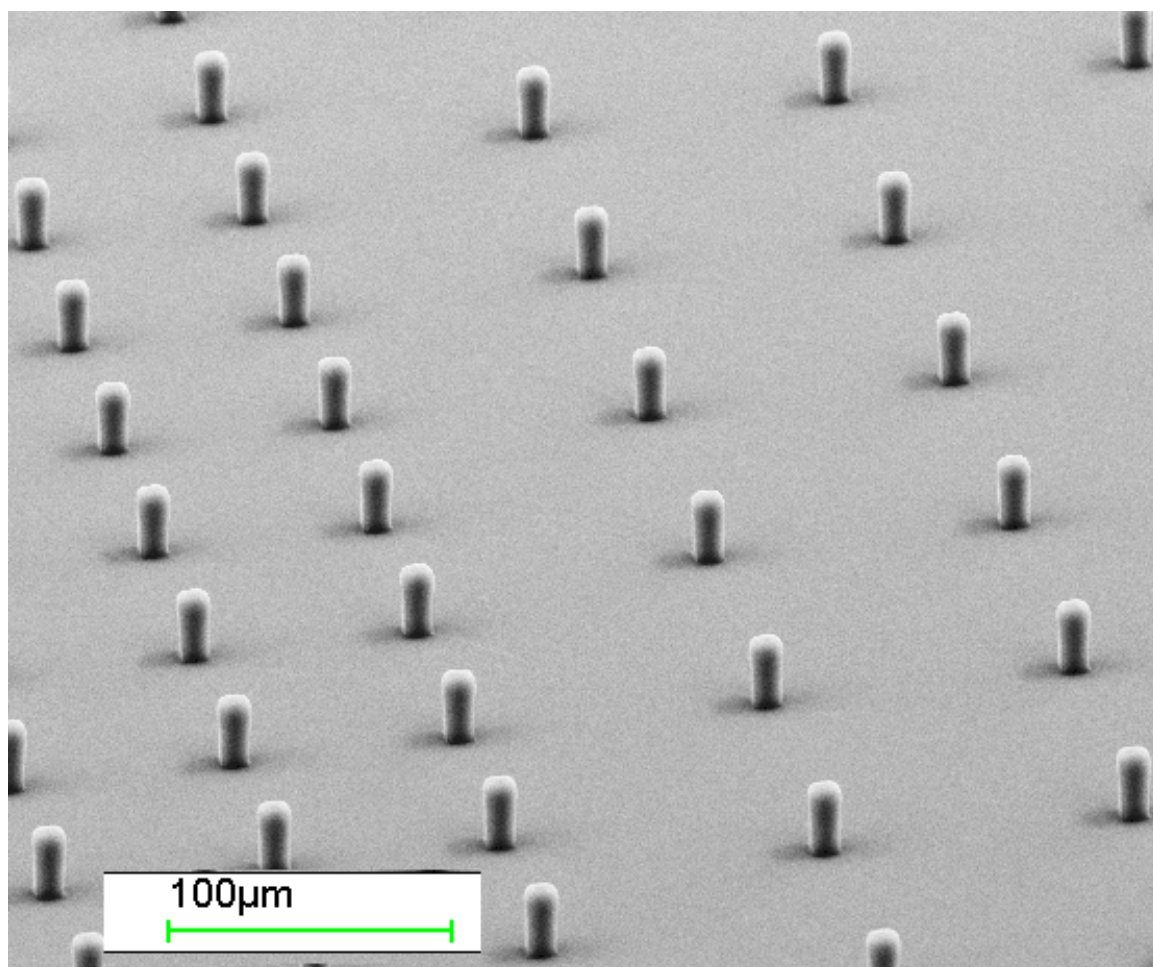
Fig. 1-U *PDMS* **elastomer micropillars, prepared from base material and crosslinker in 10 : 1 ratio seen under SEM. Note the difference between regions with two different lattice constants.**

The mechanical properties of the micropillars depended strongly on the *PDMS* prepolymer composition. We found that *PDMS* elastomer micropillars, prepared from base material and crosslinker in 20 : 1 ratio, collapsed when dried so keeping the substrates in liquid at all time was crucial to avoid micropillar bending and clumping. For that reason, softer *PDMS* elastomer substrates were immersed into 2-propanol immediately after separation from the photoresist master. That ensured both substrate sterility and served to support the delicate micropillars. First several substrates were examined under CLSM (see Figs 1-T and 1-V. This procedure was later replaced by a wide field microscope examination, as difference between tall, properly formed micropillars obtained from well-formed masters and the short 'stumps' obtained from poor ones could be easily spotted this way. 'Proper' micropillars, seen from above, were visible as regular rows of squares with sharp contours while the 'stumps' showed up as fuzzy, small dark patches. The main advantage of the optical

microscope examination was that it did not require substrate staining so that the tested substrate could be subsequently used for cell cultivation.
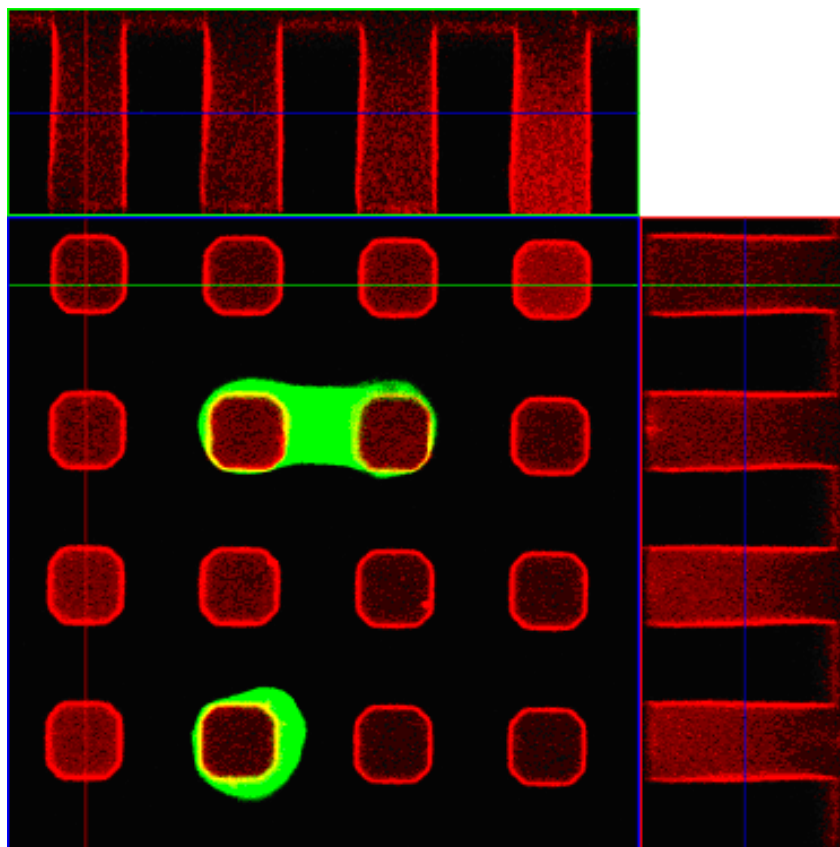
Fig. 1-V CLSM image of micropillars (red) and cells (green). The pillars are slightly rounded in cross-section and barely conical in shape. A micropillar is about 10 μm wide in diameter.

1.6.3. PREPARATION OF *PDMS* ELASTOMER SUBSTRATES FOR CELL SEEDING
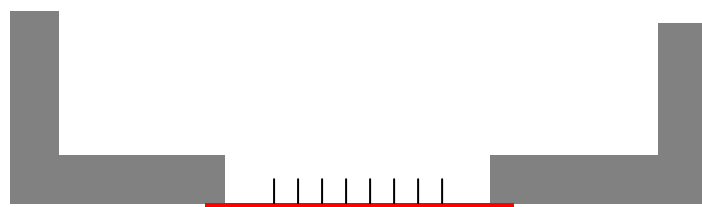
A)
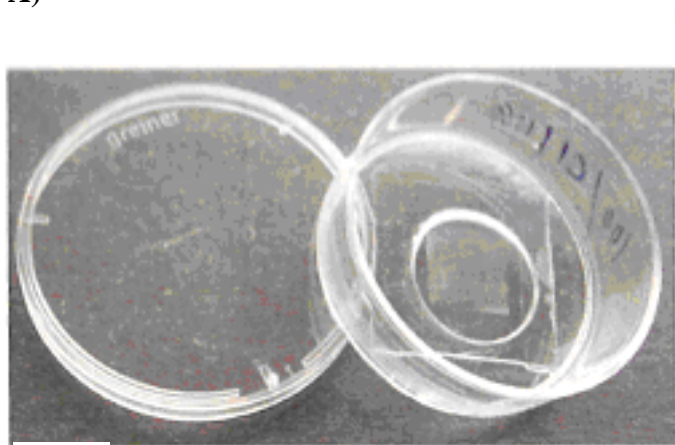
B)

Fig. 1-W *PDMS* elastomer substrate mounted on a Petri dish. As substrates with micropillars could not be dried, a similar substrate from Cesa (2007) is shown here. Petri dish diameter is 22 mm.

After verification of substrate quality, 2-propanol was replaced with sterile, distilled water under laminar flow cabinet; the washing step was repeated several times to get rid of all traces of alcohol. To enable cell seeding and CLSM examination, we essentially followed the technical solution proposed by Cesa (2007). The substrate was secured with *PDMS* (prepared from base material and crosslinker in 20 : 1 ratio) as glue at the bottom of a 22 mm plastic Petri dish with a round 15 mm hole in the center, see Fig 1-W. The *PDMS* glue was applied to the bottom of the dish with a plastic stick. The substrate was taken out of the water and quickly pressed on the glue. The Petri dish was put, bottom down, onto a screw nut (about 2 cm in outer diameter) to avoid uncontrolled sticking of the Petri dish and filled with sterile water. Leakages could be stopped by adding more glue as *PDMS* adheres even on wet surfaces. To prevent water evaporation, covers was put on the Petri dishes before the glue was cured for 90 min. at 60°C. Subsequently, water was replaced, again under laminar flow

cabinet, with *PBS* (phosphate buffered saline solution); later the substrates were checked again under wide field microscope for micropillar clumping. If the gluing was done sufficiently fast no damage occurred.

1.7. STUDY OF CELL-MICROPILLAR COMPLEXES

1.7.1.   CELL SEEDING

Before cells were seeded on the silicone rubber, *PDMS* elastomer surfaces were **stained** by immersing in 5 μl/ml DID cell-labeling solution and incubation at 37°C over the weekend. Subsequently, the surfaces were coated with fibronectin to enable cell adhesion. 300 μl of 10 g/ml fibronectin solution in *PBS* were used for this purpose. Fibronectin solution was left on the *PDMS* elastomer surfaces for 30-60 min at 37°C to allow protein adhesion.

In order to verify whether the protein covers the whole *PDMS* elastomer surface uniformly, some micropillar arrays were covered with a fluorescence-labelled[13] protein layer instead and a fluorescence CLSM scan of the substrate was taken. We found homogeneous fluorescence over the whole microarray surface, confirming uniform coverage of the whole *PDMS* elastomer array.

Prior to cell seeding the surfaces were washed with sterile *PBS* in order to remove unbound protein molecules. The cells were obtained from rat embryos using standard procedures (see Appendix D).

Freshly isolated cells were placed on the dishes (50 000 cells/dish) and incubated at 37°C and 5% CO_2. The cells were examined starting from the 2nd day after seeding for the whole week (the oldest cells were 6 days old). Cell medium was exchanged every two days. Before examination, the cell medium was exchanged to remove unadhered cells.

Examination of the micropillar substrate deformation by the cells was performed with a CLSM microscope. The cells had to be microscoped at 37°C in 5% CO_2 atmosphere, otherwise they would stop beating. For this purpose, the CLSM microscope was equipped with a heating unit and a chamber which kept the atmosphere constant. Both temperature and carbon dioxide concentration could be changed on demand; a humidifier ensured the required humidity.

---

[13] Labeled protein molecule has a small fluorescent group attached. Measuring the fluorescence intensity allows then to estimate labeled protein concentration.

1.7.2. CLSM IMAGING

Two types of scans were performed:

- A high frequency scan in a single plane to 'capture' cell dynamics (to film beating). The scan frequency was about 10 pictures/s.
- A high resolution three-dimensional scan to examine cell morphology. The whole scan lasted 20-30 min. Individual pictures were taken each 0.25 – 0.36 μm in height.

For both types of scan, LCI PlanNeofluar 63x/1.3Ph3 objective was used. To visualize the micropillars, 543 nm laser line with LP 560 filter was used and to visualize the cells – 488 nm line with LP 505 filter. The microscope was LSM510 with Axiovert 200M as microscope body, Carl Zeiss, Jena, Germany.

Cells for studies were selected with phase contrast microscopy (Carl Zeiss, Jena, Germany). Only beating cells attached to two micropillars were selected. Cells adhering to one or more than two pillars were disregarded. Also, cell clusters were excluded from measurements. Micropillar bending was determined at a CLSM focus position 15 μm above the base of the pillars in fluorescence mode. A few samples were imaged at a height of 20 μm. The index of refraction of the immersion fluid (65% glycerol in water, refractive index of 1.41) was not matched to the cell culture fluid (refractive index of 1.338) but with the refractive index of *PDMS* rubber[14]. Thus the real height of scanning was by a factor of 1.41/1.338 higher. Image sequences were taken at time intervals ranging from 0.1 s to 0.17 s using the yellow HeNe laser (543 nm) and a 560 nm long pass filter. LCI PlanNeofluar 63x/1.3Ph3 objective was used. Laser power varied from sample to sample and it was always kept as low as possible to diminish cell damage.

Subsequently, cells were stained with calcein (1 : 200 in F10 Ham's medium, Invitrogen, Carlsbad, CA) which was added to the medium for 10 min at 37 °C. The dye diffused into the cell, staining the whole cell body with exception of the nucleus. After washing twice with *PBS* solution, the medium was replaced with minimal essential medium supplemented with 10% fetal bovine serum (*FBS*, Sigma), penicillin and streptomycin (Penstrep, Sigma) and *ITS* supplement (Sigma). Calcein stains living cells and had no obvious effect on cell morphology and behaviour besides interrupting spontaneous contractions of

---

[14] To improve the optical quality of the pictures, the refraction indices of the cell culture fluid, PDMS rubber and immersion fluid should be matched. However, the cell culture fluid refraction index was not matched with the index of *PDMS* rubber as it would require an add an extra component to said medium. This, in turn, could influence cell behavior, which we wanted to avoid.

most cells. The same cells as analysed before were localized using the microstructure as marker. The cell could be re-found by recording cell position, e.g. "stripe *Ia*, 3rd row, 4-5 column". All pillars neighbouring the ones connected by the cells studied were included in the micrographs. Confocal micrographs were taken for calcein as well as DiD signals in two channels simultaneously using the yellow HeNe laser and an argon laser (488 nm) with a 505-530 nm band pass filter. The laser power again varied from sample to sample; it was kept as low as possible to minimize photodamage of the cell but to guarantee good image quality. Image stacks (so-called z-stacks) were collected at high spatial resolution in this configuration. From these stacks we determined the exact localization of the cell (by calcein staining) and the geometry of the micropillars (by DiD staining). For optimal optical resolution the refractive indices of the immersion fluid (65% glycerol in water) and the cell culture medium (addition of 32% *BSA* to culture medium had no detectable effect on cells) were matched to the one of the elastomer (refractive index of 1.41). Neglecting this match decreases image quality seriously. Geometrical parameters were read out from image stacks using the Zeiss LSM Image Browser (Version 3).

1.7.3. MEASUREMENT UNCERTAINTIES

To estimate total experimental uncertainty, the uncertainties of all input parameters were estimated. The resulting total uncertainty was calculated under the assumption that parameter contributions were uncorrelated. Gaussian propagation of uncertainties for a micropillar with average parameters was assumed. Micropillar parameters are shown in Table **1-3** while errors and their contribution to the overall uncertainty in the force estimation in Table 1-4. For the experiment only 10 x 10 μm cross-section micropillars were used. Why we abandoned the other, thinner micropillar arrays is explained in APPENDIX C.

Table 1-3 Main parameters of the micropillars and the observed cells. All data is given as averages (15 different cells exhibiting 15 contractions on average). Where applicable, lowest and highest observed values are given in parentheses.

Micropillar parameters	
Width at base, a_R (μm)	9.2 (7.8; 10.0)
Moment of inertia at pillar base, I_0 (μm^4)	610 (240; 840)
Moment of inertia at scan height[15], I (μm^4)	830 (440; 980)
Young's modulus (kPa)	608
Poisson's ratio, v	0.5
Cell parameters	
Highest point of cell, l (μm)	21.9 (17.8; 24.7)
Lowest point of cell a, [16] (μm)	5.2 (0.0; 13.8)

---

[15] Scan height – height, at which pillar displacements were scanned
[16] the highest and lowest cell points at which the cell was attached to a micropillar

Table 1-4 Conservative estimates of sources of uncertainty in the cell force measurement (*model I – see also 2.3.1* CELL - PILLAR FORCE DISTRIBUTION MODELLING).

Parameter	Uncertainty	Contribution to total force error (%)
Pillar width at base a_R (μm)	0.25	0.9
Moment of inertia at pillar base I_0 (μm^4)	60	9.8
coefficient describing pillar shape change ρ	0.03	1.5
Scan height (μm)	0.5	4.5
Young's modulus E (kPa)	20	3.2
Highest point of cell l (μm)	2	10
Deflection x (μm)	0.1	6
Overall force uncertainty	**17%**	

2. RESULTS

2.1. CELL MORPHOLOGY

When given the choice to attach to a flat *PDMS* elastomer surface or *PDMS* elastomer micropillars, the myocytes attached preferentially to micropillars. In the case of small lattice constants (regions *Ia – Ic* mainly, so 20 - 30 μm, see Table 1-2), many cells connected two neighbouring micropillars without or with very little contact to the flat part of the substrate between the micropillars. We observed some cells spanning even greater distances. In regions of the substrate where the micropillars were further apart, most cells wrapped around one pillar with connections to the flat part of the substrate, though few spanned between two micropillars. Only in regions lacking micropillars the formation of a loose cell layer on top of the flat substrate was observed, see Fig. 2-A.

Cell morphologies depended dramatically on the local environment of cells. While myocytes attached to flat substrates exhibited a spread out, 'pancake like' shape, the cells spanned between two micropillars were spindle shaped and far more compact. Cells connecting a micropillar to the flat substrate often displayed both morphologies at the same time.

2.2. CELL CONTRACTION

The observed cardiac myocytes were contracting which was accompanied by deformation of the micropillars to which the cells adhered. The regular pattern of micropillar distribution allowed calculation of the resting positions of the bent micropillars (i.e. the ones connected by cells) could be calculated from the positions of neighbouring undeflected micropillars, see Fig. 2–B.

A few percent of all the cells contracted spontaneously (usually 1 – 7 %). The smaller the lattice constant the easier it was to find a contracting cell, with most cells found in *Ia* region of the micropillar array, cf. Fig 1-P and .Table 1-2.
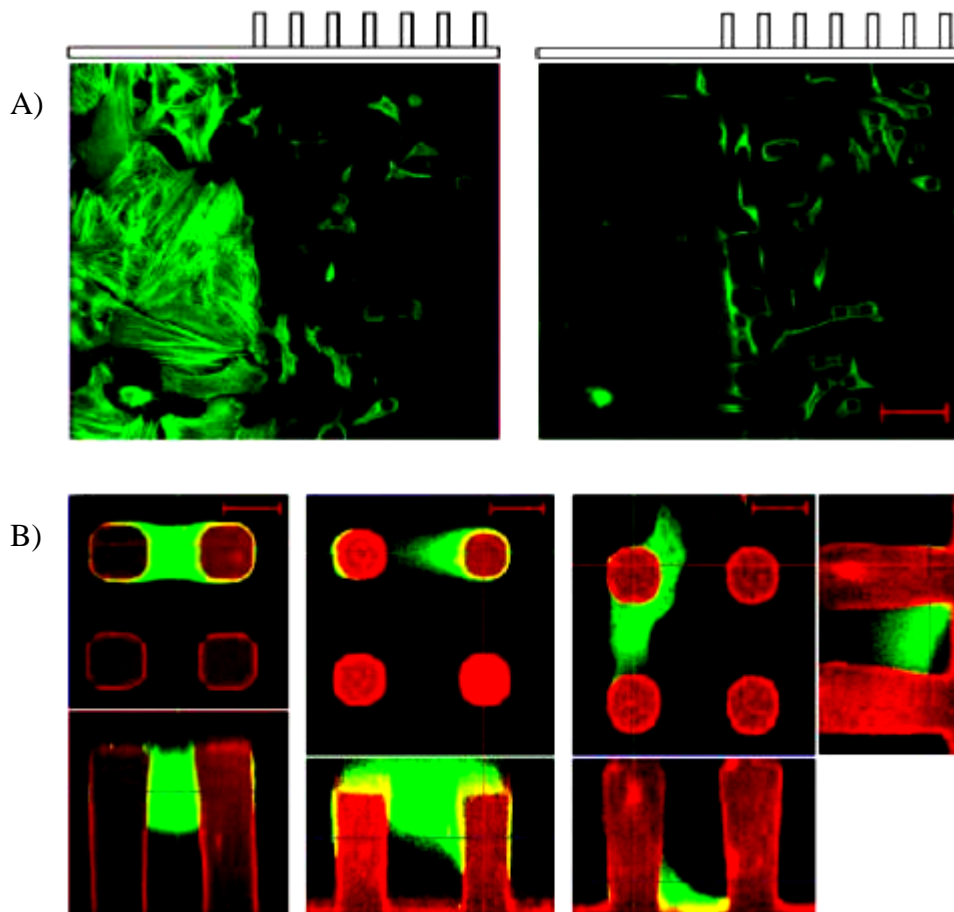
Fig. 2-A Freshly isolated cardiac myocytes were incubated for two days on *PDMS* elastomer substrates partially covered by micropillar arrays. A) Cells were fixed and subsequently stained for actin. Myocytes were analysed at the border between flat substrate and micropillar array using CLSM. Note that the same substrate area is given twice: once focused on the flat surface (left) and once at a height of approximately 20 µm above (right). Scale bars 50 µm. B) Living cells were labeled with calcein and image stacks were taken at a confocal microscope. Calcein (green) and DiD fluorescence (red) were collected simultaneously. Three possibilities of cell attachment to two micropillars are given. Each image consists of a top view at the height indicated by a blue line in the side view given below. For the last cell, side views in both directions are given. Scale bars 10 µm.

Out of 45 scanned, 15 cells were chosen for the force analysis. The other cells were rejected for various reasons. Some scans were rejected because of their optical quality. These were mainly the first scanned cells when we had little experience with optimising the scanning parameters. Second, we excluded all cells that were partly attached to the substrate between micropillars which was often not visible before cell staining. The results for all 15 cells studied are summarized in Fig. 2-G and Table 2-1.

Amplitudes in the relaxed and in contracted state of cells (i.e. during and between the beats) are reported relative to these reference positions. In few cases all columns in a field of view were connected by cells[17]. In those cases the distance between the observed columns was calculated assuming that the deviation between this distance and the lattice constant was equally distributed between the displacements of both micropillars. Examples of cell contraction transients are shown on Fig. 2-C and their properties summarized in Table 2-1.

It was also observed that clusters of cells tend to beat more often and faster than single cells, reaching the frequencies over 3 Hz. Evaluation of the obtained scans were done with stand-alone routines written by Dr Norbert Kirchgeßner (Forschungszentrum Jülich GmbH) with the MathLab software release 14.

A)   B)
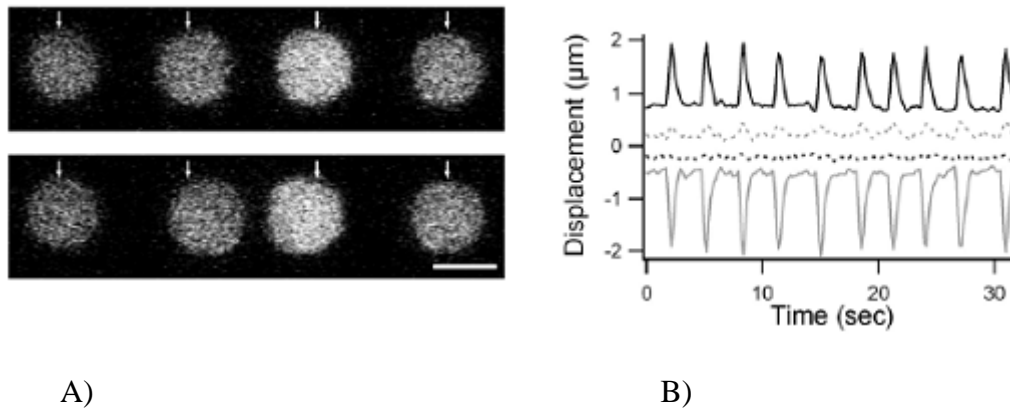
Fig. 2-B Displacement of micropillars upon myocyte beating. A) Micrographs at time 16.55 s (top) and 18.52 s (bottom). The inner two pillars are connected by a cell. The white arrows indicate the centres of undisplaced pillars. Scale bar 10 µm. B) Displacements of the pillar centres from their resting positions. Black: left pillar, grey: right pillar, full lines: x coordinates, dotted lines: y coordinates.

---

[17] It happended for three out of 15 cells taken into force analysis

Table 2-1 Summary of the properties of the observed cells. Results are given as averages (15 different cells exhibiting 15 contractions on average). Lowest and highest observed values, respectively, are given in parentheses.

Observed amplitudes	
In contracted state (μm)	1.68 (0.7; 3.0)
In relaxed state (μm)	0.66 (0; 1.8)
Contraction frequency (Hz)	0.47 (0.1; 0.8)
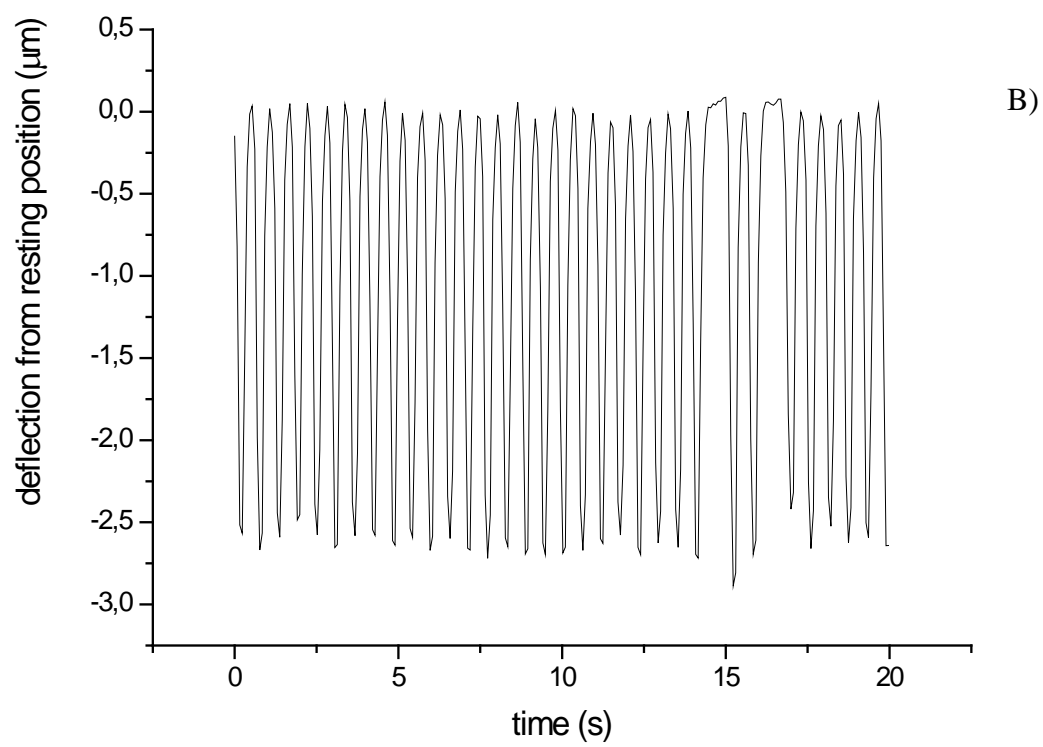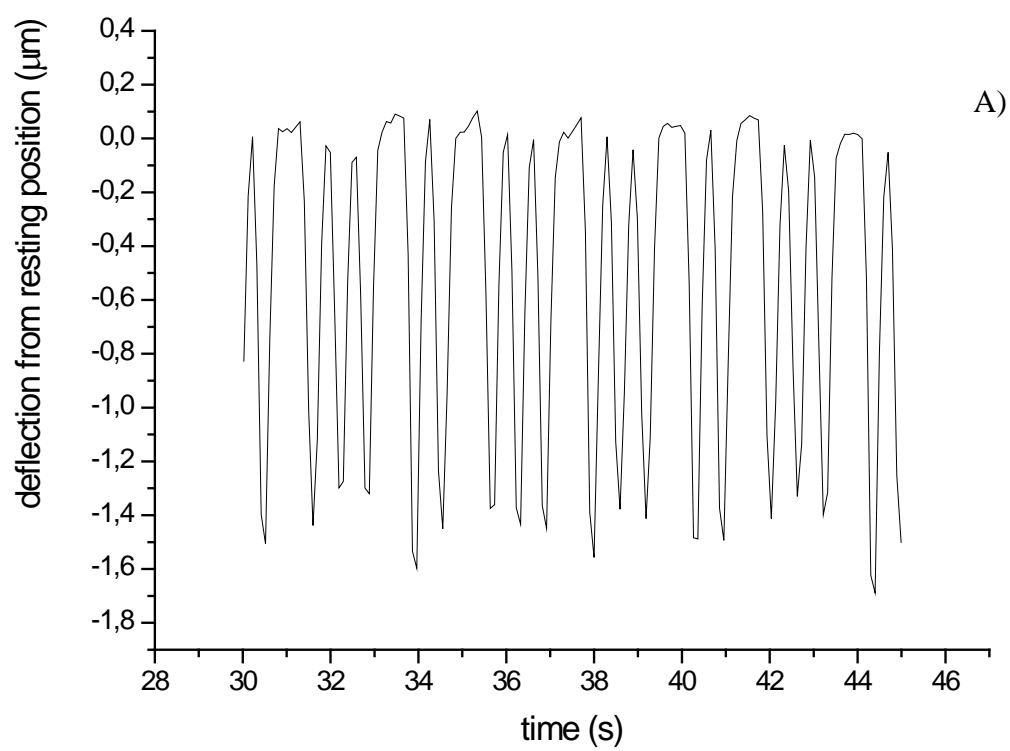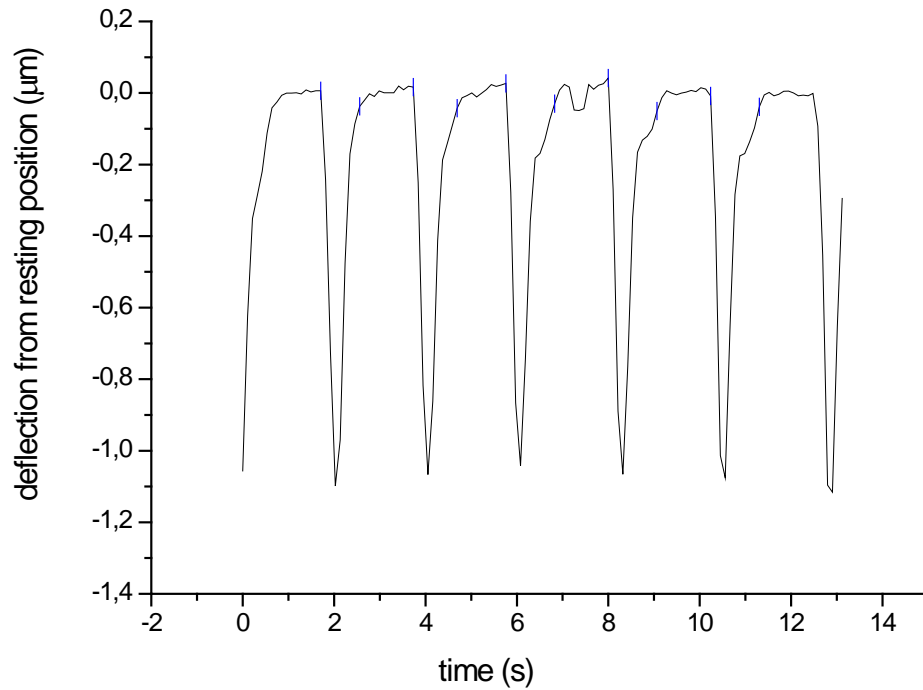
C)
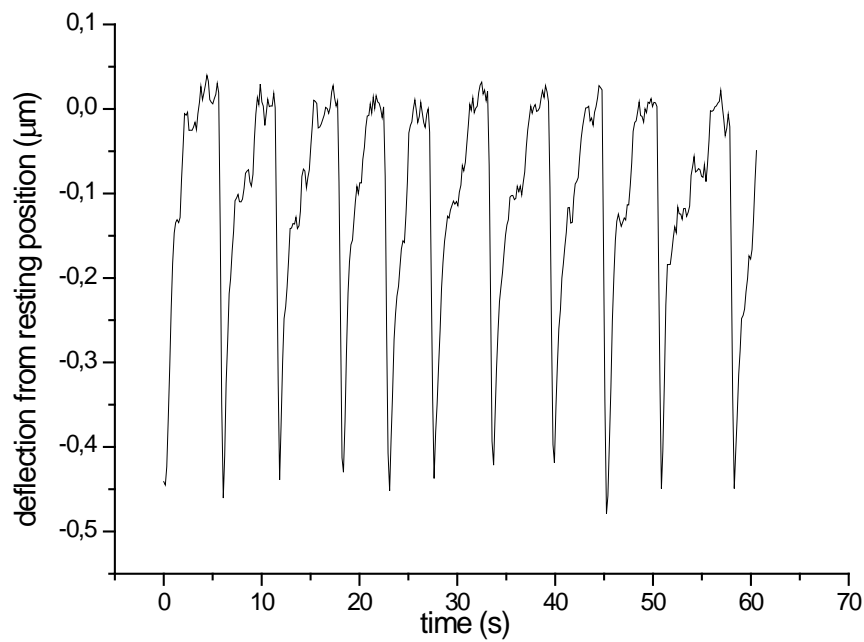
D)

Fig. 2-C Four examples for different temporal contraction patterns. A) A 'stuttering' cell with beat arrhythmia. B) A fast beating cell. Beat rhythm irregularities are also visible. C) A slow beating cell. D) A 'trembling' cell, probably due to calcium concentration fluctuations.

2.3. MODELLING OF ELASTICALLY ANCHORED PILLARS

Let us define the coordinate system in such a way that x- and y-axes lay in the plane of the base layer and z-axis points in the direction the pillar stands up. The coordinate system originates in the middle of the pillar cross-cut, at the height where the pillar emerges from the substrate (see Fig. 1-M). Far from the pillar ends, the torque bending the pillar is balanced by a distribution of axial tensions, σ_{zz}:

$$\sigma_{zz} = \frac{Mx}{I}$$ **Eq. 2-1**

where

M – entire torque acting on the micropillar

I – moment of inertia of the cross-section

x – deflection

Finite element calculation of the system consisting of both elastically anchored pillar as well as its elastic substrate is necessary to derive precise equations for the bending resistance of micropillars because the area where the substrate and the pillar merge (the contact zone) should be described in precise detail. However, the contact zone geometry, though practically the same for the micropillars on the same array sample, varied slightly from sample to sample. Thus, every micropillar array would require in principle new calculations. Moreover, the contact zone geometry was difficult to determine from CLSM stacks due to insufficient axial resolution. To avoid these problems, the following approximation was made: the distribution of tensions in the contact plane between micropillar and substrate, i.e. at the very base of the pillar, is assumed to be given by Eq. 2-2 ignoring the details of the contact zone geometry. As the thickness of the substrate layer is at least 3 times greater than the diameter of the pillar, the substrate under the pillar could be approximated with an elastic halfspace (Landau L., Lifshitz E. 1991), cf. Fig. 1–M. The displacement of an elastic substrate can be calculated if the deforming force and material properties are known. Let us define the displacement $\vec{u}(x, y) = \vec{r} - \vec{r}\,'$ where

$\vec{r}(x, y)$ the coordinate of the given point before deformation

$\vec{r}\,`(x', y')$ the coordinate of the given point after deformation.

The displacement $\vec{u}$ is obtained from the force densities $\vec{f}$ by convoluting it with the appropriate Green tensor $\vec{\mathbf{G}}$ [18]

$$\vec{u}(x,y) = \int \vec{\mathbf{G}}(x - x', y - y')\vec{f}(x',y')dx'dy' \qquad \text{Eq. 2-2}$$

Because the thickness of the substrate layer exceeded twice the diameter of the pillar, the substrate under the pillar could be approximated with an elastic halfspace (Landau L., Lifshitz E. 1991, Merkel et al. 2007), cf. Fig. 1–M. The Green tensor for the surface ($z = 0$) is given then by:

$$\vec{\mathbf{G}} = \frac{1+v}{2\pi E r}\begin{pmatrix} \dfrac{2vx^2}{r^2} + 2(1-v) & \dfrac{2vxy}{r^2} & -\dfrac{1-2v}{r}x \\[2ex] \dfrac{2vxy}{r^2} & \dfrac{2vy^2}{r^2} + 2(1-v) & -\dfrac{1-2v}{r}y \\[2ex] \dfrac{1-2v}{r}x & \dfrac{1-2v}{r}y & 2(1-v) \end{pmatrix} \qquad \text{Eq. 2-3}$$

where $r = |\vec{r}|$ and is a distance measured within the surface for $z = 0$; E and v are the Young's modulus and the Poisson's ratio respectively.

As the Poisson's ratio of *PDMS* elastomer is very close to 0.5, the calculations specific for this case can be simplified significantly because some of the coefficients equal zero. Although the cross-section of micropillars somewhat varied with the height, it was quite close to square at the base. For the square, the only nonvanishing part of the displacement can be written as :

$$\frac{u_z}{a_R^2 A} = \int_{l_1}^{l_2} ds \int_{l_3}^{l_4} dt \frac{x/a_R - s}{\sqrt{s^2 + t^2}} \qquad \text{Eq. 2-4}$$

where $s = x\text{-}x'$ and $t = y\text{-}y'$

$$A = \frac{3}{4\pi}\frac{MI}{E} \; ; \; s = \frac{x - x'}{a_R} \; ; \; t = \frac{y - y'}{a_R}$$

with the limits of integration given by

$l_1 = x/a_R -0.5; \; l_2 = x/a_R +0.5; \; l_3 = y/a_R -0.5; \; l_4 = y/a_R +0.5$

---

[18] tensors are marked with bold font, to distinguish them from vectors

These integrals were calculated with Mathematica® (Wolfram Research) and are as follows:

For x:

$$\text{int}1 = -\ln\left(-1 - 2x + \sqrt{1 + 4x + 4x^2 + 4\left(\frac{t}{a}\right)^2}\right) + \ln\left(1 - 2x + \sqrt{1 - 4x + 4x^2 + 4\left(\frac{t}{a}\right)^2}\right)$$

For y:

$$
\begin{aligned}
\text{int}2 = &-\frac{1}{2}\ln\left(-1 - 2x + \sqrt{2 + 4x + 4x^2 + 4y^2 + 4y}\right) - \frac{1}{2}\ln\left(-1 - 2x + \sqrt{2 + 4x + 4x^2 + 4y^2 + 4y}\right)y + \\
&-\frac{1}{2}\ln\left(-2 - 4y + 2\sqrt{2 + 4x + 4x^2 + 4y^2 + 4y}\right) - x\ln\left(-2 - 4y + 2\sqrt{2 + 4x + 4x^2 + 4y^2 + 4y}\right) + \\
&+\frac{1}{2}\ln\left(1 - 2x + \sqrt{2 - 4x + 4x^2 + 4y^2 + 4y}\right) + \frac{1}{2}\ln\left(1 - 2x + \sqrt{2 - 4x + 4x^2 + 4y^2 + 4y}\right)y + \\
&-\frac{1}{2}\ln\left(-2 - 4y + 2\sqrt{2 - 4x + 4x^2 + 4y^2 + 4y}\right) + x\ln\left(-2 - 4y + 2\sqrt{2 - 4x + 4x^2 + 4y^2 + 4y}\right) + \\
&-\frac{1}{2}\ln\left(-1 - 2x + \sqrt{2 + 4x + 4x^2 + 4y^2 - 4y}\right) - \frac{1}{2}\ln\left(-1 - 2x + \sqrt{2 + 4x + 4x^2 + 4y^2 - 4y}\right)y + \\
&+\frac{1}{2}\ln\left(2 - 4y + 2\sqrt{2 + 4x + 4x^2 + 4y^2 - 4y}\right) + x\ln\left(2 - 4y + 2\sqrt{2 + 4x + 4x^2 + 4y^2 - 4y}\right) + \\
&+\frac{1}{2}\ln\left(1 - 2x + \sqrt{2 - 4x + 4x^2 + 4y^2 - 4y}\right) - \frac{1}{2}\ln\left(1 - 2x + \sqrt{2 - 4x + 4x^2 + 4y^2 - 4y}\right)y + \\
&+\frac{1}{2}\ln\left(2 - 4y + 2\sqrt{2 + -4x + 4x^2 + 4y^2 - 4y}\right) - x\ln\left(2 - 4y + 2\sqrt{2 - 4x + 4x^2 + 4y^2 - 4y}\right)
\end{aligned}
$$
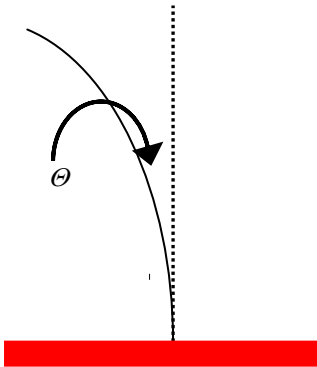
Fig. 2-D Definition of the Θ angle. Dotted line: normal to the undeformed surface; solid line: micropillar axis. The surface is shown in red.

Θ is the angle between the tangent to the pillar at its lower end and the normal to the undeformed surface (z axis, cf. Fig. 2-D). It was estimated from least square fitting a plane to the calculated deformations for the square cross-section (with a_R side length and a circular cross-section with the diameter d_0). The result is:

$$\Theta \approx b_R \frac{3M}{4\pi EI}$$

Eq. 2-5

Where $b_R = 1.18\ a_R$ or $1.05\ d_0$ for the square or circular cross-sections, respectively.

Consequently, uncertainty in the cross-section shape would add only few percent to the total error. This was indeed confirmed in the separate calibration experiment (see Appendix E). In contrast, as for a square pillar of width a_R moment I is given by $a_R^4/12$, for a cylindrical pillar of diameter d, $I = \pi d_0^4/64$ (Pilkey and Walter 2002), the uncertainty of diameter measurement adds significantly to the total error (see Table 1-4).

The bending curve, $x(z)$, of the micropillars was calculated by integrating the differential equation of a bent pillar (Landau L., Lifschitz E. 1991):

$$\frac{d^2 x}{dz^2} = -\frac{M(z)}{EI(z)}$$

Eq. 2-6

with the boundary conditions:

$$x(0) = 0, \ \left.\frac{dx}{dz}\right|_{z=0} = 1.18 a_R \frac{3M(z=0)}{4\pi EI(z=0)}$$

The moment $M(z)$ is given by

$$M(z) = -\int_z^l \int_\eta^l f(\varphi) d\varphi d\eta$$

Eq. 2-7

where $f(\varphi)$ stands for the transversal force density (e.g. force per length) acting on the micropillar.

The solution of Eq. 2-6 can be elegantly presented in dimensionless variables (denoted by a tilde). All geometrical parameters *z, a* (the lowest `contact point of the cell`) and a_R, vide Fig. 1–M), are divided by the height of the highest contact point of the cell, *l*, the torque by *Fl*, and the deflection *x* is multiplied by $EI(z=0)/(Fl^3)$. *F* denotes the entire transversal force of the cell applied to the micropillar.

The cross-section of the micropillars increased with height and rounded considerably at the same time. Variation of the moment of inertia of the micropillars with height is modelled by assuming a linear increase in diameter with height, i.e. $I(\tilde{z}) = I_0(1 + \rho\tilde{z})^4$, where ρ is the parameter describing pillar widening. The deviation of the measured *I(z)* from the approximation barely exceeded the accuracy of the determination of the moments of inertia. As a result, the dimensionless bending curve of the pillar for the case of point force acting at height *l* is given by:

$$\tilde{x} = 0.14\tilde{z}\tilde{a}_R + \frac{3\tilde{z}^2 - (1-2\rho)\tilde{z}^3}{6(1+\rho\tilde{z})^2}$$

Eq. 2-8

And the corresponding result for the case of uniform force between *a* and *l* by:

$$\tilde{x} = 0.14\tilde{z}\tilde{a}_R(1+\tilde{a}) + \frac{\tilde{z}^2[3 + 3\tilde{a} + \tilde{z}(2\tilde{a}\rho + 2\rho - 2)]}{12(1+\rho\tilde{z})^2}$$

Eq. 2-9

and for $\tilde{z} < \tilde{a}$

$$\tilde{x} = 0.14\tilde{z}\tilde{a}_R(1+\tilde{a}) + \left[12(1-\rho\tilde{a})(\tilde{a}-1)\rho^4(1+\rho\tilde{z})^2\right]^{-1}\left\{6(1+\rho\tilde{z})^2(1+\rho\tilde{a})\ln\left(\frac{\rho\tilde{z}+1}{\rho\tilde{a}+1}\right) + \right.$$
$$+ 2\rho^3\left[\rho^3\tilde{a}(\tilde{a}^2-1) + \rho^2(\tilde{a}-1) + \rho(1-\tilde{a}) - 1\right]\tilde{z}^3 +$$
$$+ 3\rho^2\left[\rho^3\tilde{a}(\tilde{a}^2-1) + \rho^2(\tilde{a}-1) - \rho\tilde{a} - 3\right]\tilde{z}^2 +$$
$$\left. + 6\rho\left[\rho^2\tilde{a}^2 + \rho\tilde{a} - 1\right]\tilde{z} - \rho\tilde{a}(\rho^2\tilde{a}^2 - \rho\tilde{a} - 6)\right\}$$

Eq. 2-10

for $1 > \tilde{z} > \tilde{a}$

The limiting case of a pillar with constant diameter ($\rho = 0$, $1 > \tilde{z} > \tilde{a}$) of Eq. 2-10 is nontrivial and becomes then

$$\tilde{x} = 0.14\tilde{z}\tilde{a}_R(1+\tilde{a}) + \frac{\tilde{z}^4 - 4\tilde{z}^3 + 6\tilde{z}^2 - 4\tilde{z}\tilde{a} + \tilde{a}^4}{24(1-\tilde{a})}$$

Eq. 2-11

Equations 2-9 to 2-11 hold for pillars of approximately square cross-section. In case of a circular cross-section, the factor 0.14 in the first term of all three equations should be replaced by 0.13.

In summary, a pillar on an elastic foundation deflects from the normal significantly more than a rigidly clamped pillar. The amount of this 'softening' depends on the aspect ratio of the pillar. For the geometry of the micropillars used in this project this effect summed up to approximately 37%. Even if the proportionality factor in Eq. 2-5 were only 70% of its calculated value as indicated by the experimental calibration, the elastically anchored pillar would still be 25% softer than the clamped one. This effect was not taken into consideration in previous works, where equations for rigidly clamped pillars were used (du Roure et al. 2005, Li et al. 2007).

2.3.1. CELL - PILLAR FORCE DISTRIBUTION MODELLING

The way cells distribute their forces along cell-pillar contact zone is unknown (see different cell-pillar contacts in Fig. 2-F). This measurement could be, in principle, performed by tracing the centre line of the bent pillar and applying Eq. 2-6. However, the equation includes a second derivative of this curve which greatly magnifies the effects of experimental uncertainty on data; thus, this measurement was not possible. Therefore, an attempt was made to measure the effective, overall torque M applied to one micropillar via the angle Θ to the surface normal at the base of the micropillar, using Eq. 2-5. However, within a range of 1-2 µm above the substrate surface a blurred image was seen simultaneously with pillar cross-sections. These blurred images caused artifacts in all tested image processing algorithms and prevented the measurement of Θ (cf Fig 2-E).

A)   B)
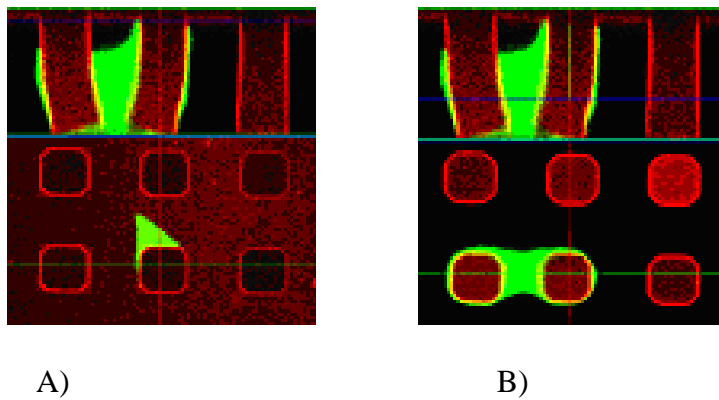
Fig. 2-E Blur problem. A) A cross-section through a *PDMS* elastomer substrate, taken about 1 μm over substrate level. B) The same sample, cross-section 15 μm above the substrate level. Note substantial blur in A).

A)   B)
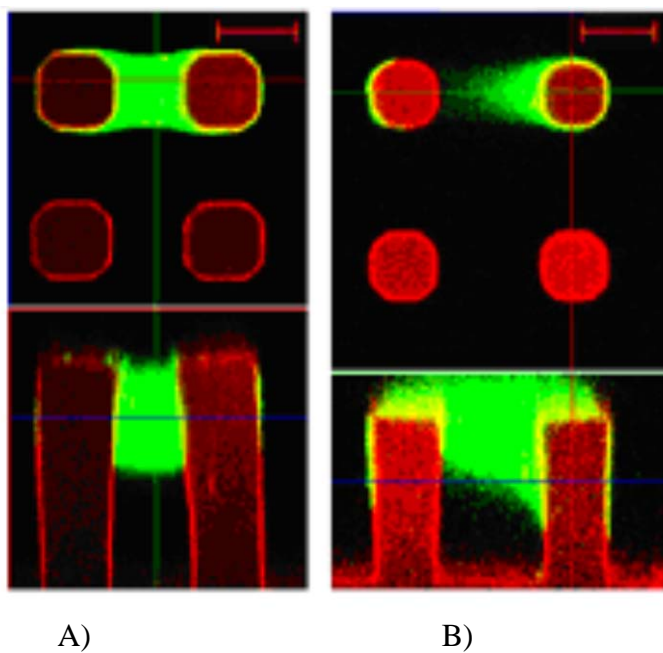
Fig. 2-F Micropillar-cell adhesion. Living cells were labelled with calcein and image stacks were taken at a confocal microscope. Calcein (green) and DiD fluorescence (red) were collected simultaneously. Each image consists of a top view at the height indicated by a blue line in the side view given below. Scale bars 10 μm.

Due to these experimental problems, we resorted to use two models.

1. ***Model I*** – calculation of the smallest cell force that could be necessary to create the observed deformation of two micropillars connected by the same cell. To obtain the limit, it was assumed that the cell applies **the force locally (point force) to the very highest point of cell-micropillar contact zone.**

2. ***Model II*** – it was assumed that the **cell force is uniformly distributed over the whole length of the cell-micropillar contact zone**.

Model I gives the very lowest forces that are compatible with physics. *Model II* is a much more likely scenario as actin-myosin is distributed all over a cross-section of a cell. Thus *model II* yields the likely forces of a given cell and *model I* a lower limit. Both estimates (most likely and limit) are necessary.
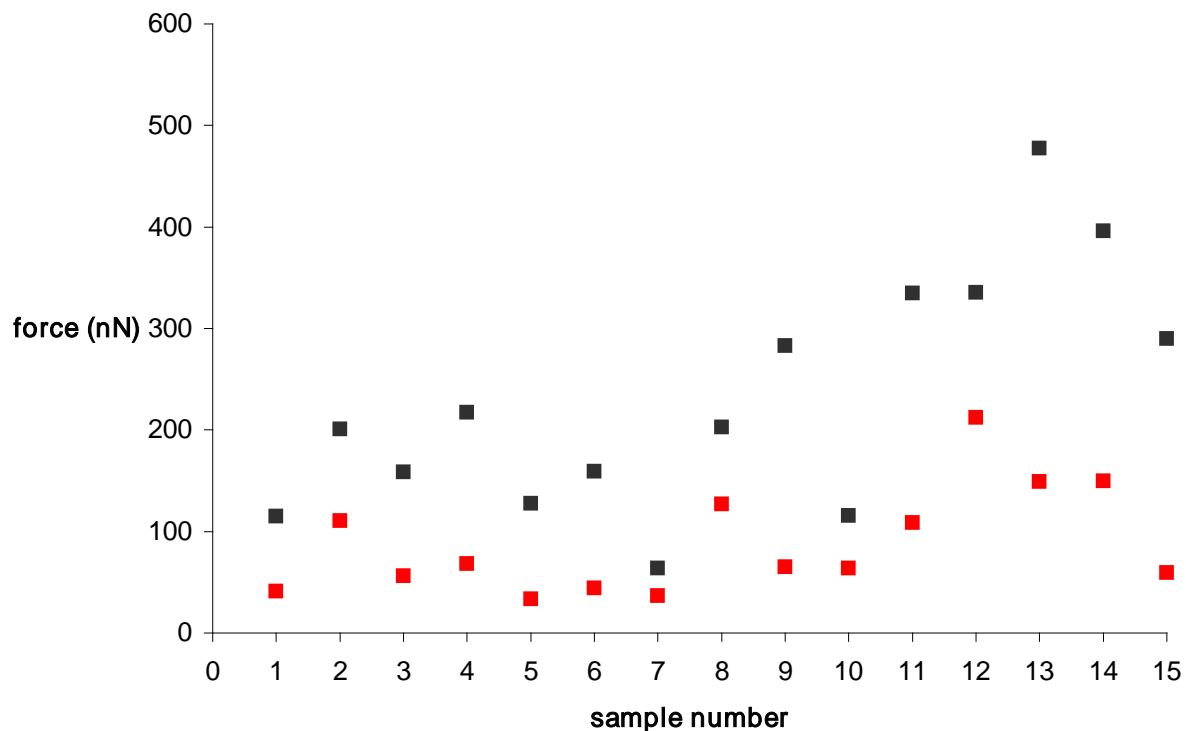
Fig. 2-G *Model I*. Red squares: Myocytes in relaxed state, black squares: cells in contracted state. The model gives estimates of the lowest possible cell forces sufficient to cause the observed pillar deflections.

The highest point of both cell-pillar contact zones of a given cell was selected as the point of force application. The classical Newtonian action-reaction principle was applied to calculate at which height same force had to be applied on the other micropillar to cause its observed deflection. In all cases the calculated height was well within the observed contact zone between cell and micropillar. Thus, *Model I* yielded force distributions consistent with all observations. For the *Model I*, the forces on average equalled 90 ± 20 nN in the relaxed state, and 230 ± 20 nN in the contracted state, see also Fig. 2-H.
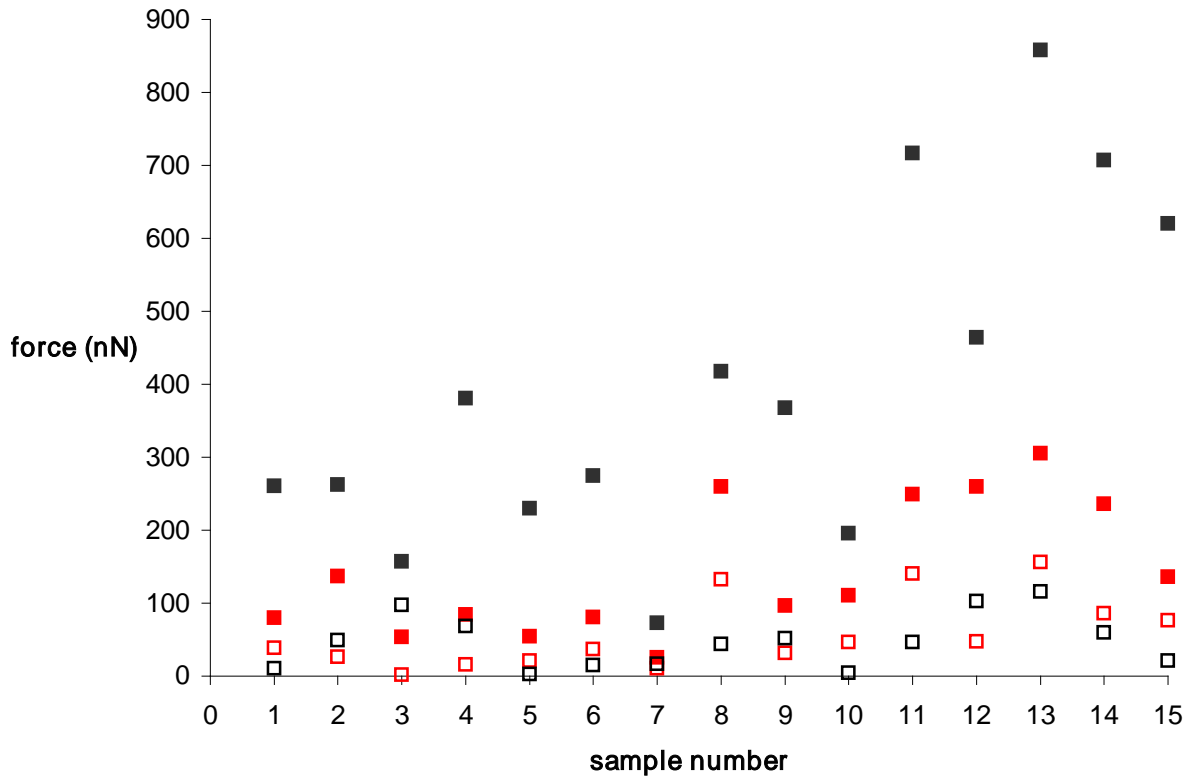
Fig. 2-H *Model II*. Contraction forces of cells assuming even force distribution over the continuous contact zone between the cell and micropillars. Forces were averaged over both columns. Black filled squares: contracted state, red filled squares: relaxed state. Difference between the forces measured at both columns for contracted and relaxed state is also shown (black and red open squares, respectively). The model gives estimates of mean cell forces sufficient to cause the observed pillar deflections.

Model II assumes uniform force distribution all over the cell-pillar contact zone. Equations 2-9 to 2-11 were used to calculate the cell forces in this case. As the cell usually attached at different heights to each micropillar, forces for both micropillars connected by one cell were obtained independently. Nonetheless, forces must balance for a system in mechanical equilibrium so the mean of the forces determined for both micropillars connected by the cell was taken and it was checked whether the differences between these two forces were within the range of experimental uncertainty (see Fig. 2-H).

3. DISCUSSION

3.1. INFLUENCE OF EXPERIMENTAL CONDITIONS ON CARDIAC MYOCYTES

3.1.1. CHOICE OF CELLS

Present work was carried out on rat cells, as these cells have been frequently used for similar experiments in the past (see Table 3-1) and it is known that cells obtained from different animal species behave differently (Gao et al. 1997). We used cells from embryos prepared from embryonic hearts resulting in a higher number of surviving cells and a higher fraction of spontaneously contracting cells as compared to preparation from adult hearts. Due to their small sizes, entire rat embryonic hearts were used as raw material for cell preparation. A further specialization to ventricular tissue as usual for adult hearts (see Table 3-1) was not possible. However, it is known that cells from different regions of the heart exhibit different properties (James 2002, 2003). Frequency and strength of the electric oscillations vary according the origin of the cardiac myocytes. As in intact heart cells are electrically connected by gap junctions, the fastest cells act as pacemakers and the capability of ventricular for spontaneous oscillations never comes to bear. In culture, however, the cells are not connected, therefore even the slowest may show contractions at "their own speed".

3.1.2. TEMPERATURE

We decided to perform our experiments at 37°C in order to approach physiological conditions as closely as possible. Experiments on mammalian cells at non-physiological temperatures as frequently reported in the literature (Table 3-1) are, in my opinion, of limited scientific value. Rabbits, guinea pigs and rats, used in the experiments do not hibernate and, being endotherms, keep their body temperature at constant level. In such organisms, all the enzymes are optimised to cooperate in a narrow range of temperatures. This balance is very subtle and is brutally disrupted by temperature change (Schmidt-Nielsen 2008). The cause of death is the lose of equilibrium between molecular processes in the body, changed cell membrane fluidity etc. A non-hibernating mammal dies in temperatures much higher then actually required to cause ice formation in its tissues (~20°C for humans). Such temperatures do not kill the heart cells, though, so myocytes can be investigated at lower temperatures. Those temperatures are, nonetheless, non-physiological and the question arises how they affect the cells. Sweitzer and Moss (1990) noticed an influence of temperature on myocyte

maximum force. For the temperature range they investigated (10°C and 15°C) the force rose with temperature. There is, however, to our best knowledge no model which would allow the calculation of body-temperature cellular forces out of the data gathered at lower temperatures. As the temperature does influence the myocytes, the comparison of low-temperature data with the data obtained at physiological temperatures becomes highly debatable.

A noteworthy exception is the work of Cecchi and coworkers who used *Rana esculenta* frogs which undergo huge body temperature changes as the frog is a hibernating and ectothermic animal (Mazgajska, 2005). Obviously, studying cardiac myocyte function at different temperatures is a profound strategy to gain insight into heart physiology of **ectothermic** animals.

3.1.3.   EXTERNAL STIMULATION

In most of the cases shown in Table 3-1, cardiac myocytes were stimulated to contract. It is indeed very important to study the behaviour of heart muscle cells under external stimulation as in the heart said cells are excited in this way. However, Bluhm et al. (1995) and Cecchi et al (1992) found in experiments on external electrical stimulation of cardiac myocytes that contraction forces depend on the stimulus interval for electrical excitation. Moreover, Gao et al. (1997) demonstrated for cells stimulated with Ca^{2+} - containing solution, that both the contraction amplitude and force increase with external Ca^{2+} concentration. Furthermore, rat cardiac myocytes reacted differently to unphysiologically high Ca^{2+} concentration than mouse myocytes. Thus, utmost care must be taken when comparing such experiments.

Experimental systems which do not require external cell stimulation allow, on the other hand, to study the spontaneous or autonomous contractions of cell. As the cells are not excited, no electrode system or stimulating solutions are necessary which simplifies the experimental system and procedures. However, the question remains how these two different approaches influence cell behaviour. From works of Bluhm et al. (1995) and Cecchi et al. (1992) one can conclude that – at least up to frequencies up to 1 Hz - the increase of frequency causes the increase of contraction force. This may explain why the forces obtained in our work are usually lower than those obtained from experiments with stimulated cells. It is then reasonable to compare the forces of non-excited cardiac myocytes with the force of myocytes stimulated with lowest frequencies. According to Bluhm, cardiac myocytes stimulated with 0.1 Hz stimulus exerted forces of about 300 nm; Cecchi reported values in the range of 100-150 nN which is in the range of forces exerted by unstimulated cells, compare Table 3-1.

3.1.4. CELL PRE-TREATMENT

As we did not stimulate the cells, cell skinning or permeabilization were not necessary. These procedures serve to decrease the barrier function of cell membranes. Their perforation facilitates stimulation of the cells chemically with Ca^{2+} ions and, as shown in Table 3-1, is a commonly used experimental technique. Please note that permeabilized and skinned cardiac myocytes usually exhibit higher forces compared to intact cells. It can be explained by stronger excitation of skinned and permeabilized cells, especially that most the cells exhibiting the greatest forces were skinned or permeabilized cells stimulated with solutions containing different concentrations of Ca^{2+}. It is plausible that ions penetrate such cells easier and faster. As cell contraction forces increase with Ca^{2+} concentration (Gao et al. 1997), permeabilized and skinned cells may react with higher contraction forces to rapid influx of calcium.

The only exception was reported by Yin and coworkers (2005). Their cells, though intact, exhibit forces in range of 10 μN. They, however, used myocytes extracted from ischemic rats (which underwent deliberately induced heart attack). It is well possible that the reported low contraction forces were a consequence of this pathological situation.

Judging from the data collected in Table 3-1 'skinning' affected the myocyte contraction forces, by increasing them. A plausible explanation would be as follows: myocyte contraction is caused by a biochemical mechanism based on ion flow through the cell membrane. Partial disruption of the cell membrane changes the ion transport through the membrane, affecting the cellular contractile mechanism.

3.1.5. MICROARRAY LATTICE CONSTANTS

We observed the highest cell activity in the micropillar array regions with the lowest lattice constant, i. e. region *Ia* (c.f. Table 1-2). As a micropillar is about 10 μm wide and the myocytes tended to wrap around them, the myocyte length was about 30 μm in this region of the sample. For the second lattice constant region - *Ib* - myocyte length was approximately 35 μm.

Our myocytes were not forced to elongate when actively adjusting to their environment (which is the case in experiments where the cells are spanned between microfibres, micropipettes or a micromanipulator and a force transducer). Once they 'decided' to attach to the neighbouring micropillars, their length had to be fitted to the microarray lattice constant. Interestingly, we observed that myocytes attached all over the microarray, also in regions *Ie* and *If* but there they adhered to one micropillar only. It is plausible that myocytes

attached to two or more micropillars only if they touched them when floating in the medium. Should a myocyte adhere to only one micropillar, it did most likely not spread in order to seek another pillar. This is well possible as cardiac myocytes are stationary cells with limited locomotion capabilities.

3.1.6.   ISOMETRIC CONDITIONS

In some experiments (see Table 3-1) cellular forces are measured under isometric conditions, i.e. the compliance of the measuring device is changed during the measurement so that the myocyte length remains constant. If the cell pulls harder, the device stiffens so that the cell cannot contract any further. I believe this measurement method is not optimal for cardiac myocytes. First, if myocytes strive to achieve certain contraction amplitude, not force (see detailed discussion in section 3.3.2 CONCLUSION), isometric measurement conditions may spur them to exhibit nonphysiologically high forces. Second, cardiac myocytes do not work under isometric conditions *in vivo*, (though skeletal muscles may) so isometric conditions are not biomimetic. On the other hand, this approach may provide information about maximal forces the cell is able to exert.

3.2. FORCE COMPARISON

In this context it is instructive to compare the results of all cardiac myocyte contraction force studies performed up to now. Myocyte contraction forces observed varied from tenths to tens of μN, c.f. Table 3-1. This huge spread reflects the differences in the cellular material and complexity of the cellular force measurements, detection techniques and experimental conditions. Not only myocytes of different animal species and of animals of different ages were used (rat, guinea pig, rabbit; grown-up, neonatal, foetus) but also from different heart regions (whole organ, ventricles only). Moreover, in some cases the cells were subjected to **external excitation**. The experiments required various forms of cell manipulation, like adhesive use or placing a cell in a magnetic field, which may have affected the cell performance. In spite of those difficulties it is possible to draw several conclusions and to explain – at least partly – which experimental parameter affected the results.

Forces of individual cells measured by the same authors with identical techniques varied substantially. In some cases the credibility of the presented results may be questioned: several authors published mean force values with errors as large as the mean values themselves, see Table 3-1. The standard deviation is of limited value for the description of data with such large scatter. Instead it would be better to show mean, maximal and minimal

force magnitudes or, as the number of investigated cells is usually low, show all values on one graph.

Table 3-1 Comparison of cardiac myocyte forces, measured in different experiments.

Authors	Measurement set-up	Source of cardiac myocyte	External stimulation	Conditions	Number of cells studied	Force (nN)
This work	**Micropillar array system**	**Rat embryos, intact, node cells**	**None**	**37°C** **Model I, upon contraction**	**15**	**230** **Average over cells**
				Model I, relaxed state	**15**	**90** **Average over cells**
				Model II, upon contraction,	**15**	**400** **Average over cells**
				Model I, relaxed state	**15**	**140** **Average over cells**
Balaban et al. (2001)	Ultrasoft, flat, patterned substrates	Neonatal rat, Intact cells	None	37°C		Up to hundreds[19]
Bluhm et al. (1995)	A cell is attached between a force transducer and a micromanipulator	Rabbit, intact, ventricular	Stimulation with electrodes	30°C 2 s stimulus interval	5	2700 (strong stimulus interval/force dependence) isometric force

---

[19] total cell force; the forces were measured on subcellular level

Cecchi et al. 1992	A cell is stretched with micropipettes. The pipette bending is used to calculate cellular force.	Frog, atrial and ventricular cells tested separately Intact cells	Stimulation with electrodes	20 - 23°C Peak twitch force 10 s stimulation pulse intervals	39 atrial	42.1 ± 4.4 Effect of Ca^{2+} and isoprenaline[20] concentration is discussed
					60 ventricular	70.6 ± 6.7
				20 - 23°C Peak twitch force 10 s stimulation pulse intervals	12 atrial	34.4 ± 6.8
					10 ventricular	69.6 ± 19.4
				20 - 23°C 1 s stimulation pulse intervals	12 atrial	55.5 ± 10.4
					10 ventricular	113.1 ± 27.3
Cesa (2007)	Ultrasoft, flat, patterned substrates	Rat embryos Intact cells	None	37°C	12	Up to hundreds
Colomo et al. (1997)	A cell is stretched with micropipettes. The pipette bending is used to calculate cellular force.	Frog, skinned cells	Stimulation with solutions comprising Ca^{2+} ions	15°C	45	500 – 3500

---

[20] a drug altering cardiac myocyte contraction force

Herron et al (2001)	A cell is attached between a force transducer and a micromanipulator.	Rat, skinned cells	Stimulation with solutions comprising Ca^{2+} ions	13°C Control	5	7 000 ± 1 800 or 8 200 ± 9 700 (depending on stimulating solution) Isometric force
				13°C, Adrenergic stimulation	5	8 600 ± 1 700 or 10 000 ± 5 620 (depending on stimulating solution) isometric force
Korte and McDonald (2007)	A cell is attached between a force transducer and a micromanipulator.	Adult rat, ventricular, skinned cells	Stimulation with solutions comprising Ca^{2+} ions	12°C	12	5900 ± 1800 maximal isotonic
Le Guennec et al. (1990)	A cell is stretched with carbon microfibres. The fibre bending is used to calculate cellular force.	Guinea pig, Intact cells	Stimulation with solutions comprising Ca^{2+} ions. In some cases also electrode stimulation was used.	Room temperature	4	154 (maximum)
Lin et al. (2000)	A cell is attached between a force transducer and a micromanipulator.	Adult rat, ventricular, skinned cells	Stimulation with solutions comprising Ca^{2+} ions		7	12 600 ± 4 660
McDonald et al. (1998)	A cell is attached between a force transducer and a micromanipulator.	Rat, skinned cells	Stimulation with solutions comprising Ca^{2+} ions	12°C Prestretched cell	13	7800 ± 2 400 (Maximum)
Shepherd et al (1990)	A cell is stretched with micropipettes.	Guinea pig, ventricular myocytes	Stimulation with electrodes	35°C	11	1 230 ± 440 Isometric force

	The pipette bending is used to calculate cellular force.	Intact cells				
Shepherd and Fisher (1990)	A cell is attached between a force transducer and a micromanipulator.	Guinea pig, ventricular myocytes Intact cells	Stimulation with electrodes	35°C	11	1 230± 440 Isometric force
Sweitzer and Moss (1990)	A cell is attached between a force transducer and a micromanipulator.	Rat, permeabilized cells	Stimulation with solutions comprising Ca^{2+} ions	15°C	6	2 800 - 14 700 Maximal isometric force
						920 – 2 060 Rest tension
Tasche et al. (1999)	A cell is stretched with tungsten microneedles. The needle bending is used to calculate cellular force.	Rat, ventricular, skinned cell	Stimulation with solutions comprising Ca^{2+} ions.	12°C, cell glued with polyurethane varnish	6	About 8 000
Yasuda et al. (2001)	A cell is stretched with carbon microfibres. The fibre bending is used to calculate cellular force.	Adult rat, left ventricle, intact cell	Stimulation with electrodes.	37°C, Treated with isoproterenol. No adhesive	5	1060 ± 200 Isometric force
				37°C, Control No adhesive	5	730 ± 170 Isometric force
Yin et. al. (2005)	A cell is attached between a force transducer and a micromanipulator.	Adult rat, ventricles, intact cells Ischemic rat	Stimulation with electrodes.	37°C Cells attached to beads via ECM proteins		About 10 000

3.3. CELL FORCE – PILLAR STIFFNESS RELATION

The dependence of cell force magnitude on micropillar stiffness was modelled as a linear law, see Eq. 3-1. Least square fitting was used to find proportionality constant. If we denote the bending force as *F* and stiffness as *s*, we obtain:

$$F = xs + b \qquad\qquad\qquad \textbf{Eq. 3-1}$$

where b is the *y*-intercept.

According to Eq. 3-1 the micropillar stiffness can be defined as the ratio of the applied force to micropillar deflection amplitude. I would like to stress that though all the micropillars were cast of the same polymer and are of similar height and width, micropillar stiffness **experienced** by cells varied because of the different height of cell adhesion as well as variations in pillar diameter and shape. A cell which adhered close to the micropillar top sensed smaller stiffness than a cell adhered closer to the micropillar foundations (see cells in Fig. 2-F). The values obtained depended on the model (*I* or *II*) used to analyse our data. The results in Fig. 3-B indicate of a clear force - stiffness correlation for both models.

We observe strong scattering of force results, independent of the model used, although we utilized the same type of cells and maintained identical experimental conditions throughout our study (see Fig. 2-G, Fig. 2-H and Fig. 3-B). Similarly, a huge scatter of the contraction forces was also observed in other works (see Table 3-1), regardless of experimental techniques and cell preparation. A similar scatter of values was observed also for other cell parameters, like length (le Guennec 1990) or beat frequency (see below). Even cells originating from the same cell region differ. This 'individuality' of cells makes interpretation and comparison of data a very challenging task.
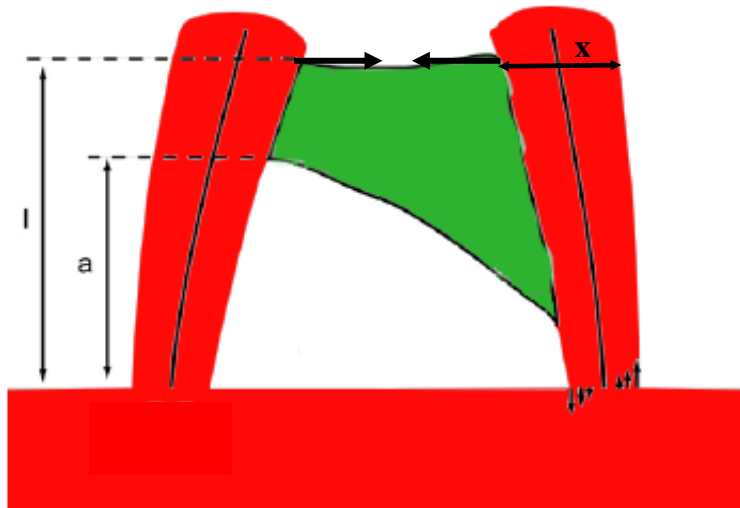
A)
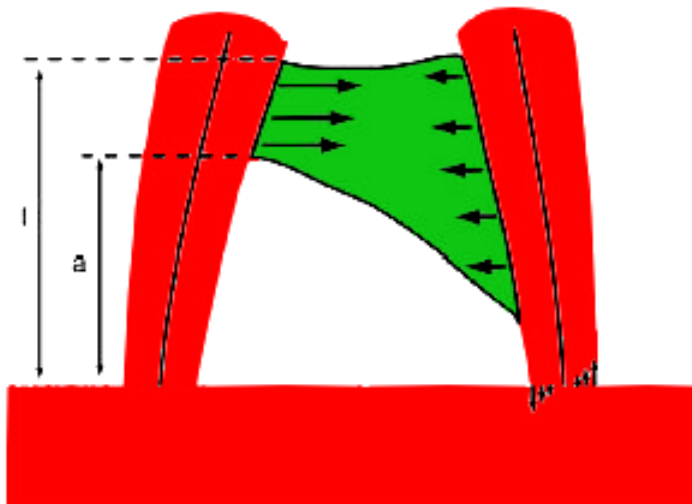
B)

Fig. 3-A Cell between the micropillars – A) *Model I* B) *Model II*. The arrows illustrate how the force is applied to the micropillars. Note that the highest point of cell-micropillar contact *l* can be lower than the micropillar top and that the lowest point of cell-micropillar contact *a* can be higher than the 'floor' level. Both *l* and *a* can differ for both micropillars connected by the same cell.
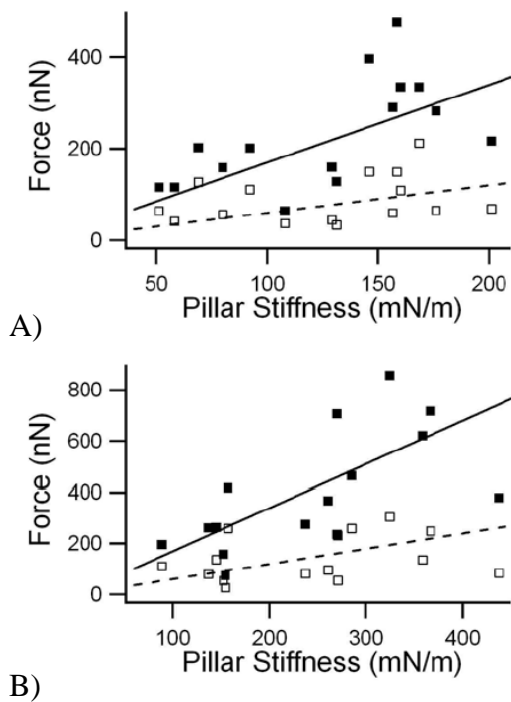
Fig. 3-B Myocyte contraction forces (filled squares: contracted state, open squares: relaxed state) plotted versus stiffness of micropillars. A) *Model I.* **Forces and stiffness evaluated assuming a point force at the highest cell point. B)** *Model II.* **Forces assumed to be equally distributed over the cell-micropillar contact. The lines correspond to a proportional law.**

For *model II* the following values for micropillar deflection are obtained for the forces during contraction of the cells (see Eq. 3-1): **1.6 µm and 0.6 µm** in contracted and relaxed states, respectively.

Analogically, for point force *model I*, we obtained 0.8 µm and 0.7 µm contracted and relaxed states, respectively.

The values obtained from *model II* remarkably match with the mean amplitudes of micropillar deflection in the respective states, see Table 2-1. This noteworthy fact can be understood as follows: since cells adhere to micropillars at random, cell properties and pillar stiffness were not correlated. Contraction amplitude and stiffness are uncorrelated random variables, whereas force is just the product of these two variables. In this situation a fit of the dependence of force on stiffness to a proportional law must yield the average value of the amplitude just as observed.

Model II seems to be more appropriate, as "our" myocytes adhered to the micropillars via costamers which indeed is distributed fairly uniformly over the contact area. Moreover, even cells that do adhere via focal adhesions usually exhibit dozens or hundreds of these

complexes. Therefore, the cellular force distribution cannot be expected to be due to a single point force exactly at the highest contact point between cell and micropillar.

3.3.1. CONTRACTION AMPLITUDE

The algebraic mean contraction amplitude, obtained in this work, 1.68 μm (see Table **2-1**) is in contrast with substantially larger values of cardiac myocyte contraction amplitudes observed by others (see Table 3-2). However, RELATIVE cell shortening measured in our experiment is similar to values obtained by several other authors, that is about 6%, see Table 3-2.

Table 3-2 Myocyte contraction amplitude.

authors	Approximate mean contraction amplitude (μm)	amplitude divided by cell length (%)
This work	1.68	~6
Han et al. (1998)	10	9,2
Herron et al. (2001)	25	~13
Lin et al. (2000)	19	~23
McDonald et al. (1998)	14	6.7
Ren et al. (2002)	10	~6
Tasche, et al. (1999)	15	20
Vizgirda et al (2002)	8	~9

3.3.2. CONCLUSION

The cell force magnitude vs. micropillar stiffness correlation may be explained by **cell's self-regulation of its contraction forces in order to achieve a constant contraction amplitude, not constant contraction force.** However, the "preferred" contraction amplitude varies from cell to cell which masks this regulation mechanism if the standard deviations of

measured amplitudes and measured forces are compared. It was already suggested by some authors that the cells may adjust their forces according to the stiffness of their environment (Saez et al. 2005, Choquet at al. 1997). It is a possible solution for cardiac myocytes as the heart should adjust to eject a given volume of blood (so given amplitude of contraction), not the force.

This is indeed the case for the whole heart muscle (Klabunde, 2004). **The Frank-Starling law of the heart (also known as Starling's law or the Frank-Starling mechanism)** states that the greater the volume of blood entering the heart during diastole (relaxation phase) the greater the volume of blood ejected during contraction. Thus, if the heart fills with more blood than usual, the force of the muscular contractions will increase. The force that any single muscle fibre generates is proportional to the initial sarcomere length and the stretch on the individual fibres is related to the end-diastolic volume of the ventricle[21].

Tesi and coworkers (2002) measuring the contractile forces of single myofibres, obtained the contraction forces per cross-section of about 10^5 N/m^2. Puceat at al. (1990) reported a similar value of 1.78 10^5 N/m^2. Based on that result, one calculates that already a cross-section area of several μm^2 would suffice to generate the average forces measured for whole cells in our experiment, c.f. Table 3-1. Thus, it seems likely that myocytes connecting micropillars with stiffness in the range of several hundred mN/m are limited not by the force they can generate but by the cell specific contraction amplitude.

This hypothesis could be tested by using the same kind of cardiac myocytes on micropillar arrays made of different *PDMS* mixtures. Then the chemical and geometrical properties of the micropillar would be the same but their stiffness would differ. If the hypothesis is true for cardiac myocytes, they would exhibit greater forces on stiffer micropillars and smaller forces on more compliant ones.

The hypothesis has also one important consequence. If the cells regulate their forces according to the stiffness of the environment, one cannot define the 'correct' cell force magnitude as it will differ even for the same cell depending on its environment. One could only estimate the maximal force magnitude a cell is able to apply by using very stiff material as cellular environment.

This does **not** mean, nonetheless, that measurements of cell forces are pointless. **Yet it means that cellular force measurements should be done in as biomimetic conditions as possible**. Chemical, mechanical and all other parameters of the cellular environment must be

---

[21] This is correct in a certain range only. At very large sarcomere lengths the overlapp of thick and thin filaments is too small and the force drops again.

similar to that *in vivo*; otherwise cells, adjusting to the change, may modify their behaviour significantly. By performing experiments in biomimetic conditions one may observe cellular forces **as they are** *in vivo* and so get information about the natural behaviour of cells.

Finally I would like to emphasize the fact that, as described it section **2.3** MODELLING OF ELASTICALLY ANCHORED PILLARS, there was significant force overestimation in previous experiments which applied the elastomer micropost bending. According to our calculations (see **2.3**), the overestimation is in the 25-37 % range. Although microposts are not usually used to measure cardiac myocyte contraction forces, they are a popular tool in studies of migrating cells and studies of forces on sub-cellular level (du Roure et al. 2005, Li et al. 2007). Commonly, no correction due to elastic anchorage of the microposts was done. Therefore, the published forces are overestimated.

3.4. CELL MORPHOLOGY

Cell morphologies changed spectacularly with the local environment of cells. Cells spanned between two micropillars were spindle shaped and relatively compact, see Fig. 3-C. Usually their length was below 40 μm. The identical cells adhering to flat substrates exhibited a very flat, pancake-like geometry, see Fig. 3-C. Their diameter was about 50 to 100 μm and their shape was highly irregular. I would like to stress again that it was the environment geometry only that varied – the cells displaying these two morphologies were present on the same substrate, made of the same elastomer of identical stiffness and chemical composition, immersed in the same medium. Cells adhering to a pillar and to the flat substrate at the same time often exhibited both morphologies. (see Fig. 2-A).

Such an adhesion selectivity has been already observed by many authors. Lateef and coworkers (2005) also observed cells wrapping around substrate protrusions. In their experiment, neonatal cardiac myocytes were allowed to adhere on flat silicone substrate with microscopic beads protruding from the substrate surface. Cells responded to polylysine or laminin-coated beads by either terminating at or wrapping around them. Boateng et al. (2003) observed a similar phenomenon, with myocytes attaching to micropillars 10 μm tall and several μm in diameter. Deutsch at al. (2000) described cardiac myocytes preferentially adhering to square micropillars (10 x 10 μm and 5 μm tall). Mata and coworkers (2002) studied cell-*PDMS* elastomer post interactions for human connective tissue progenitor cells. They noted that cells growing on flat surfaces exhibited a 'flat' morphology and their shape varied significantly from the shape of cells growing between *PDMS* elastomer posts.

It was observed by many authors that other substrate textures also influence cell attachment. For example, microgrooves cause cells to align along them (Deutsch et al. 2000, Curtis and Wilkinson 1997).

Generally, one observes a tendency of cells to treat substrate textures as anchoring points. This may be due to the fact that many cell types reorient when in contact with fibres of diameter in the 5–50 µm range (so called contact guidance) (Curtis and Riehle 2001, Badylak 2002). Micro-posts, beads and pillars are in that range and may induce a rearrangement response from cells.

3.5. CELL MECHANICS MODELS

3.5.1. ROLE OF FAS

It is generally accepted that cells transmit forces along cytoskeleton fibres (Geiger and Bershadsky 2001, Lauffenburger and Horwitz, 1996). In many cell types on flat and rigid substrates, focal adhesion sites (FAS), sophisticated protein complexes, serve to link the cell to their environment and to transmit cellular forces (Geiger and Bershadsky 2002, Hu et al. 2003, Sastry and Burrigde 2000). Thus, staining of cytoskeleton proteins could result in deeper understanding of cell force transduction and distribution. The question arose whether the differences of the cell outer geometry evoked pronounced changes in the cytoskeleton and in the adhesion structures. The answer is positive. The protein staining was made by B. Hoffmann and N. Hersch (Forschungszentrum Jülich GmbH, Jülich, Germany).

On flat parts of the substrate the cytoskeleton exhibited numerous, clearly visible actin stress fibres. Myofibres, responsible for cell contraction, were relatively unordered and mostly connected to stress fibres at their ends (Fig. 3-C). Stress fibres connected the myofibres to the surface via FAS (c.f. chapter 1.1.2 CYTOSKELETON).

However, FAS were not observed for myocytes adhered between two micropillars. In this case, actin stress fibres were basically absent. Instead, actin was predominantly organized in sarcomeric myofibres displaying a regular pattern of prominent Z-bands (Fig. 3-C). The allocation of adhesion proteins indicated absence of FAS. Instead, the cell and the micropillar were linked by costameric protein complexes at the site of Z-bands (c.f. chapter 1.1.2 CYTOSKELETON). This type of adhesion together with the absence of stress fibres bears a close resemblance to myocyte

morphology in the myocardium (heart tissue). Thus it implies close to native growth conditions in the micropillar system.

Focal adhesion structures are highly dynamic, assembling and disassembling according to cellular needs. They consist of at least 50 different types of proteins, linked with intricate network of correlations among themselves and with other types of proteins (Martin et al. 2002, Giancotti & Ruoslahti 1999, Giancotti 2000, Zamir & Geiger 2001). Costamere and FAS differ in their protein arrangement. Different kinds of cell-ECM adhesion complexes can be found in the same cell (Katz et al. 2000). FAS appearance seems to be connected with increased ECM rigidity (Tomasek 2002, Wang et al. 2003). Thus, cells adhering to micropillars may not form FAS due to the lower rigidity they sense.

There are several other models describing FAS and stress fibre formation (Novak et al. 2004) or describing estimation of cellular force magnitudes and directions (Schwarz et al. 2002 and 2003) in case of cells adhered to flat surfaces. They correctly foresee such phenomena like pancake, irregular cell shape, formation of FAS on the cell periphery etc. They are very useful when describing cells in 2D environment. Their applicability to the 3D environment of cells in our experiment is, I believe, limited. First, we observed neither FAS nor stress fibres, described by those models. Second, the models treat cells as two-dimensional which is not a good approximation of our myocytes. However, the model proposed by Deshpande et al. (2006), though developed for a 2D case, can be useful in the case of our myocytes as well. It assumes that cellular forces are not strongly correlated with big stress fibres but can be transmitted by tiny fibres that cannot be visualized by staining techniques. Deshpande and co-workers discuss a square cell attached to four elastic supports by sets of springs. Modifying the model by introducing a rectangular- or parallelogram-like cell stretched between two supports one would obtain a model resembling our myocytes.
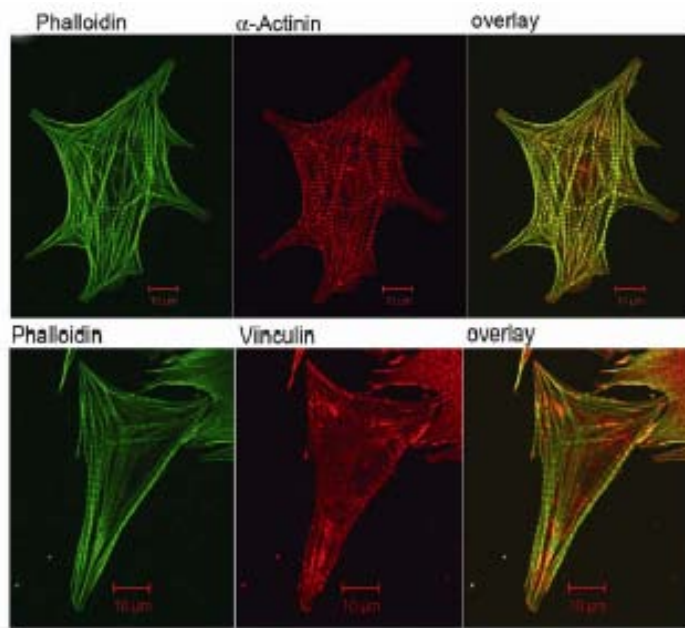
A)
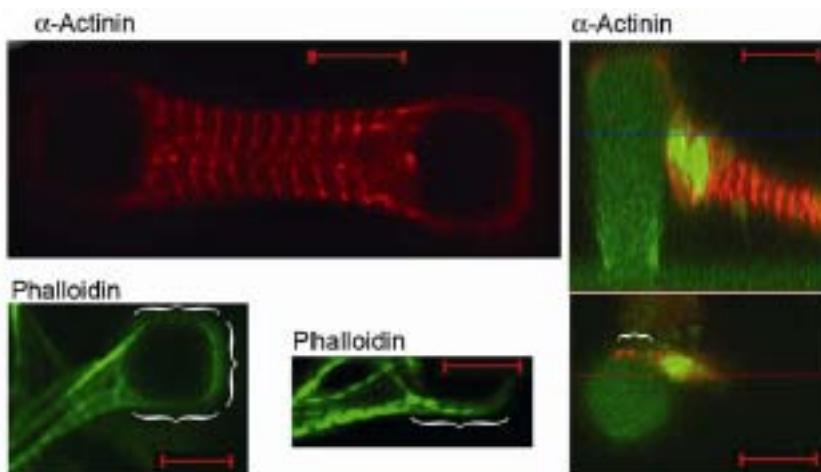
B)

Fig. 3-C Cardiac myocytes incubated for two days on either flat glass surfaces A) or *PDMS* elastomer micropillar arrays B). After fixation, cells were immunofluorescently labelled for actin (phalloidin, green) and cytoskeletal α-actinin (red). Some cells on glass were labelled for vinculin (red) instead of α-actinin. Note the DID staining of micropillars (green) is partially present in B), right. Here, a top view at the height indicated by a blue line is given below the side view. Brackets mark close sarcomere (phalloidin, green) and costamere (α-actinin) contact of myocytes to the micropillars. Scale bars, 10 μm.

3.5.2. OTHER CONCEPTS

1. **Cellular tensegrity**. The idea of tensegrity ("tensional integrity") was created by the architect R. Buckminster Fuller and the first tensegral structures were constructed by the sculptor K. Snelson. Tensegrity refers to the interplay between tension and compression members in any structure[22]. A tensegrity structure is composed of a tensed network of parts (prestressed cables or wires and other supporting elements that resist compression like stiff bars). The overall structure is very stable because the forces transmitted in both types of elements cancel. In particular, the tensegrity concept was applied to describe the mechanics of organisms, tissues, cells and complex molecules (Ingber 1998, 1998a, 2003, 2003a, 2003b, King 2005). The cellular tensegrity concept predicts such phenomena like cell stiffening under stretch which was observed for cardiac myocytes by le Guennec et al. (1990) and Bluhm et al. (1995), describes the cell – ECM interactions indeed observed, like irregular, pancake cell shape on flat surfaces (Ingber 1998, 1998a, 2003, 2003a, 2003b, King 2005). Also Bar-Ziv et al. (1999) considers the balance between cytoskeleton compression and cellular membrane surface tension as decisive for cell shape. The cellular tensegrity concept treats cytoskeletal microfilaments and intermediate filaments as tension bearing elements, while the microtubules are considered to be under compression. However, individual filaments can have both functions and (e.g. actin filament bundles bear compression in filopodia) (Ingber 1993, 2003a, b).

2. **Erythrocyte models** (Boey et al. 1998, Discher et al 1998), which treat the mammalian erythrocyte (red blood cell) membrane as a triangulated dome, wrapping the cell. Due to this highly elastic and robust structure, erythrocytes are able to resist bending forces they face as they are forced through blood capillaries. As some authors, including Fuller, consider triangulated dome structure as another type of tensegrity structure (Ingber 1998, 1998a 2003, 2003a, 2003b), the erythrocyte model can be, in my opinion, viewed as a tensegrity concept tailored to the specific architecture of the mammalian red blood cell. Therefore, the erythrocyte models are not a competition but a completion of the tensegrity concept.

3. **Soft glass** hypothesis – an interesting model, comparing the behavior of cells under stress to the behavior of glasses under temperature changes (Nguyen and Fredberg

---

[22] The idea is ancient: for example tents and sail ships are stabilized with guy ropes (which transmit tension) and poles or masts which undergo compression. Buckminster Fuller and Snelson realized that this principle can be widely used in architecture. This change of paradigm from predominantly compression bearing structures in architecture to a mixture of tension and compression elements was possible only because old fashioned building materials like stone and mortar which are strong under compression only were replaced by more modern materials like steel, plastic or reinforced concrete which are also resist tension well.

2008, Gunst and Fredberg 2003). Glasses change their fluidity as the temperature changes, behaving like an elastic solid in lower and like a viscous fluid in the higher temperatures. Their mechanics is viscoelastic: they have "memory" i. e. their behavior depends on how the stress was applied to them earlier (Taub and Spaepen 1981; Tervoort 1996). Moreover, glasses are NOT in thermal equilibrium. Their behaviour is described by several, not just one relaxation time (divergence of relaxation times) (Sastry et al. 1998; Tervoort 1996) or their responses to external forces are not tied to any particular relaxation times and are thus scale-free (Sollich 1998). Interestingly, living cells also show viscoelastic behaviour, including scale-free relaxation behaviour, creeping and aging. They are also out-of-equilibrium systems (Bursac et al. 2005; Kumar et al. 2006; Lenormand et al. 2004, Maksym et al. 2000).

However, according to the authors the soft glass model, is inappropriate for the striated muscle (Gunst and Fredberg 2003). Therefore it may be not optimal to describe cardiac myocytes. Nonetheless, I believe the model is well worth of consideration and further experiments as it nicely combines the mechanical and chemical changes in the cytoskeleton. What is more, the model bears resemblance to the 'sol-gel' transition model, described below.

4. The **'sol – gel'** model, being actually a set of several models assuming that a cell reacts to stress by crosslinking and uncrosslinking cytoskeleton proteins (Janmey et al. 1990, van Citters et al. 2006, Xu et al. 2000). The oldest models assume an actin sol – gel transition under shear or stress but more recent experiments conclude that the mechanism must be far more complex and is not well understood yet. Like the soft glass model, it stresses the chemomechanical coupling in the cell and bases on a 'phase transition' of the cytoskeleton. Thus, I think the both models may be actually considered as parts of one, more general model, especially that Kumar et al. (2006) combined both approaches.

5. The **percolation** model (Forgacs 1995) which concentrates rather on HOW the information is propagated inside the cell on any specific mechanical mechanism. The percolation model stresses the need of redundancy and the corresponding robustness of the disordered molecular network. According to the author, the tensegrity concept lacks redundancy which makes it fragile to any disruption. The more advanced tensegrity concepts, however, do not suffer any more from that problem: the cell is treated as a multimodular tensegrity structure which accounts for the fact that redundancy is omnipresent in the cell (Ingber 2003b). Should some parts of it be destroyed, only a few modules would collapse. Therefore Forgacs believes – and I agree with him – that percolation model can be considered not the competition but completion of the tensegrity concept.

The above list is by no means complete. However, one can group the existing models in three categories: tensegrity based, phase transition based and percolation based. Each group stresses one – equally important in my opinion – cellular feature. Tensegrity based models shows how the cytoskeleton is able to sense, transfer and exert forces mechanically. It sees the cell as a highly complex, dynamic and sensitive "scaffold". Phase transition models couple the chemical and the mechanical processes in the cell while the percolation model deals with the redundancy and disorder of the cytoskeleton. In my opinion, it is the tensegrity concept which describes the cardiac myocytes best. It is because they are cells which evolved to exert strong forces in a regular and controlled pattern, cells whose role is to create mechanical work. Therefore, they seem to fit well into the model which concentrates on mechanical aspects of the cell behaviour. Nonetheless, the other models should not be disregarded. I believe that each cell could be best described by their combination. Moreover, there is no single model – neither their single combination – that is optimal to describe all kinds of cells and tissues. The diversity of cell properties of the same organism is incredible and each type of cell should be treated individually.

3.6. FREQUENCY AND RHYTHM OF MYOCYTE CONTRACTIONS

Beat amplitude and rhythm varied between cells and for a single cell (see chapter 2.2 CELL CONTRACTION). Some cells were 'stuttering' i.e. missing some beats. Rhythm irregularities are typical for healthy hearts. Breath rhythm, stress, day-night rhythm are commonly given reasons for heart rate variability but the problem has not been fully understood yet (Kristal-Boneh et al. 1995). Rochetti and coworkers (2000) observed contraction rate variability for isolated rabbit sinoatrial[23] myocytes; they also described the dependence of the contraction irregularity on acetylocholine. Wilders and Jongsma (1995) constructed a model for describing single myocyte activation. They concluded that fluctuations in interbeat interval opening and closing of single sinoatrial node pacemaker cells they investigated were due to the stochastic opening and closing kinetics of the ion channels in the cell membrane. Thus, the contraction rate and amplitude variability observed in our experiment may be intrinsic property of the cardiac myocytes. Moreover, local variation of the environment, for example like coverage with ECM proteins, crosslink density or local sub-micron roughness may also influence cell behaviour.

However, no time series analysis of beat series was possible because the measured series were too short[24]. It was decided, however, not to scan beating cells for longer periods of time

---

[23] obtained from so called sinus node (part of the heart) which is one of the heart pacemakers
[24] They contained a small number of contractions – usually less than 20.

in order to keep cell damage as low as possible for further analysis. In this respect it should be noted that confocal laser scanning microscopy may damage the cells within minutes unless care is taken to keep the laser power very low. To diminish the possible laser damage, mainly caused by radicals produced by photobleaching, the laser power was kept as low and the scanning speed as high as it was possible without compromising the picture quality. Moreover, only the micropillars were stained before cell contraction filming which decreased the number of radicals produced inside the cells considerably.

APPENDICES

APPENDIX A: YOUNG'S MODULUS AND POISSON'S RATIO

YOUNG'S MODULUS *E*

For a rod of initial length l and cross-section area A, $\vec{F}$ is defined as the force needed to elongate it to the length $L+\Delta L$ (ΔL is the change of rod length caused by the force, see Fig. A-1). The **elastic modulus E (Young's modulus**) is given by Hooke's law:

$$\frac{|F|}{A} = \frac{E\Delta L}{L}$$

Eq. 1A

Therefore:

$$E = \frac{|F|L}{A\Delta L}$$

Eq. 2A

For linear elastic materials E is time independent; for isotropic ones E also does not depend on direction. Young's modulus unit is N/m^2 or Pascal (Pa). For comparison, Young's moduli of several materials are as follows: *PDMS* rubber (depending on the base material to crosslinking agent ratio): 28 kPa for base material and crosslinker in 55 : 1 ratio (Cesa 2007) to 850 kPa for base material and crosslinker in 5 : 1 ratio (Armani et al. 1999); polystyrene 3.37 GPa (Lubarsky et al. 2004), SU-8 photoresist (cured): 4.4 GPa (Guerin 2005); glass 65-90 GPa (Fluegel 2007).

POISSON'S RATIO *v*

Change in length normalized to length is called **strain ε**:

$$\varepsilon = \frac{\Delta L}{L}$$

Eq. 3A

For an elongated rod, we can distinguish longitudal extension strain $\varepsilon_{//}$ (a stretched rod elongates) and transverse contraction strain $\varepsilon_{\perp}$ (the rod gets thinner). The initial rod width w[25] decreases by Δw during stretch. **Poisson's ratio v is the absolute value of the ratio between $\varepsilon_{//}$ and $\varepsilon_{\perp}$:**

$$v = -\frac{\varepsilon_{\perp}}{\varepsilon_{II}}$$
Eq. 4A

where $\varepsilon_{\perp} = \Delta w/w$ and $\varepsilon_{//} = \Delta L/L$

The negative sign in Eq. 4A comes from the fact that Δw is negative (the rod diameter decreases during stretch). It is easy to see that Poisson's ratio is a dimensionless parameter; for uncompressible materials $v = 0.5$. Common materials like concrete or steel have v between 0.2 and 0.3.
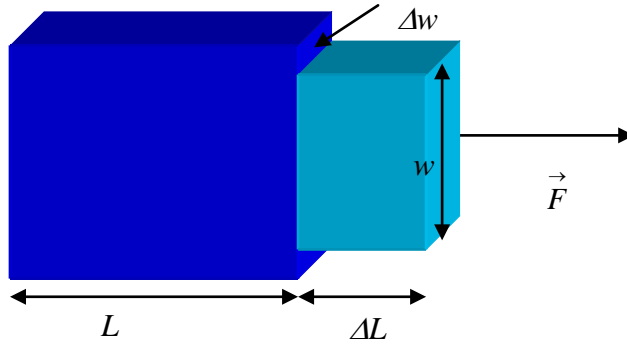
Fig. A-1 Young's modulus and Poisson's ratio schema. Young's modulus E is the force per area, necessary to induce material elongation by an unit value ; Poisson's ratio is the ratio of cross-sectional area change to the change of length during stretching or compression.

For *PDMS* elastomer, prepared from base material and crosslinker in 20 : 1 ratio, the following values were obtained:

$E = 608 \pm 20$ kPa (for 6 samples)
$v = 0.49 \pm 0.04$

---

[25] I use *w* instead of commonly used *l* to describe rod width in order to avoid confusion with another meaning of symbol *l* already present in this work

APPENDIX B: CHEMICALS AND MATERIALS

SU-8 25 PHOTORESIST

SU-8 (MicroChem) is a family of high contrast[26], epoxy-based photoresist mixtures. *SU-8's* have very high optical transparency above 360 nm, which makes them ideal for imaging near vertical sidewalls in films of great thickness[27]. *SU-8s* are **negative photoresists** which means that it is the irradiated part of the photoresist that remains and the non-irradiated is removed in further processing. As the photoresist layer turns hard and resistant to many chemical agents, *SU-8* is well-suited to create matrices that can be repetitively used over time. *SU-8* compound molecules can be seen in Fig. B–1. Chemically, *SU-8* is a mixture of γ-butyrolactone (22-60%) as a epoxy resin solvent, mixed with triarylsulfonium-hexafluoroantimonate salt (catalyst), propylene carbonate (1-5%) (a polar, aprotic solvent, added to increase salt solubility) and epoxy resin (35-75%) – the main photoresist compound which polymerizes when exposed to UV light (I used 365 nm wavelenght). The polymerization reaction schema is depicted on Fig. B–2. The exact composition varies between the different SU-8 photoresists, giving them various properties - each member of *SU-8* family is optimised for different layer thickness. For the needs of this experiment *SU-8 25* was used, capable of forming 15-40 µm thick layers.

After *SU-8* is exposed to UV light, a special *SU-8* **developer** (MicroChem), 1-methoxy-2-propyl acetate, can be used to remove the unwanted parts of the photoresist.

WAFERS

3'' **silicon wafers** single-side polished (Si-Mat – Silicon Materials, Landsberg am Lech, Germany) of <100> crystallographic orientation and 1-10 Ω·cm resistivity were used as substrates for photolithography processes. Doping of the wafer was not of vital importance, as no integrated circuits were created[28]. Therefore, price and availability only were taken into consideration when choosing the wafer type. Still, only one type of wafer was used to ensure

---

[26] it means that the border between the irradiated and non-irradiated parts of the photoresist is sharp.

[27] the photoresist is irradiated with light of a specific wavelength. In order to assure that the structures created in this way have proper depth and vertical walls, the light must penetrate the photoresist deep and without scattering. Therefore, the photoresist must be transparent for the irradiating light.

[28] Doping is adding a small amount of other substances to pure semiconductor materials. Even small amounts of the doping material affect conductivity of the semiconductor tremendously. In this case, however, as no electrical circuit was created, wafer conductivity was not important.

experiment repeatability and exclude unexpected variations stemming from wafer variability. Si wafers were preferred to GaAs ones due to their nontoxicity.

PHOTOMASK CLEANING AGENT – HOT PIRANHA

This (aptly named) mixture consisted of hydrogen peroxide (30% H_2O_2 solution, medical, extra pure) and sulfuric acid (95-97% H_2SO_4, pro analysis) mixed in 1 : 2 (or 1 : 3) ratio. It is usually used as heavy duty glass cleaner, removing even the most stubborn organic residues. This caustic and explosive mixture should be never made or used by a person without experience in handling dangerous chemicals! Proper protection – acid gown, thick gloves and a face mask is mandatory. Fresh Hot Piranha mixture is indeed hot, as the reaction between the peroxide and the acid releases a huge amount of heat so caution must be taken when handling hot containers.

A dirty chromium mask was slowly immersed into Hot Piranha solution for about 8 minutes and then rinsed in deionised water (16 minutes immersion in flowing water). The mask was then dried in a nitrogen stream.

PDMS ELASTOMER - SYLGARD

Sylgard (Dow Corning GmbH, Wiesbaden, Germany), is a highly elastic polymer, perfect for micromolding. It forms by crosslinking out of poly(dimethylosiloxane) – *PDMS* linear polymer**.** *Sylgard* has good thermal and chemical stability and is permeable to gases but not hygroscopic (does not swell when in contact with water or humidity). Crosslinked *PDMS* elastomer is also transparent for light wavelengths in the visible range what makes it useful in microscopy. Also, it is biocompatible i.e. well tolerated by living cells. Moreover*, PDMS* rubber is homogenous and isotropic facilitating mechanical studies considerably. All these properties make *Sylgard* an optimal material for micropillar experiments.

Out of numerous silicone rubber types, Sylgard 184 was used in our work; it consists of base and crosslinking agent (plus platinum catalyst). The base agent contains siloxane oligomers with vinyl groups; the crosslinker – oligomers with at least 3 silicon hydride bonds each. The catalysts accelerates the reaction between base and crosslinking agent in which a Si-H bond is added to a vinyl group, forming Si-CH_2-CH_2-Si links (see Fig. B-3). The reaction starts when the base and the crosslinker are mixed and is accelerated by heat. As a result, a three-dimensional elastomer mesh is formed. Elastomer stiffness increases with crosslink density.

Mixing base and the crosslinker in different proportions results in *PDMS* elastomer of varied stiffness but the same chemical structure; *PDMS* rubber is therefore ideal for experiments where the influence of different mechanical stimuli is to be tested in a chemically uniform and stable environment. *PDMS* components have to be shaken before use and mixed throughout to obtain uniform meshwork; the mixture must be subsequently degassed to remove air bubbles.

PDMS PREPOLYMER MIXTURE PREPARATION

.

PDMS elastomer consists of base and crosslinking agent which have to be mixed in order to start the polymerisation reaction. Using different ratios of the two ingredients, elastomers of different mechanical properties can be created. The Young's modulus increases if more crosslinking agent is added as its molecules crosslink base oligomeres. Thus, a three-dimensional mesh of polymer is formed and the more crosslinking molecules there are, the stiffer the mesh is.

The prepolymer mixture was prepared in a desired base to crosslinking agent ratio in a 50 ml Falcon tube and carefully mixed with a metal rod to ensure uniform mixture. As polymerisation began immediately upon first contact of both materials, the prepolymer was prepared directly before substrate preparation and used immediately after mixing. The prepolymer was then poured on the photoresist masters and degassed for 30 min.

Young's modulus and Poisson's ratio for *PDMS* rubber were measured with the method described by Cesa (2007). Briefly, thin *PDMS* elastomer rods were slowly stretched with the stretch force being registered. Rod elongation and diameter change were quantified with essentially the same set-up described in Appendix E for the measurement on a magnified model of the pillars. Evaluation of the measurements was done with stand-alone routines written by Dr Norbert Kirchgeßner (Forschungszentrum Jülich GmbH) using the MathLab software release 14. I am grateful to Norbert Kirchgeßner for the enormous amount of work and know-how he put into creating the software.
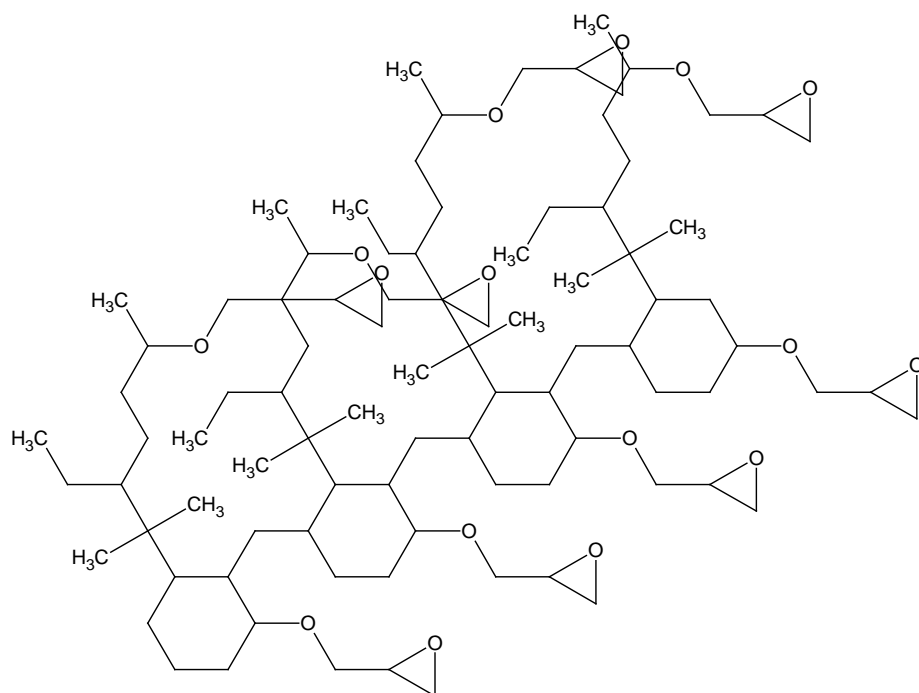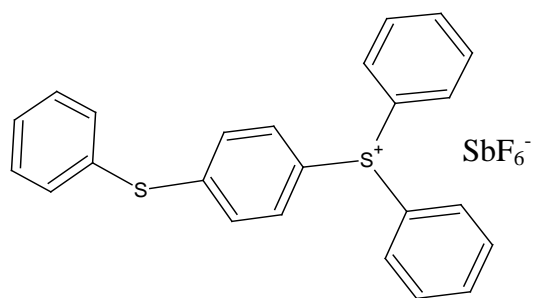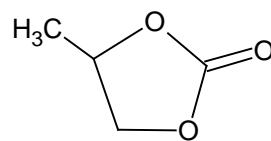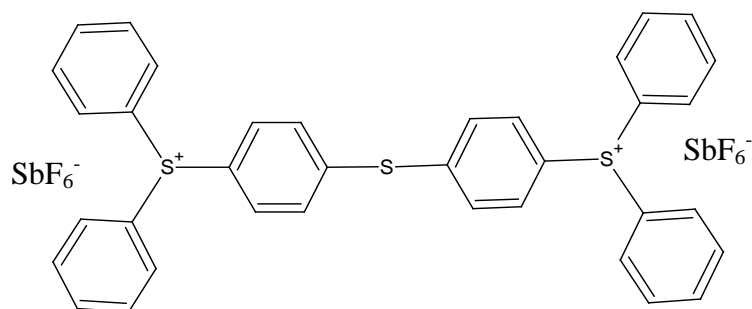
Fig. B-1 *SU-8* **compounds (after Sigma-Aldrich and Guerin (2005)) A)** *SU-8* **molecular structure (a fragment),   B) triarylsulfonium/hexafluoroantimonate   salt   C)   gamma-butyrolactone, D) propylene carbonate**
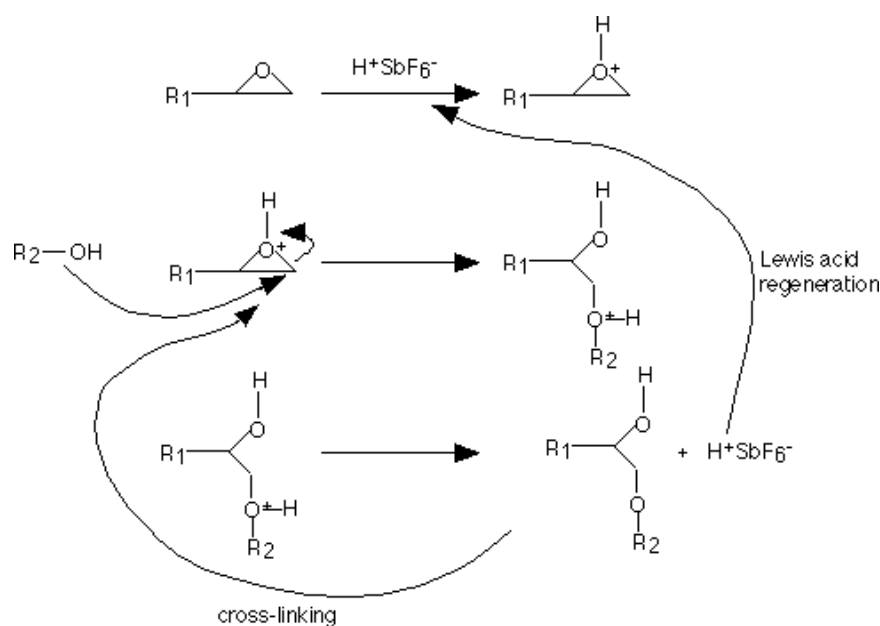
Fig. B-2. *SU-8* **crosslinking. The hexafluoroantimonate salt (H+SbF6-) catalyses the process. Upon exposure, crosslinking proceeds in two steps: formation of a strong acid (H+SbF6-) during the exposure process, followed by acid-initiated, thermally driven epoxy crosslinking during the post exposure bake (PEB) step. After (Guerin 2005).**
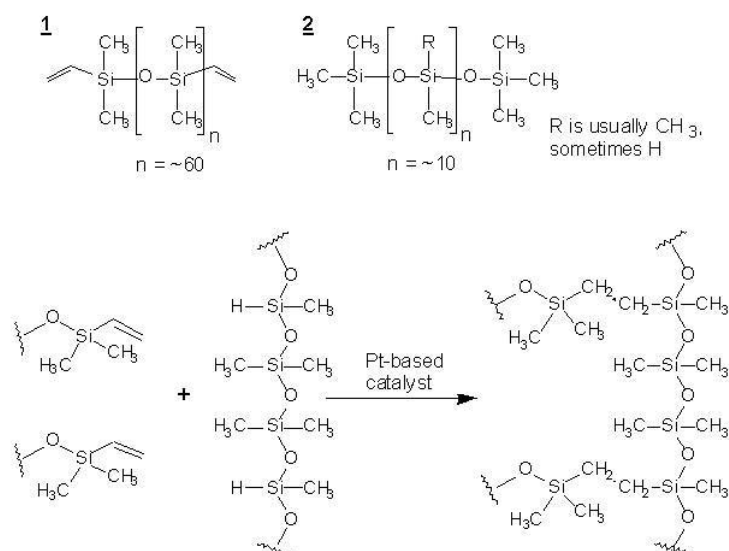
Fig. B-3 *PDMS* **crosslinking. 1. A base oligomere, containing vinyl groups. 2. An example of an crosslinker molecule. The oligomeres react, forming a three-dimensional mesh. Image taken from Cesa (2007).**

SILANE

If *PDMS* elastomer is cured on silicon wafers, it adheres so strongly to their surfaces that subsequent separation is practically impossible. Thus, in order to minimize adhesion between silicon and *PDMS* rubber, the wafers have to pretreated before first use. As described by Cesa (2007), silanization is a quick and reliable procedure to reduce adhesion between silicon wafer and silicone rubber.

Silanization is the process of silicon surface passivation with the help of a long-chain fluorinated alkylchlorosilane. The silane reacts with free hydrodyl groups on the surface of the wafer, forming a surface with low interfacial free energy. This thin layer serves as releasing agent, facilitating the separation of silicone rubber from the wafer. Many types of chlorosilanes are available. $[CF_3(CF_2)_5CH_2CH_2SiCl_3]$ (1H,1H',2H,2H'–perfluorooctyl–trichlorosilane) (Sigma-Aldrich, Fig. B-4) was chosen for our work.
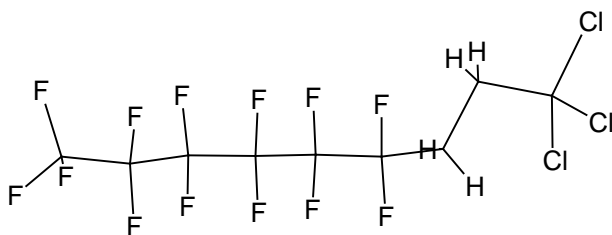
Fig. B-4 The chemical structure of the silane used here (according to Sigma-Aldrich).

SILANIZATION

Following Cesa's receipt, the wafers were cleaned in 2-propanol and dried in nitrogen stream. The wafers were then placed horizontally in an desiccator and a silane drop was added to the desiccators, below the masters (see Fig. B-5). The desiccators was closed and pumped out. Silane vapors adhered to the wafer surfaces. After about 15 min. at room temperature the masters were removed and used for *PDMS* elastomer formation.

As the masters could be used several times, they had to be cleaned after each use. For that purpose, they were placed into n-heptane and gently shaken with a rotary shaker overnight. Subsequently, they were dried with a nitrogen stream and re-silanized. Thus, each master could be used twice a week.
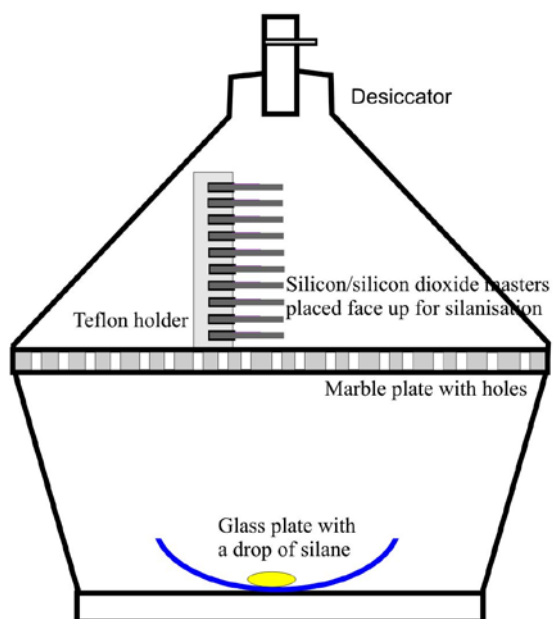
Fig. B-5. Silanization. The device used to silanized the masters. It is essential that the whole master is exposed to the silane vapours. (after Cesa 2007).

APPENDIX C: PHOTOLITHOGRAPHY AND MICROMOLDING

PHOTOMASK CREATION PROCESS

The photomask is a transparent quartz glass plate covered with a chromium pattern created by **Electron Beam Lithography**. **EBL** is a lithographic process using a focused beam of electrons to write patterns into photoresist layers. Electron lithography offers higher resolution than optical lithography because electron optics can easily achieve much higher resolutions than optical imaging. The most common application of EBL is writing of chrome-on-glass masks. An EBL system needs no mask itself but 'draws' the pattern in the photoresist using the electron beam as its 'pencil'. Thus, EBL systems produces the mask 'point by point' while optical lithography copies the pattern as a whole. As a drawback, EBL works slowly compared to conventional photolithography.

A typical EBL system consists of:

a) an electron gun or electron source
b) an electron beam focusing optics
c) a mechanical stage that positions the wafer under the electron beam, a wafer handling system
d) a computer system to control the equipment

A Leica lithography system (EBPG-5HR Leica, Germany) was used for our project. Writing of the mask was kindly done by Mrs. Mona Nonn, ISG, Froschungszentrum Jülich, Germany. The EBL set-up is depicted on Fig. C-1.

As quartz glass is transparent to UV light while chromium is not, a photomask is used to transfer patterns into photoresists in photolithographical processes. Before the mask is created, the file describing the aforementioned pattern must be written. The file may either contain the geometric layout or the mathematical description of the desired structure. Usually, a CAD program is written for this purpose.

Blank masks used in this work were square (5×5 inch) quartz glass plates. The factory (Hoya, Tokyo, Japan) covered them with a chromium layer (80 nm thick) and a negative

photoresist layer (SAL 601, 500 nm thick). The protocol described below was optimised for SAL 601 only – other photoresists may require different procedures.
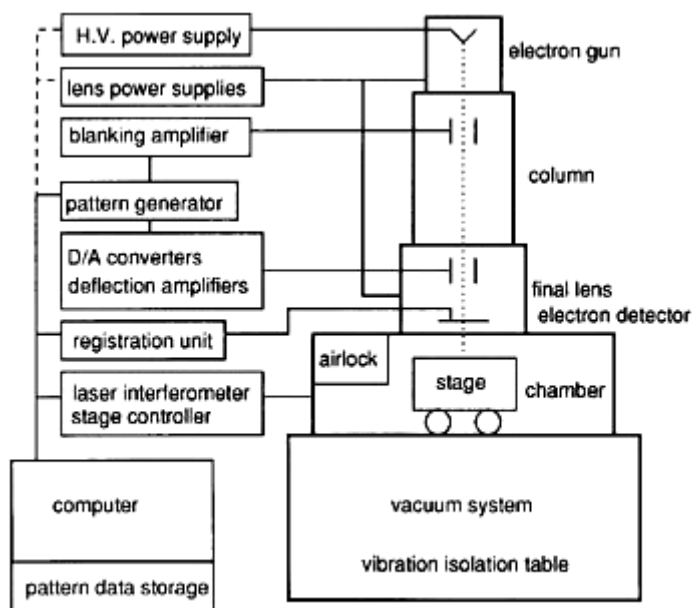
Fig. C-1. EBL set-up. Image taken from (Rai-Choudhury 1997).

The typical mask creation proceeded as follows:

1.   **Exposure** to electron beam. The negative photoresist *SAL 601* crosslinks when exposed to electron beam so in subsequent steps the exposed part of the photoresist would stay on the mask whereas the unexposed would be washed away during the developing step.

2.   **Post-exposure bake** (2 min. at 105°C) allowed the reactions started by exposition to spread through the whole photoresist layer uniformly. Therefore, post-exposure bake made the photolithographic process more controllable and reproducible.

3.   **Development** – here the uncrosslinked photoresist was washed off the mask. A mixture of *AZ 400K* developer (Clariant, Somerville, NJ, USA) and deionized water in 1 : 2 ratio was used for the purpose. The developing process was stopped by dipping the mask into deionized water.

4. **Control and further development** (if necessary): The mask quality was checked under the optical microscope after the development. If underdeveloped, the structure was developed again.

5. **Hardbake** – which allowed photoresist polymerization to continue through the whole layer thickness, resulting in polymer hardening and longer mask usability. Hardbake was performed in three steps: 15 min. at 100°C, 15 min. at 130°C and finally 15 min. at 150°C.

6. **Etching.** The etching time varied from 10 to 120 s and was conducted with AMR80 plasma reactor (Oxford Instruments, Tubney Woods, UK). Due to electron scattering (mainly backscattering at the photoresist-Cr interface), the dimensions of the structures may be wider than expected. Backscattering caused an extra amount of photoresist to polymerise at the base of the structures or may even result in formation of a thin polymer film on the photoresist surface. Additional etching was then necessary to remove the unwanted crosslinked photoresist.

    a) The thin polymer layer could be removed with oxygen plasma (so called descumming). Descumming affected the patterned areas as well, but if only little of the total photoresist amount was removed, the impact of descumming on the patterned part was negligible.

    b) Wet etching was used to remove these chromium areas that were no longer covered with photoresist. Etching was done by dipping the masks for about 1 min. in a special chemical mixture named Chrom-etch (MicroChemicals). Etching was stopped by immersing the mask in deionised water. Masks were subsequently dried with a gentle nitrogen stream.

   c) The remnants of the photoresist were removed with oxygen plasma.

PHOTOLITHOGRAPHY

The standard photolithographical procedure consists of the following steps:

1. Wafer pretreatment
2. Spin-coating
3. Pre-exposure bake
4. Exposure
5. Post-exposure bake
6. Development
7. Testing
8. Hard-bake

1. The wafer surface must be **clean and free of dust particles** so that the photoresist layer would be uniform all over the wafer. A 3'' wafer was taken out of the wafer box under clean-room conditions and its surface was dusted with a nitrogen stream (for more information about wafers, see Appendix B). No chemical **pretreatment** of the wafer surface was necessary. The only pretreatment was dehydration – removing a thin water layer that inevitably condensed on the silicon surface. Dehydration was done by simply heating the wafers on a hot-plate (ca. 10 min. at 180°C). If the dehydration step were skipped, the photoresist might not adhere to the wafer properly which would result in *SU-8* peeling off during development.

2. The wafer was placed on the rotating holder (a chuck, see Fig. C-2) of the spin-coating machine, carefully centred and fixed. If centring is neglected, the photoresist layer is uneven. The photoresist drop should be placed in the centre of the wafer; pouring must be slow and cautious so that no air bubbles form in the photoresist and no dust particles get trapped within. For *SU-8* it was found best to transfer the photoresist directly from the original bottle since usage of pipettes causes formation of air bubbles in the photoresist. About 1/3 of the wafer surface should be covered with photoresist. The wafer with the photoresist drop was accelerated till the desired rotation speed was reached and was spun at constant speed for a while. The wafer was spin-coated with 2000 rpm (rotations per minute) speed to produce a *SU-8* photoresist layer about 25 μm thick. During rotation the photoresists spread all over the wafer surface and some solvent evaporated. On the wafer edge, a thicker photoresist layer (the built-up edge) accumulated during the spinning; it was removed by letting the wafers rest (horizontally) at room temperature for several minutes. To ensure the sticky photoresist layer was not contaminated with dust, the wafers were covered with beakers during this period. Should an air bubble or any other kind of contamination destroy the uniformity of the photoresist layer in any way, the wafer was thrown away. The thickness of the final photoresist layer depended on photoresist properties like viscosity, surface tension or drying rate but was independent of the amount of the liquid. If too little photoresist was poured, the wafer surface was not uniformly covered; photoresist excess was removed during spin-coating.

3. The wafers underwent the **prebake** step, serving to remove excess solvent from the photoresist. Unnecessary solvent may cause wafer-mask sticking during the exposure step and by increasing the mobility of photoresist molecules (since they keep the photoresist in a liquid state), it could destroy structures written into the photoresist. Additionally, prebake relaxes inhomogeneities that remained after spin-coating. The photoresist was prebaked for 5 min. on a hotplate at 90°C and then left to rest for about 5 min. at room temperature. *SU-8* photoresist tended to shrink during baking;

therefore some wafers, on which shrinkage was huge, could not be further used. The shrinkage may also contribute to the observed slight variation of photoresist thickness from wafer to wafer.
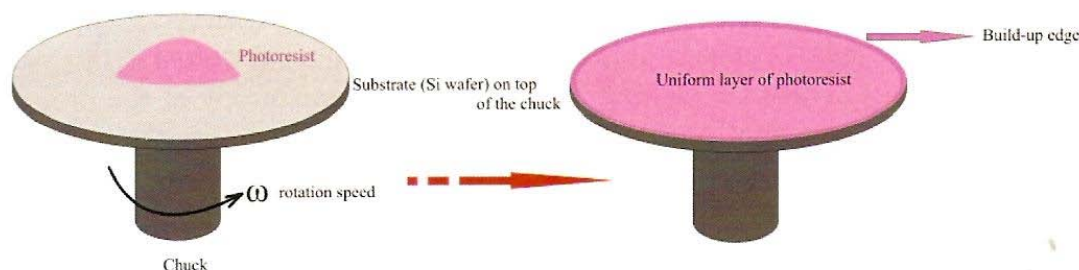
Fig. C-2 A drop of photoresist is placed in the middle of the wafer held by the spin-coating chuck. The chuck rotates, causing the photoresist to spread. (Picture taken from Cesa 2007).

4. The photomask and the wafer were mounted on mask aligner (MA6, Karl Süss, Germany) to be **exposed to UV radiation**. The apparatus was equipped with a mercury arc lamp having a strong emission line at 365 nm. Exposure time depended on the lamp power, photoresist sensitivity and thickness and structure size. The wafer was mounted on the mask aligner, dusted and brought into contact with the photomask. **The mask must be cleaned before and after each use to ensure proper alignment during exposure**. This was done in a mask cleaner APT 195 (Applied Process Technologies, San Jose, USA) or by rinsing the mask with isopropanol and acetone. The mask was dried in a nitrogen stream. It is extremely important that the photomask is clean and the photoresist layer even: inhomogeneities result in replica failure. Exposure time was 25 s and the wafer was allowed to rest for about 5 min. before the next step.

5. The exposed wafer underwent a **post-exposure bake** (PEB) step. PEB ensured that the chemical reactions triggered by UV light continued and spread uniformly through the exposed areas of the photoresist. *SU-8* is a negative photoresist which means its exposed parts polymerised and turned insoluble while the unexposed parts remained uncrosslinked. Postbake is a crucial and critical step, as both time and temperature must be controlled meticulously and, moreover, their optimal values depend greatly on the transferred pattern. The wafers were heated for 30 s at 90°C on a hotplate and then left to rest for at least 15 min. at room temperature.

6. The photoresist was finally **developed**. The wafer was immersed into a suitable developer (see Appendix B). It removed the uncrossliked photoresist while leaving the crosslinked parts intact. As the result, a three-dimensional 'copy' of a pattern written

by the photomask was formed. The wafer was gently agitated manually to speed up developing. **Since no overdeveloping is possible and as underdevelopment is hard to notice for this kind of structure, longer development times should be preferred when in doubt.** The developing process was stopped by immersing the wafer in isopropanol and agitating it manually. The developed wafer was blown dry with a nitrogen stream. For the structures created in this work, at least 6 min. of development was needed.

7. The final **hardbake** step serves to ensure greater mechanical stability of the photoresist. It was skipped as the photoresist turned out to be very stable.

The protocol described above was optimised for 10 x 10 µm structures on the photomask that would give about 25 µm deep 'microholes' in the photoresist. It turned out to be impossible to obtain 10 x 10 as well as 5 x 5 µm structures during same preparation as not only the instruments and chemicals but also the pattern characteristics affect the process parameters.

Summarizing, the parameters of the process were as follows:

1. Wafer pretreatment: 180°C, 10 min.
2. Spin-coating: 2000 rpm
3. Pre-exposure bake: 90°C, 5 min
4. Exposure: 25 s
5. Post-exposure bake: 90°C, 30 s
6. Development ~ 6 min.
7. Hard-bake: skipped

ALTERNATIVE MICROARRAY PREPARATION PROCEDURES

As discussed in chapter 1.6 PROCESSING TECHNOLOGY FOR MICROPILLAR ARRAYS , the photomasks created for our project, bore 10 x 10 µm structures and 5 x 5 µm ones. Experiment showed that the both microhole types cannot be produced simultaneously. I did not, however, optimise separately the process for 5 x 5 µm microholes because of the problems I faced with the elastomer structures produced on the photoresist masters. Since 10 x 10x25 µm micropillars were already so soft that they often collapsed, 5 x 5 x 25 µm ones would turn out to be so difficult to handle that I considered their creation futile.

Another approach, inspired by the work of Tan et. al. (2003) was also tested. Instead of microholes, micropillars were produced in the photoresist. Next, the negative of the micropillar structure was created in elastomer, resulting in microhole pattern in silicone

rubber. This microhole array, after being covered with a separative silane layer, served to create a final, micropillar array from silicone rubber. This approach showed several drawbacks, compared to the preparation of silicone rubber micropillars directly from *SU-8* masters with microholes. First, it required an extra preparation step which took the whole day. Second, photoresist micropillars were much more fragile than photoresist microholes and often were ripped off the wafer during master-elastomer separation while the photoresist master with microholes could be used several times without problems occurring. The greatest problem, however, was separation of two silicone elastomer layers – it usually failed and both rubber layers remained stuck together.

ELASTOMER MICROPILLAR ARRAY PREPARATION

1.   A master created with photolithography (cf. APPENDIX C). was silanized (see Appendix B). The photoresist layer was silanized before every use to avoid master – substrate sticking. If the master had been used before, it was also cleaned before the next application. For cleaning, the masters were left on a shaker in a bowl filled with n-heptane overnight and subsequently dried in nitrogen stream.

2.   A liquid prepolymer mixture was prepared; Sylgard base and crosslinking agent were mixed in chosen proportions and degassed to remove air bubbles. For more information about silicone rubber see Appendix B.

3.   The mixture was poured on the master surface and degassing was repeated. In case of deep structures degassing is essential for entrance of the viscous prepolymer into deep structures of the master.

4.   A coverslip was put on the prepolymer. Spacers were used to ensure defined rubber thickness. On the coverslip, a thick glass plate was placed and the whole assembly was clamped to assure the required thickness.

5.   The prepolymer was cured (heated to speed up the crosslinking process).

6.   The master and the elastomer part were separated. This step would be impossible without prior silanization of the master. Also, 2-propanol was used to facilitate the separation.

POLYMER SELECTION

Silicone rubber rigidity depends on the base/crosslinking agent ratio of the prepolymer. The crosslinking agent causes the crosslinking of base molecules so the more crosslinking agent is added, the stiffer the resulting *PDMS* elastomer. In first tests *PDMS* rubber, prepared from base material and crosslinker in 10 : 1 ratio, was used. It was, however, too stiff for the cells to bend so that mixtures in 20 : 1 ratio were prepared for experiments

with cells. Even softer *PDMS* rubber substrates were also prepared (25 : 1 and 30 : 1 base material and crosslinker ratio) but they were extremely difficult to handle – the micropillars clumped more easily than in the case of 20 : 1 ratio mixtures. Also, 25 : 1 and 30 : 1 ratio elastomers were too pliable for the cardiac myocytes. They could be, however, used for weaker kinds of cells.

PDMS rubber pillars (10 : 1 base material to crosslinker ratio) were prepared for SEM analysis. After peeling, silicone rubber micropillars were sputtered with gold, mounted onto SEM stubs and visualized. Softer pillars were examined using a CLSM microscope (LSM510 with Axiovert 200M as microscope body, Carl Zeiss, Jena, Germany). For this purpose, *PDMS* elastomer structures were stained with DiD Vybrant cell labeling solution (Molecular Probes, Eugene, OR) in a 1 : 300 dilution. Staining was performed at 37°C for two days to allow diffusion of the dye into the elastomer. After staining, substrates were washed twice in *PBS* and either directly analysed at the CLSM using a yellow HeNe laser (543 nm) or used as substrates for cultivating cells.

APPENDIX D: CELL PREPARATION AND IMAGING

MATERIALS

The following materials and chemicals were used:

1. A female rat, 19 days pregnant

2. Myocyte medium: nutrient mixture F10 Ham powder (Sigma, Traufkirchen, Germany), 9.8 g for 1 l of sterile water. 4 ml of sodium bicarbonate ($NaHCO_3$) 7.5% solution has to be added to 1 l of F10 solution to keep pH at 7.2.

Out of myocyte medium, the following mixtures are prepared:

a) Blocking-solution: mix 33 % FKS (foetal calf serum) with 25 ml myocyte medium (containing $NaHCO_3$)

b) **Cell culture medium**: mix 5 % FKS with 50 ml of myocyte medium containing: $NaHCO_3$, 1 : 100 dilution of antibiotics - solution penicillin-streptomycin (10 mg streptomycin and 10 000 units of penicillin in 0,9 % NaCl, Sigma) and 1 : 200 *ITS* liquid media supplement[29], Sigma.

4. Hank's balanced solution (*HBSS*, Sigma)

5. 0,5% Trypsin and 0,2 % EDTA solution (Sigma)

6. DNAse 10 000 units/ml (Sigma)

7. phosphate buffered saline solution (PBS 10x, pH 7.2), containing:

   NaCl 80 g/l

   Na_2PO_3 11 g/l

   KH_2PO_4 2.0 g/l

8. Cell culture dishes, 35 mm (Greiner, Germany)

9. 15 and 50 ml Falcon tubes

10. Pasteur pipettes

---

[29] *ITS* contains: 1.0 mg/ml insulin from bovine pancreas, 0.55 mg/ml human transferrin (substantially iron-free), and 0.5 µg/ml sodium selenite (according to Sigma-Aldrich).

11. sterile scalpels

CELL ISOLATION

Cardiac myocyte isolation was done by Mr. Nils Hersch (IBN 4, Jülich, Germany).

- The pregnant rat was anaesthetised using CO_2 and then decapitated with a guillotine.
- The embryos were taken out, stored on ice and then decapitated.
- Embryos' thoraxes were opened; hearts were taken out and put into *HBSS* (in a 15 ml tube with 14 ml *HBSS*) on ice till all the hearts were collected; the hearts were then 2-3 times washed in *HBSS*.
- The hearts were removed from *HBSS* and put into Petri dishes containing fresh *HBSS* on ice and, to complete the washing, transferred 2 times into new dishes containing fresh *HBSS*.
- The hearts were cut into small pieces with a sterile scalpel in the presence of trypsin-EDTA-solution
- Heart fragments were transferred into a 15 ml Falcon tube containing 8 ml of trypsin-EDTA solution and left for about 8 min. at 37°C. After that time, a part of the solution was removed. Care was taken not to remove floating cell aggregates.
- 100 μl of DNAse (10 000 units/ml) were added to the solution and the content of the Falcon tube was gently stirred for 3 min at room temperature with a sterile Pasteur pipette tip in order to break cell aggregates.
- 4 ml of warm (37°C) fresh trypsin-EDTA solution was added to the tube and subsequently the tube was shaken for next 4 min at 37°C.
- The suspension of floating cells was transferred into a fresh 15 ml Falcon tube containing 4 ml *FKS* 33% solution and stored on ice. Here, the cells began to sediment.
- The cells were centrifuged for 10 min at 200 g at 4°C.
- The supernatant was removed and the cell pellet was resuspended in 8 ml 5% *FKS* solution.
- The cell suspension was plated on 2 cell culture dishes for 30 min. Then the remaining supernatant was centrifuged for 10 min at 200 g and 25°C.
- The pellet was re-suspended in 400 μl medium and the cell number was estimated using a Bürker counting chamber.
- The cells were seeded in appropriate concentrations on the fibronectin[30] coated, elastomeric surfaces.
- The cells were then incubated at 37°C and 5% CO_2.

---

[30] Fibronectin is a ECM protein cells can adhere to

CLSM

Confocal laser scanning microscopy (CLSM) is a powerful technique, allowing both fast probe scans and precise three dimensional scanning of samples even tens of micrometers thick. This is achieved by excluding most of the light from the specimen coming not from the microscope's focal plane. The image has less haze and better contrast than that of a conventional microscope and represents a thin cross-section of the specimen. Thus, apart from allowing better observation of fine details, it is possible to build three-dimensional (3D) reconstructions of a volume of the specimen by assembling a series of thin slices taken along the vertical axis. The majority of confocal microscopes image either by reflecting light off the specimen or by stimulating fluorescence from dyes (fluorophores) applied to the specimen.

FLUORESCENCE

If a molecule absorbs a photon and emits another photon of lower energy, emission of the light is called **fluorescence**. At room temperature most molecules are in their ground (lowest energy) states, therefore unable to emit photons. They may, however, absorb photons so one of their electrons 'jumps' to a higher energy level (excitation). Usually, some this extra energy is dissipated in collisions with other molecules and dielectric relaxation of the solvent and the excited electron falls on a lower (but still not ground!) energy level. If the energy gap is large enough and non-radiative decay processes are of low efficiency, the electronic system of the molecule relaxes by emitting a photon. Fluorescence is red shifted compared to the excitation light because of these vibronic and dielectric relaxation processes.

Fluorescence microscopy offers far greater selectivity than conventional microscopy. Often it is possible to attach a fluorophore to one type of molecule only or to use the natural fluorescence of some chemical compounds. Moreover, several specific fluorophores may be used simultaneously in one sample. Thus, by using different wavelengths, different molecules within the sample may be visualized simultaneously in different colours.

CLSM MICROSCOPING PRINCIPLES

The principles of CLSM are illustrated on Fig. D-1. Light from the light source (a laser) passed through a pinhole and is, with the help of dichroic mirrors, cast on the specimen. Mirrors rotate so that the specimen can be scanned all over, point by point. Reflected laser light is blocked by a combination of dichroic mirrors and long pass filter and the fluorescent light, passing another pinhole, reaches the detector. The set of two confocal pinholes is decisive for CLSM resolution. The pinhole guarantees that only light originating

in the focal point reaches the detector; photons coming from other places are blocked by the pinhole. Therefore, CLSM can be used on thick samples as the fluorescence originating from the layers above and below the focal plane are greatly attenuated. It implies, however, that only one voxel (3D pixel) of a specimen is observed at a time point. Therefore, to image the whole sample, scanning point by point is necessary. A computer program then rearranges the data into a 2 or 3D image of the specimen. If two or more fluorescent molecules are excited, scanning must be repeated several times or several detection channels must be used simultaneously. CLSM is a powerful but time-consuming microscopic technique; photodamage of the living specimen due to the powerful laser radiation must also be taken into consideration.

A)

B)
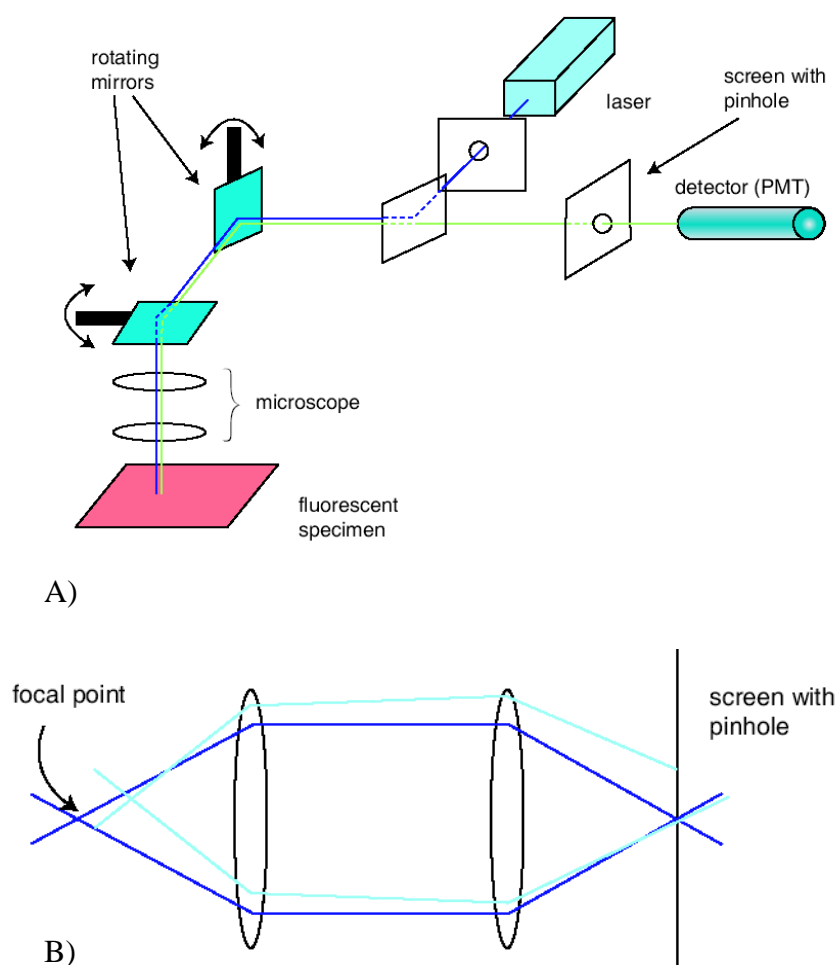
Fig. D-1 A) CLSM set-up. Blue line: a light beam emitted by the laser; green line: light re-emitted by the sample B) Effect of confocal pinholes. Pictures taken from (after Semwogerere and Weeks 2005). Dark blue line: a light beam originating from the focal point; light blue line: a light beam originating from another place

APPENDIX E: *PDMS* ELASTOMER MICROPILLAR CALIBRATION

MAGNIFIED MODEL OF THE MICROPILLAR

In engineering science, miniscule models of the tested systems are often built, in order to make first measurements and experiments cheaper and faster than with the real object. For this project a similar approach was proposed: creation of a 'macropillar' – a magnified model of the *PDMS* elastomer micropillar. A model consisted of a single pillar magnified 500 times. All the dimensions, also substrate thickness, were kept to scale. The macropillar was about 1.2 cm long. Instead of a glass coverslip, which served as a base for a real substrate, a thick metal slab was used. *PDMS* rubber stiffness was the same as in the case of the micropillars.

For ease of fabrication of this model a cylindrical pillar (diameter 5.1 mm) was used. This macro model was mounted vertically on a micromanipulator (MHW3, Narishige International, Tokyo, Japan) and lowered gently onto a chisel shaped edge placed on a precision scale (Labstyle 204, Mettler Toledo, Giessen, Germany, see **Fig.** E-1). Both the distance between the substrate and the edge as well as the loading force were varied to alter the torque acting on the macropillar. The whole assembly was observed with a stereomicroscope (Stemi2000, Carl Zeiss, Jena, Germany) equipped with a XCD-X710 CCD camera (Sony, Tokyo, Japan). Images were captured with ICcapture 1.1 (Imaging Source Europe GmbH, Bremen, Germany). The outer edges of the substrate and the macropillar were found by fitting lines through the maxima of the local variance of the images. From these lines the angle, Θ, was determined.

Using Eq. 2-5 which predicted the following relation between the angle Θ between the tangent to the pillar at its lower end and the normal to the undeformed surface and the torque *M*:

$$\Theta \approx 1.18 a_R \frac{3M}{4\pi EI}$$

a linear equation for the $\Theta(M)$ relationship was expected.

$$\Theta = \alpha a_R \frac{3M}{4\pi EI} + \beta$$

The proportionality factor of 44 rad/(Nm) was **found** (see Fig. E-2). However, using Eq. 2-5 with the corresponding factor for a cylindrical pillar yields a factor of 64 rad/Nm. This finding implies that the correct proportionality factor may be only 70% of the values calculated by the approximate approach which neglects transverse stresses. The factor of 1.18 was used for calculations shown in our work. However, if this factor was overestimated by as much as indicated by the experimental calibration, all forces given in this publication would be underestimated by 10%. This is below the statistical uncertainty of the measurement (see also chapter **MEASUREMENT UNCERTAINTIES**). Therefore the accuracy of the calculation was not further improved.
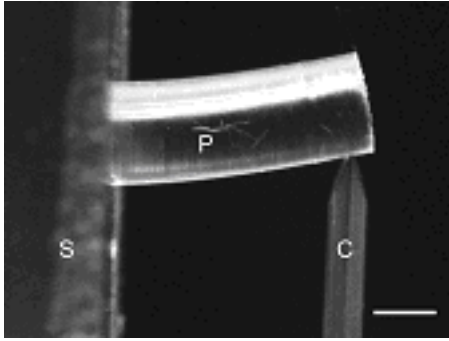
Fig. E-1 A macroscopic pillar (P) was bent by pressing it down on a chisel shaped point (C) mounted to a precision scale. The angle between substrate (S) surface and pillar contour was determined by tracing the outer contours of pillar and substrate (see text). Scale bar 3 mm.
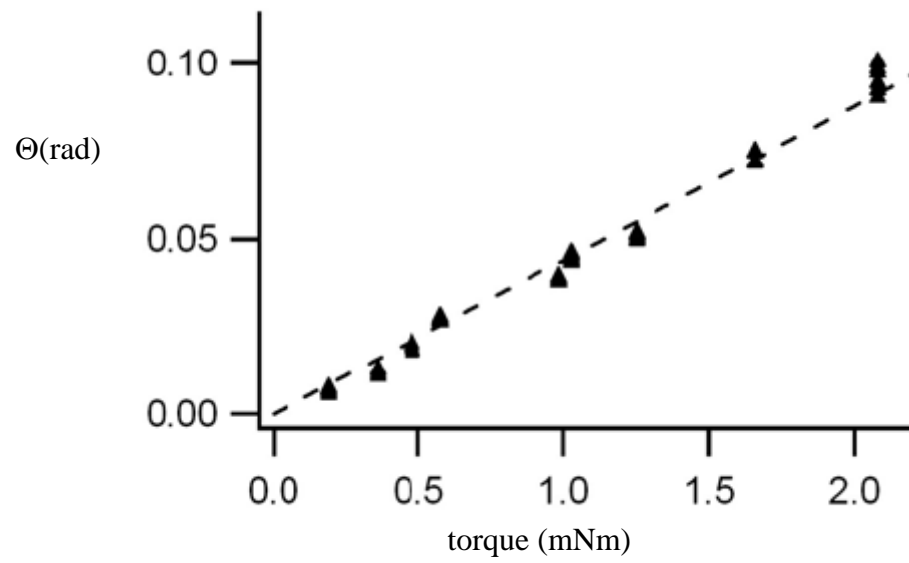
Fig. E-2 Results of the macropillar bending test. Points: measured data. Straight line: least square fit, slope 44 rad/(Nm).

LITERATURE

1. Armani D., Liu C., Aluru N. 1999 *Re-configurable fluid circuits by PDMS elastomer micromachining.* Micro Electro Mechanical Systems, 1999. MEMS '99. Twelfth IEEE International Conference on**. 222-227**

2. Badylak S. F. 2002 *The extracellular matrix as a scaffold for tissue reconstruction.* Cell & Developmental Biology **13** 377-383

3. Balaban N. Q., Schwarz U., Riveline D., Golchberg P., Tzur G., Sabanay I., Mahalu D., Safran S., Bershadsky A., Addadi L., Geiger B. 2001 *Force and focal adhesion assembly: a close relationship studied using elastic micropatterned substrates*. Nature Cell Biology **3** 466-472

4. Bao G. 2002 *Mechanics of biomolecules*. Journal of the Mechanics and Physics of Solids, **50** 2237 – 2274

5. Bar-Ziv R, Tlusty T., Moses E. Safran S. A., Bershadsky A. 1999 *Pearling in cells: a clue to understanding cell shape.* Cell Biology 96 10140-10145

6. Ben Ze'ev A., Robinson G., Bucher N., Farmer S. 1988 *Cell-cell and cell-matrix interactions differentially regulate the expression of hepatic and cytoskeletal genes in primary cultures of rat hepatocytes*. Proc. Nati. Acad. Sci. USA **85** 2161-2165

7. Beningo K. A., Wang L. 2002 *Flexible substrata for the detection of cellular traction forces.* Trends in Cell Biology **12(2)** 79-84

8. Berg J. M., Stryer L., Tymoczko J. 1997 *Biochemia.* Wydawnictwo Naukowe PWN, Warszawa

9. Bluhm W. F., McCulloch A., Lew W. 1995 *Active force in rabbit ventricular myocytes*. J Biomechanics **28(9)** 1119-1122

10. Boateng S. Y., Hartman T., Ahluwalia N., Vidula H., Desai T., Russell B. 2003 *Inhibition of fibroblast proliferation in cardiac myocyte cultures by surface microtopography.* Am J Call Physiol **285** C171-C182

11. Boey S. K., Boal D. H., Fischer D. E. 1998 *Simulations of the Erythrocyte Cytoskeleton at Large Deformation. I. Microscopic Models.* Biophysical Journal **75** 1573–1583

12. Britland S., Perridge C., Denyer M., Morgan H., Curtis A., Wilkinson C. 1997 *Morphogenetic guidance cues can interact synergistically and hierarchically in steering nerve cell growth* Exp. Biol. Online-EBO **1(2)** 1430-3418

13. Brunette D. M. 1984 *Mechanical stretching increases the number of epithelial cells synthesizing DNA in culture*. Journal of Cell Science **69(1)** 35-45

14. Bryszewska M., Leyko W. 1997 *Biofizyka dla biologów*. PWN, Warszawa

15. Bursac N., Parker K., Iravanian S., Tung L. 2002 *Cardiomyocyte cultures with controlled macroscopic anisotropy – A model for functional electrophysiological studies of cardiac muscle.* Circ. Res. **91** e45-e54

16. Bursac P., Lenormand G., Fabry B., Oliver M., Weitz D. A., Viasnoff V., Butler J. P., Fredberg J. J. 2005 Cytoskeletal remodelling and slow dynamics in the living cell. Nature Materials **4** 557-561

17. Cecchi G., Colomo F., Poggesi C., Tesi C. 1992 *The stimulus interval-tension relation in enzymatically isolated single myocytes of the frog heart.* Journal of Physiology **448** 275-291

18. Cesa C. M. 2007 *Microstructured elastomer films to measure dynamic traction forces of living animal cells with high spatial resolution – establishement of the technique and first results on cardiac myocytes.* Berichte des Forschungszentrums Jülich 4186, Jülich, Germany

19. Cesa, C., Kirchgeßner N., Mayer D., Schwarz U., Hoffmann B., Merkel R. 2007. *Micropatterned silicon elastomer for high resolution analysis of cell force patterns.* Rev. Sci. Instrum. **78** 034301-1– 034301-10

20. Chen C. S., Mrkisich M., Huang S., Whitesides G., Ingber D. 1997 *Geometric control of cell life and death.* Science **276** 1425-1428

21. Choquet D., Felsenfeld D. P. Sheetz M. P. 1997 *Extracellular Matrix Rigidity Causes Strengthening of Integrin–Cytoskeleton Linkages.* Cell, **88** 39–48

22. Citters, van K. M., Hoffman B. D., Massiera G.,Cocker J. C. 2006 *The Role of F-Actin and Myosin in Epithelial Cell Rheology.* Biophysical Journal **91(10)** 3946–3956

23. Colomo F., Piroddi N., Poggesi C., te Kronnie G., Tesi C. 1997 *Active and passive forces of isolated myofibrils from cardiac and fast skeletal muscle of the frog.* Journal of Physiology 500.2 535-548

24. Cooper G.M.,. Hausman R. E., 2007 *The Cell: A molecular approach,* 4th edition, ASM Press and Sinauer Associates, Inc.

25. Craighhead H. G., James C., Turner A. 2001 *Chemical and topographical patterning for directed cell attachment.* Current Opinion in Solid State and Materials Science, **5** 177-184

26. Curtis A., Riehle M. 2001 *Tissue engineering: the biophysical background.* Phys. Med. Biol. **46** R47-R65

27. Curtis A., Wilkinson C. 1997 *Topographical control of cells.* Biomaterials **18** 1573-1583

28. Dalby M. J., Riehle M., Sutherland D., Agheli H., Curtis A. 2005 *Morphological and mircoarray analysis of human fibroblasts cultured on nanocolumns produced by colloidal lithography.* European Cells and Materials **9** 1-8

29. Dalby M. J., Yarwood S., Johnstone H., Affrossman S., Riehle M. 2002 *Fibroblast Signaling Events in Response to Nanotopography: A Gene Array Study.* IEEE Transactions of Nanobioscience **1(1)** 12-17

30. Danowski B. A., Imanaka-Yoshida K., Sanger J. M., Sanger J. W. 1992 *Costameres are sites of force transmission to the substratum in adult rat cardiomyocytes.* J Cell Biol **118** 1411-1420

31. Dembo M., Oliver T., Ishihara A., Jacobson K. 1996 *Imaging the traction stresses exerted by locomoting cells with the elastic substratum method.* Biophys J **70** 2008-2022

32. Deshpande V. S., McMeeking R. M., Evans A. G. 2006 *A bio-chemo-mechanical model for cell contractility.* **103** 14015–14020

33. Deutsch J., Motlagh D., Russell B., Desai T. A. 2000 *Fabrication of Microtextured Membranes for Cardiac MyocyteAttachment and Orientation.* J Biomed Mater Res (Appl Biomater) 53: 267–275

34. Dike L. E., Chen C., Mrksich M., Tien J., Whitesides G., Ingber D. 1999 *Geometric control of switching between growth, apoptosis and differentiation during angiogenesis using micropatterned substrates.* In Vitro Cell. Dev. Biol. – Animal **35** 441-448

35. Discher D. E., Boal D. H., Boey S. K. 1998 *Simulations of the Erythrocyte Cytoskeleton at Large Deformation. II. Micropipette Aspiration.* Biophysical Journal **75** 1584–1597

36. Discher D. E., Jammey P., Wang Y. 2005 *Tissue cells feel and respond to the stiffness of their substrate.* Science **310** 1139-1143

37. Doolabh V. B., Hertl M., Mackinnon S. 1996 *The role of conduits in nerve repair: a review.* Rev Neurosci **7** 47-84

38. Engler A. J., Griffin M., Sen S., Bönnemann C., Sweeney H., Discher D. 2004 *Myotubes differentiate optimally on substrates with tissue-like stiffness: pathological implications for soft or stiff microenvironments.* J Cell Biol **166(6)** 877-887

39. Entcheva E., Bien H. 2003 *Tension development and nuclear eccentricity in topographically controlled cardiac syncytium.* Biomedical Microdevices **5(2)** 162-168

40. Entcheva E., Bien H., Yin L., Chung C., Farrell M., Kostom Y. 2004 *Functional cardiac cell constructs on cellulose-based scaffolding.* Biomaterials **25** 5753–5762

41. Fluegel A. (2007) *Statistical Calculation and Development of Glass Properties http://www.glassproperties.com/young_modulus/*

42. Forgacs G. 1995 *On the possible role of cytoskeletal filamentous networks in intracellular signaling: an approach based on percolation.* Journal of Cell Science **108** 2131-2143

43. Geiger B., Bershadsky A. 2001 *Assembly and mechanosensory function of focal contacts.* Curr Op Cell Biol **13** 584-592

44. Geiger B., Bershadsky A. 2002 *Exploring the neighbourhood: adhesion-coupled cells mechanosensor.* Cell **110** 139-142

45. Geiger B., Bershadsky A., Pankov R., Yamada K. 2001 *Transmembrane crosstalk between the extracellular matrix-cytoskeleton crosstalk.* Nat Rev Mol Cell Biol. **2** 793-805

46. Giancotti F. G. 2000 *Complexity and specificityof integrin signalling.* Nature Cell Biology **2** E13-E14

47. Giancotti F. G. Ruoslahti E. 1999 *Integrin Signaling.* Science **285** 1028-1032

48. Gray D. S., Tien J., Chen C. 2003 *Repositioning of cells by mechanotaxis on surfaces with micropatterned Young's modulus.* J Biomed Mater Res A, **66(3)** 605-614

49. Guerin L. J. 2005 *SU-8 homepage http://www.geocities.com/guerinlj/*

50. Gumbiner B. M. 1996 Cell Adhesion: The Molecular Basis of Tissue Architecture and Morphogenesis. Cell **84** 345-357

51. Gunst S. J., Fredberg J. J. 2003 *Airway Hyperresponsiveness: From Molecules to Bedside Invited Review: The first three minutes: smooth muszle contraction, cytoskeletal events, and soft glasses.* J Appl Physiol **95** 413–425

52. Hamilton D. W., Maul T., Vorp D. 2004 *Characterization of the Response of Bone Marrow-Derived Progenitor Cells to Cyclic Strain: Implications for Vascular Tissue-Engineering Applications.* Tissue Engineering **10(3/4)** 361-369

53. Han X., Kubota I., Feron O. Opel D., Arstall M., Zhao Y., Huang P., Fishman M., Kelly R. 1998 *Muscarinic cholinergic regulation of cardiac myocyte ICa-L is absent in mice with targeted disruption of endothelial nitric oxide synthase* Proc. Natl. Acad. Sci. USA **95** 6510–6515

54. Harris A. K., Wild P., Stopak D. 1980 *Silicone rubber substrata: a new wrinkle in the study of cell locomotion.* Science **208(4440)** 177-179

55. Herron T. J., Korte F., McDonald K. 2001 *Power output is increased after phosphorylation of myofibrillar proteins in rat skinned cardiac myocytes.* **89** 1184-1190

56. Hu S., Chen J., Fabry B., Numaguchi Y.,Gouldstone A., Ingber D. E., Fredberg J. J., Butler J. P., Wang N. 2003 *Intracellular stress tomography reveals stress focusing and structural anisotropy in cytoskeleton of living cells.* Am J Physiol Cell Physiol **285** C1082–C1090

57. Huang S., Ingber D. 1999 *The structural and mechanical complexity of cell-growth control.* Nature Cell Biology **1** E131-E138

58. Ingber D. E. 1993 *Cellular tensegrity: defining new rules of biological design that govern the cytoskeleton.* Journal of Cell Science **104** 613-627

59. Ingber D. E. 1998 *Cellular Basis of Mechanotransduction.* Biol. Bull. **194** 323-327

60. Ingber D. E. 1998a *The Architecture of Life.* Scientific American 48-57

61. Ingber D. E. 2003 *Mechanosensation through integrins: Cells act locally but think globally.* PNAS **100** 1472–1474

62. Ingber D. E. 2003a *Tensegrity I. Cell structure and hierarchical systems biology.* Journal of Cell Science 116, 1157-1173

63. Ingber D. E. 2003b *Tensegrity II. How structural networks influence cellular information processing networks.* Journal of Cell Science **116**, 1397-1408

64. James, T. N. 2002. *Structure and function of the sinus node, AV node and His bundle of the human heart: part I-structure.* Prog Cardiovasc Dis 45 235-267

65. James, T. N. 2003. *Structure and function of the sinus node, AV node and his bundle of the human heart: part II--function.* Prog Cardiovasc Dis 45 327-360

66. Janmey, P. A., Hvidt S., Lamb J., Stossel T. P. 1990. *Resemblance of actin-binding protein/actin gels to covalently crosslinked networks.* Nature. **345**:89–92

67. Juliano, R. L. & Haskill, S. J. 1993 *Signal transduction from the extracellular matrix.* J. Cell Biol. **120** 577–585

68. Katsumi A., Naoes T., Matsushita T., Kaibuchi K., Schwartz M. A. 2005 *Integin activation and matrix binding mediate cellular responses to mechanical stress.* J Biol chem **280** 16546-16549

69. Katz B., Zamir E., Bershadsky A., Kam Z., Yamada K. M., Geiger B. 2000 *Physical State of the Extracellular Matrix Regulates the Structure and Molecular Composition of Cell-Matrix Adhesions.* Molecular Biology of the Cell. **11** 1047–1060

70. Khan S., Sheetz M. 1997 *Force effects on biochemical kinetics.* Annu. Rev. Biochem. **66** 785–805

71. King M. R. 2005 *Priniples of Cellular Engineering: Understamding the biomolecular interface. Chapter 4.* Academic Press

72. Klabunde R. E.2004 *Cardiovascular Physiology Concepts.* Lippincott Williams & Wilkins (2004)

73. Korte F. S., McDonald K. S. 2007 *Sarcomere length dependence of rat skinned cardiac myocyte mechanical properties: dependence on Mosin heavy chain.* J Physiol **581.2** 725–739

74. Kristal-Boneh E., Raifel M., Froom P., Ribak J. 1995 *Heart rate variability in health and disease.* Scandinavian journal of work, environment & health. **21(2)** 85-95

75. Kumar S., Maxwell I. Z., Heisterkamp A., Polte T. R., Lele T. P., Salanga M., Mazur E., Ingber D. E. 2006 *Viscoelastic Retraction of Single Living Stress Fibers and Its Impact on Cell Shape, Cytoskeletal Organization, and Extracellular Matrix Mechanics.* Biophysical Journal **90** 3762–3773

76. Kung C. 2005 *A possible unifying principle for mechanosensation.* Nature **436** 647-654

77. Landau L. D., Lifszyc E. 1991 *Elastizitätstheorie.* Berlin, Akademie Verl.

78. Lateef S. S., Boateng S., Ahluwalia N., Hartman T., Russell B., Hanley L. 2005 *Three-dimensional chemical structures by protein functionalized micron-sized beads bound to polylisine-coated silicone surfaces.* J Biomed Mater Res A. **72(4)** 373-380

79. Lauffenburger D. A., Horwitz A. 1996 *Cell migration: a physically integrated molecular process.* Cell **84** 359-369

80. Le Guennec J. Y., Peineau N., Argibay J., Mongo K., Garnier D. 1990 *A new method of attachment of isolated mammalian ventricular myocytes for tension re-cording: Length dependence of passive and active tension.* J. Mol. Cell. Cardiol. **22** 1083-1093

81. Le Guennec J. Y., White E., Gannier F., Argibay J., Garnier D. 1991 *Stretch-induced increase of resting intracellular calcium concentration in single guinea-pig ventricular myocyte.* Exp Physiol **76** 975-978

82. Lenormand G., Millet E., Fabry B., Butler J. P. 2004 *Linearity and time-scale invariance of the creep function in living cells.* J. R. Soc. Interface **1** 91–97

83. Li B., Xie L., Starr Z., Yang Z., Lin J.,Wang J 2007 *Development of micropost force sensor array with culture experiments for determination* of cell traction forces. Cell Motility and the Cytoskeleton **64** 509-518

84. Liew C., Dzau V. 2004 *Molecular genetics and genomics of heart failure.* Nature Reviews Genetics **5**, 811-825

85. Lin G., Pister K., Roos K. 2000 *Surface micromachined polysilicon heart cell force transducer.* J of Microelectromechanical systems **9** 9-17

86. Lin, G., Pister K., Roos K. 1995 *Novel microelectromechanical system force transducer to quantify contractile characteristics from isolated cardiac muscle cells.* J. Electrochem. Soc. **142** L31-L33

87. Lo C., Wang H., Dembo M., Wang Y. 2000 *Cell movement is guided by the rigidity of the substrate.* Biophysical Journal **79** 144-152

88. Lubarsky G. V., Davidson M. R.; BRADLEY R. H. 2004 *Elastic modulus, oxidation depth and adhesion force of surface modified polystyrene studied by AFM and XPS*. Surface Science **558(1-3)** 135-144

89. Ma Z., Kotaki M., Inai R., Ramakrishna S. 2005 *Potential of Nanofiber Matrix as Tissue-Engineering Scaffolds*. Tissue Engineering **11(1/2)** 101-109

90. Maksym G. N., Fabry B., Butler J.P., Navajas D., Tschumperlin D. J., Laporte J. D., Fredberg J. J. 2000 *Mechanical properties of cultured human airway smooth muscle cells from 0.05 to 0.4 Hz.* J Appl Physiol **89** 1619–1632

91. Malmivuo J. Plonsey R. 1995 Principles and Applications of Bioelectric and Biomagnetic Fields.

92. Martin K. H., Slack J. K., Boerner S. A., Martin C. C., Parsons J. T. 2002 *Integrin Connections Map: To Infinity and Beyond.* Science **296** 1652-165

93. Martinac B. 2004 *Mechanosensitive ion channels: molecules of mechanotransduction*. J Cell Science **117** 2449-2460

94. Mata A., Boehm C., Fleischman A., Muschler G., Roy S. 2002 *Growth of connective tissue progenitor cells on microtextured polidimethylsiloxane surfaces*. J Biomed Mater Res. **62(4)** 499-506

95. Mazgajska J. 2005 *Płazy i gady Europy.* Internet issue www.herpetologia.waw.pl

96. McDonald K. S., Wolff M., Moss R. 1998 *Force-velocity and power-load curves in rat skinned cardiac myocytes.* Journal of Physiology **511** 519-531

97. Merkel R., Kirchgeßner N., Cesa C., Hoffmann B. 2007 *Cell Force Microscopy on Elastic Layers of Finite Thickness.* Biophysical Journal **93** 3314–3323

98. Michie K. A., Löwe J. 2006 *Dynamic filaments of the bacterial cytoskeleton.* Annu. Rev. Biochem. **75** 467–92

99. Mossman K. D., Campi G., Groves J., Dustin M. 2005 Alter*ed TCR signaling from geometrically repatterned immunological synapses.* Science **310** 1191-1193

100. Motlagh D., Senyo S., Desai T., Russell B. 2003 *Microtextured substrata alter gene expression, protein localization and the shape of cardiac myocytes.* Biomaterials **24(14)** 2463-2476

101. *Nature Insight Lab on a chip* 2006 **442** no. 7101

102. Nguyen T. T. B., Fredberg J. J. 2008 *Strange Dynamics of a Dynamic Cytoskeleton.* Proc Am Thorac Soc **5.** 58–61

103. Nishimura S., Yasuda S., Katoh M., Yamada K., Yamashita H., Saeki Y., Sunagawa K., Nagai R., Hisada T., Sugiura S. 2004 *Single cell mechanics of rat cardiomyocytes under isometric, unloaded and physiologically loaded conditions.* AJP- Heart **287** 196-202

104. Norman J. J., Desai T. 2005 *Control of cellular organization in three dimensions using a microfabricated polydimethylsiloxane-collage composite tissue scaffold*. Tissue Engineering **11** 378-386

105. Numaguchi Y., Huang S., Polte T. Eichler G., Wang N., Ingber D. 2003 *Caldesmon-dependent switching between capillary endothelial cell growth and apoptosis through modulation of cell shape and contractility*. Angiogenesis **6** 55–64

106. Oliver T. Dembo M., Jacobson K. 1995 *Traction forces in locomoting cells.* Cell Motil. Cytoskeleton **31(3)** 225–240

107. Pardo J. V., d'Angelo Siliciano J. D., Craig S. W. 1983 *A vinculin-containing cortical lattice in skeletal muscle: Transverse lattice elements ("costameres") mark sites of attachment between myofibrils and sarcolemma.* Cell Biology **80** 1008-1012

108. Pelham R. J. Jr., Wang Y. 1997 *Cell locomotion and focal adhesions are regulated by substrate flexibility,* Proc. Natl. Acad. Sci. USA **94** 13661-13665

109. Perozo E., Cortes D., Sompornpisut P., Kloda A., Martinac B. 2002 *Structure of MscL in the open state and the molecular mechanism of gating in mechanosensitive channels.* Nature **418** 942–948

110. Pilkey, W. D. 2002. *Analysis and Design of Elastic Beams.* John Wiley & Sons, Inc.

111. Pizzo A.M., Kokini K., Vaughn L., Waisner B., Voytik-Harbin S. 2005 *Extracellular matrix (ECM) microstructural composition regulates local cell-ECM biomechanics and fundamental fibroblast behavior: a multidimensional perspective.* J Appl Physiol **98** 1909–1921

112. Powers M. J., Domansky K., Kaazempur-Mofrad M., Kalezi A., Capitano A., Upadhyaya A. Kurzawski P., Wack K., Stolz D., Kamm R., Griffith L. 2002 *A microfabricated array bioreactor for perfused D liver culture.* Biotechnology and Bioengineering, **78(3)** 257-269

113. Puceat, M., Clement O., Lechene P., Pelosin J, Ventura-Clapier R., Vassort G. 1990 *Neurohormonal control of calcium sensitivity of myofilaments in rat single heart cells.* Circ. Res. **67** 517–124

114. Rai-Choudhury P. 1997 *SPIE Handbook of Microlithography, Micromachining and Microfabrication Volume 1: Microlithography.* SPIE Press Monograph Vol. PM39

115. Ren J., Ren B., Sharma A. 2002 *Sepsis-induced depressed contractile function of isolated ventricular myocytes is due to altered calcium transient properties.* Shock **18(3)** 285-288

116. Rochetti M., Malfatto G., Lombardi F., Zaza A. *2000 Role of the Input/Output Relation of Sinoatrial Myocytes In Cholinergic Modulation of Heart Rate Variability.* J Curdiovasc Electrophysiol, **2** 522-530

117. Roure O. du, Saez A., Buguin A., Austin R., Chavrier P., Siberzan P., Ladoux B. 2005 *Force mapping in epithelial cell migration.* Biophysics **102(7)** 2390-2395

118. Roy P., Petroll W., Cavanagh H., Chuong C., Jester V. 1997 *An in vitro force measurement assay to study the early mechanical interaction between corneal fibroblasts and collagen matrix.* Exp Cell Res **232** 106-117

119. Saez, A., Buguin A., Silberzan P., Ladoux B. 2005 *Is the mechanical activity of epithelial cells controlled by deformations or forces?* Biophys J **89** L52-54.

120. Sarkar S., Dadhania M., Rourke P., Dasia T., Wong J. 2005 *Vascular tissue engineering: microtextured scaffold templates to control organization of vascular smooth muscle cells and extracellular matrix* Acta Biomaterialia **1** 39-100

121. Sastry S. K., Burridge K. 2000 *Focal adhesions: a nexus for intracellular signalling and cytoskeleton dynamics.* Experimental Cell Research 261 25-36

122. Sastry S., Debenedetti P. G., Stillinger F. H 1998 *Signatures of distinct dynamical regimes in the energy landscape of a glass-forming liquid.* Nature 393 554-557

123. Schmidt – Nielsen K. 2008 *Fizjologia zwierząt***.** Adaptacja do środowiska. Wydawnictwo Naukowe PWN

124. Schwartz M. A., Ingber D. 1994 *Integrating with integrins.* Molecular Biology of the Cell **5** 389-393

125. Schwarz U. S., Balaban N. Q., Riveline D., Addadi L., Bershadsky A., Safran S. A., Geiger B. 2003 *Measurement of cellular forces at focal adhesions using elastic micro-patterned substrates.* Materials Science and Engineering **C 23** 387–394

126. Schwarz U. S., Balaban N. Q., Riveline D., Bershadsky A., Geiger B., Safran S. A. 2002 *Calculation of Forces at Focal Adhesions from Elastic Substrate Data:The Effect of Localized Force and the Need for Regularization.* Biophysical Journal **83** 1380–1394

127. Seko Y., Seko Y., Takahashi N., Tobe K., Kadowaki T., Yazaki Y. 1999 *Pulsatile Stretch Activates Mitogen-Activated Protein Kinase (MAPK) Family Members and Focal Adhesion Kinase (p125FAK) in Cultured Rat Cardiac Myocytes.* Biochemical and Biophysical Research Communications **259** 8–14

128. Semwogerere D., Weeks E. 2005 *Confocal microscopy.* Encyclopedia of Biomaterials and Biomedical Ingeneering Emory University, Atlanta, Georgia, U.S.A.

129. Shepherd N., Fisher V. 1990 *Combined force and voltage measurement in rapidly superfused guinea pig heart cells.* Am J Physiol **258** C739-C748

130. Shepherd N., Vornanen M., Isenberg G. 1990 *Force measurements from voltage-clamped guinea pig ventricular myocytes.* AJP - Heart and Circulatory Physiology, **258(2)** H452-H459

131. Sheu M. T., Huang J., Yeh G., Ho H. 2001 *Characterization of collagen gel solutions and collagen matrices for cell culture.* Biomaterials **22** 1713-1719

132. Shih Y., Rothfield L. 2006 *The bacterial cytoskeleton.* Microbiology and Molecular Biology Reviews **70(3)** 729-754

133. Simpson D. G., Decker M., Clark W., Decker R. 1993 *Contractile activity and cell-cell contact regulate myofibrillar organization in cultured cardiac myocytes.* J Cell Biol **123** 323-336

134. Sollich P. 1998 *Rheological constitutive equation for a model of soft glassy materials.* Phys. Rev. E **58**, 738−759

135. Sotowska-Brochocka J. 2001 *Fizjologia zwierząt.* Wydawnictwa Uniwersytetu Warszawskiego, Warszawa

136. Sweitzer N. K., Moss R. 1990 *The Effect of Altered Temperature on Ca2+-sensitive Force in Permeabilized Myocardium and Skeletal Muscle Evidence for Force Dependence of Thin Filament Activation.* J. Gen. Physiol. **96** 1221-1245

137. Tamada M., Sheetz M. P., Sawada Y. 2004 *Activation of a signaling cascade by cytoskeleton stretch.* Developmental Cell **7** 709-718

138. Tan J. L., Tien J., Pirone D., Gray D., Bhadriraju K., Chen C. 2003 *Cells lying on a bed of microneedles: an approach to isolate mechanical force.* Appl Physical Sciences **100** 1484-1489Tan J., Shen H., Saltzman W. 2001 *Micron-Scale Positioning of Features Influences the Rate of Polymorphonuclear Leukocyte Migration.* Biophysical Journal **81** 2569–2579

139. Tasche C., Meyhöfer E., Brenner B. 1999 *A force transducer for measuring mechanical properties of single cardiac myocytes.* APJ- Heart 277 2400-2408

140. Taub A. I., Spaepen F. 1981 Ideal.elastic, anelastic and viscoelasticdeformation of a metallic glass. Journal of Materials Science 16 3087-3092

141. Tervoort T. A. 1996 *A multi-mode approach to finite, three-dimensional, nonlinear viscoelastic behavior of polymer glasses*. J. Rheol. **40**(5) 779-797

142. Tesi, C., Piroddi N., Colomo F., Poggesi C. 2002. *Relaxation kinetics following sudden Ca(2+) re in single myofibrils from skeletal muscle.* Biophys J **83** 2142-2151

143. Tomasek J. J. ,Gabbiani G., Hinz B., Chaponnier C., Brown R. 2002 *Myofibroblasts and mechanoregulation of connective tissue remodeling.* Nature Reviews Molecular Cell Biology **3** 349-363

144. Vizgirda V. M., Wahler G., Sondgeroth K., Ziolo M., Schwertz D. 2002 *Mechanisms of sex differences in rat cardiac myocyte response to β-adrenergic stimulation.* Am J Physiol Heart Circ Physiol **282** H256-H263

145. Vogel V. 2006 *Mechanotransduction involvin multimodular proteins: converting force into biochemical signals.* Annu. Rev. Biophys. Biomol. Struct. **35** 459-488

146. Vogel V., Sheetz M. 2006 *Local force and geometry sensing regulate cell functions.* Mol Cell Biol **7** 265-275

147. Wang N., Naruse K., Stamenović D., Fredberg J., Mijailovich S., Tolić-Nørelykke I., Polte T., Mannix R., Ingber D. 2001 *Mechanical behavior in living cells consistent with the tensegrity model.* Biophysics **98(14)** 7765–7770

148. Webb K., Li W., Hitchcock R., Smeal R., Gray S., Tresco P. 2003 *Comparison of human fibroblast ECM-related gene expression on elastic three-dimensional substrates relative to two-dimensional films of the same material.* Biomaterials **24** 4681–4690

149. Wilders R., Jongsma H. J. 1993 *Beating Irregularity of Single Pacemaker Cells Isolated from the Rabbit Sinoatrial Node.* Biophysical Journal **65** 2601-2613

150. Xu J., Steng Y., Wirtz D. 2000 *Strain Hardening of Actin Filament Networks: Regulation by the dynamic crosslinking protein α-actinin.* The Journal of Biological Chemistry 275(46) 35886-35892

151. Yasuda S., Sugiura S., Kobayakawa N., Fujita H., Yamashita H., Katoh K., Saeki Y., Kaneko H., Suda Y., Nagai R., Sugi H. 2001 *A novel method to study contraction characteristics of a single cardiac myocyte using carbon fibres.* Am J Physiol Heart Circ Physiol, **281** H1442-H1446

152. Yeung T., Georges P., Flanagan L., Marg B., Ortiz M., Funaki M., Zahir N., Ming W., Weaver V., Janmey P. 2004 *Effects of substrate stiffness on cell morphology, cytoskeletal structure and adhesion.* Cell Motility and the Cytoskeleton, **60** 24-34

153. Yi X. P., Wang X., Gerdes A., Li F. 2003 *Subcellular Redistribution of Focal Adhesion Kinase and Its Related Nonkinase in Hypertrophic Myocardium.* Hypertension **41** 1317-1323

154. Yin L., Bien H., Entcheva E. 2004 *Scaffold topography alters intracellular calcium dynamics in cultured cardiomyocyte networks.* Am J Physiol Heart Circ Physiol **287** H1276-H1285

155. Yin S., Zhang Y., Zhan C., Wu J., Xu J., Cheung J. 2005 *Measuring single cardiac myocyte contractile force via moving a magnetic bead.* Biophysical Journal **88** 1489-1495

156. Zamir E. Geiger B. 2001 *Molecular complexity and dynamics of cell-matrix adhesions.* Journal of Cell Science **114** 3583-3590

157. Zhao I., Lim C., Sawyer D., Liao R., Zhang X. 2006 *Microchip for subcellular mechanics study in living cells.* Sensors and Actuators B: Chemical **114(2)** 1108-1115

158. Zimmermann W. H., Fink C., Kralisch D., Remmers U., Weil J., Eschenhagen T. 2000 *Three-Dimensional Engineered Heart Tissue from Neonatal Rat Cardiac Myocytes.* Biotechnology and Bioengineering 68(1) 106-114